The thesis committee for Christopher Archer McKinstry

Certifies that this is the approved version of the following thesis:

Frequency Response of Damaged External Post-Tensioned Tendons

APPROVED BY
SUPERVISING COMMITTEE:

Sharon L. Wood, Supervisor

James O. Jirsa

Frequency Response of Damaged External Post-Tensioned Tendons

by

Christopher Archer McKinstry, B.S.C.E.

Thesis

Presented to the Faculty of the Graduate School of

The University of Texas at Austin

in Partial Fulfillment

of the Requirements

for the Degree of

Master of Science in Engineering

The University of Texas at Austin

May 2010

Dedication

To my parents,

For their guidance, love, and support.

Acknowledgements

I never considered pursuing a Master's degree until my last month as an undergraduate. I would like to thank those that encouraged me to further my education, especially my parents and professors at the University of Houston. It has been a very gratifying and invaluable experience. Without the generous support of Samsung Construction and Trading Corporation much of my learning experience would not be possible. Your contributions are greatly appreciated. And Jun Ki Lee, for his guidance and assistance throughout the project.

My sincere thanks go to Dr. Sharon L. Wood, my supervising professor, whose guidance, encouragement, patience, and friendship were instrumental in the completion of this project. It has truly been a pleasure working with you.

This project would not have been possible without the generous support from the faculty at the Ferguson Structural Engineering Laboratory. Special thanks are owed to Andrew Valentine, Eric Schnell, Mike Wason, Blake Stassney, Dennis Fillip, Jessica Hanten, Wendy Harrison, and Barbara Howard foe their dedicated support.

Lastly, I would also like to thank my peers for their assistance during the project, including: Andy Moore, Alejandro Avendano, Kevin Quinn, Jeremiah Fasl, Miguel Forero, and Nancy Larson.

April 23, 2010

Frequency Response of Damaged External Post-Tensioned Tendons

Christopher Archer McKinstry, M.S.E.
The University of Texas at Austin, 2010
SUPERVISOR: Sharon L. Wood

Bridges with external post-tensioned tendons are considered to be more durable than bridges with internal tendons (tendons within the webs and flanges), because external tendons are easier to inspect. In addition, in the event that extensive corrosion damage is detected, it is possible to replace an external tendon. However, an appropriate inspection for detecting damage needs to be determined for external tendons. This investigation focuses on the vibration technique, which uses the dynamic properties of the external tendon to infer the effective prestress force.

Four large-scale external tendons, designed to simulate one section of an external tendon between two deviators in a post-tensioned bridge, were tested. In the study, damage to the tendons was induced in a quantifiable fashion at a

specific location and the tensile force was measured directly. In addition, free-vibration tests were conducted periodically. This provided a direct means of measuring the sensitivity of measured natural frequencies and measured tensile force to local damage. The measured data were correlated with an approximation of the stiff string vibration model. In addition to the laboratory specimens, field testing was conducted on a bridge with external post-tensioned tendons.

The findings from the study show that a loss in tensile force was not linear with a loss in the cross-sectional area of the strand, which results from stress redistribution within the tendon. Also, the natural frequencies were much less sensitive to the level of induced damage than the tensile force. While the measured data from the laboratory data compared very well with the analytical model, the field measurements exhibited a much greater deviation from the model. Due to several factors, the difference between the laboratory specimens and the bridge tendons are believed to be caused by larger levels of inherent error in the model. The findings from the investigation support the notion that vibration testing is most appropriately used in comparing relative differences between peer tendons.

Table of Contents

List of Tables

List of Figures

CHAPTER 1
Introduction

Post-tensioning of concrete bridges was first introduced in Germany in 1936 (Weiher and Zilch, 2006). Since its inception, post-tensioning has developed into a variety of structural forms, namely bonded tendons located within the concrete section, unbonded tendons internal to the concrete, and unbonded tendons external to the concrete (Tilly, 2002). A widely-used structural form is external post-tensioned tendons, consisting of bonded strands running through grouted ducts and positioned internal to continuous or segmental concrete construction.

External-post-tensioned tendons provide two primary advantages over internal tendons with respect to durability: (1) the tendons are easier to inspect since the majority of the tendon is exposed, and (2) if necessary, an external tendon can be replaced without damage to the structure. As with internal tendons, corrosion damage in external tendons has been reported in several bridges around the world. A loss in the cross-sectional area of the tendon due to corrosion has the potential of reducing the prestress force – thereby reducing the capacity of the bridge. Developing a procedure to detect changes in the in-situ prestress force is critical for evaluating the capacity of an existing post-tensioned bridge.

In recent years several non-destructive tests have been developed or improved to evaluate the condition of the tendons, including: magnetic flux, stress-wave methods, and a vibration technique. This study focuses on using the vibration technique for external post-tensioned tendons. The goal is to be able to measure the dynamic properties of an external tendon in a post-tensioned bridge and infer the effective prestress force. The primary focus of the study is formulating the sensitivity of the measured vibrations to local damage accumulation.

In the investigations of external tendons, the occurrence of corrosion damage is associated with the presence of local voids from bleed water formation during grouting, often with chloride ion contamination as an aggravating factor (Sagues et al, 2003). In some cases, the corrosion led to the fracture of strands and complete tendon failure, usually at or near the anchorage region (Figure 1.1).

Figure 1.1: Niles Channel Bridge – Corrosion at Anchor Region (Corven, 2002)

The loss of cross-sectional area of strand would typically be assumed to be directly related to a loss in prestress force. However, this simple assumption has been shown to not be valid. A portion of the tensile stress has been found to be recovered after a wire fractures. Through inter-wire friction, a portion of the load can be redistributed to adjacent wires in a particular strand. Also, grout provides the ability for load to transfer to adjacent strands in a multi-strand tendon.

The current study is intended to build on the research performed by Lee (2007). While discovering a reduction in the measured vibration response of external tendons as damage accumulated, many questions remained unanswered because the tension force was not measured directly. It was found that the variations in the natural frequencies were not linearly related to the loss in cross-sectional area.

In the current study damage was induced in a quantifiable fashion at a specific location and the tensile force was measured directly. These data provide a direct means of measuring the sensitivity of measured natural frequencies to local damage.

The presentation of the subsequent study is shown in Table 1.1. Information on stress redistribution in external tendons is discussed in Chapter 2, as well as the vibration technique and vibration model used in the study. The construction phase of this study and highlights of the necessary instrumentation in extracting relevant data from the specimens is detailed in Chapter 3. In addition, the method of inducing damage to the tendons is discussed. The measured data from the test specimens is presented in Chapter 4. The presented data focuses on measured natural frequencies and tension force, as well as noticeable stress redistribution behavior. The measured variations in the natural frequencies are correlated with analytical models in Chapter 5. In Chapter 6, the measured response and evaluation of external tendons in the field are discussed. A brief summary on findings from the study is provided in Chapter 7.

Table 1.1: Presentation of Report

Chapter	Topic
2	Literature Review
3	Construction of Specimens and Test Procedures
4	Measured Response
5	Evaluation of Measured Response
6	Field Measurements
7	Summary

CHAPTER 2

Literature Review

In order to understand and interpret observed research data, information on relevant structural properties and system behavior is essential. The following section summarizes such pertinent background information.

The ability of stress redistribution in post-tensioning strands is discussed in Section 2.1. The vibration technique used to evaluate the condition of external tendons is explained in Section 2.2. Vibration models that have been formulated to predict the behavior of external tendons are described in Section 2.3. The measured vibration response of external tendons on the Mid-Bay Bridge in Florida is summarized in Section 2.4.

2.1 STRESS REDISTRIBUTION IN STRANDS

Although typically modeled as tension elements with no redundancy, external post-tensioned tendons have the ability to redistribute stress when local damage in the form of wire breaks occurs. This is achieved through inter-wire friction within an individual strand and also by the ability of load to be transferred through surrounding grout and into adjacent strands in a tendon. These mechanisms are discussed in the following section.

2.1.1 Stress Redistribution through Inter-wire Friction

Most previous research on wire breaks have focused on the recovery length of large-diameter, wire rope. The recovery length is defined as the distance from a fracture in which a wire is able to carry its share of the axial load again. Table 2.1 summarizes the recovery length calculated using data reported by various researchers for different configurations of wire rope.

Table 2.1: Recovery Length of Various Large-Diameter Wire Rope (Evans and Ridge, 2001)

Source of data	Transfer length (rope lay lengths)	Rope types	Derived from	Break types
Shitkow and Pospechow	1–6	Various six strand	Pull-out force	External
Davidsson	1–2 for external, 0.5–1 for internal	Seale/filler and (12/6/1)	Breaking strength	Internal and external
Cholewa and Hansel	0.4	Triangular six-strand (6 × 32) FC	Breaking strength	External
Cholewa	0.65–1	Seale RHO FC	Breaking strength	Internal and external
Chaplin and Tantrum	0.75–1.5	Seale RHO IWRC	Breaking strength	External
Wiek	1	Seale RHO IWRC	Strain gauge	External
Chien and Costello	1.18	Seale RHO IWRC	Theory	External

Typically the recovery (transfer) length is 1 to 1.5 times the lay length, which is the distance for one wire to make a complete revolution about the longitudinal axis of the rope. The lay length for a 0.6-in. diameter seven-wire strand is typically 10-in.

In general, the models developed for the large-diameter wire ropes cannot be applied to seven-wire prestressing strands embedded in concrete or grout (MacDougall and Bartlett, 2006). The presence of far fewer individual wires, as well as the interaction between the strand and concrete/grout drastically changes the behavior. A mechanical model was introduced by MacDougall and Bartlett (2005) to approximate the behavior of seven-wire strands. At the location of a wire fracture, the strain of the broken wire is zero, but the strain increases with distance from the fracture. The maximum strain in the intact wires of the strand occurs directly adjacent to the wire break. It was determined that the axial strain in the broken wire increased exponentially with distance from the break and the actual distribution depends on the tendon geometry, coefficient of inter-wire friction, and the tendon axial force (MacDougall and Bartlett, 2006).

In post-tensioned applications, the prestressing steel in the tendon is elongated during construction. When a wire breaks, the tensile force in the tendon is reduced, but the total elongation remains constant. MacDougall and Bartlett (2006) conducted several verification tests using 60-ft, single, ungrouted, seven-wire strands with different diameters (0.35-in., 0.5-in., and 0.6-in.).

Initially, the tendons were loaded to a predetermined tensile load, which varied between 50 and 70% GUTS (guaranteed ultimate tensile force). The elongation of the

tendon was recorded and the tendon was unloaded. A single wire was then cut at mid-length and the tendon was loaded again until the elongation of the undamaged specimen was reached. The difference in the tensile force before and after the damage was considered to be the loss in prestress force due to the single wire fracture. The measured reduction in the load of the 0.35-in., 0.5-in., and 0.6-in. diameter single-strand tendons were approximately 6%, 9%, and 10%, respectively. A reduction of 14% represents the loss in prestress if one-seventh of the tendon cross-sectional area is lost and no inter-wire friction exists. Therefore, the strands experienced a smaller reduction in load due to the inter-wire friction between the individual wires.

Before the single wire was cut, strain gages were attached to the outer wires in the strand at varying distances along the length in order to measure the distribution of strain after damage. The comparison between the predicted and experimental individual wire strains for the 0.6-in. diameter strand is displayed in Figure 2.1.

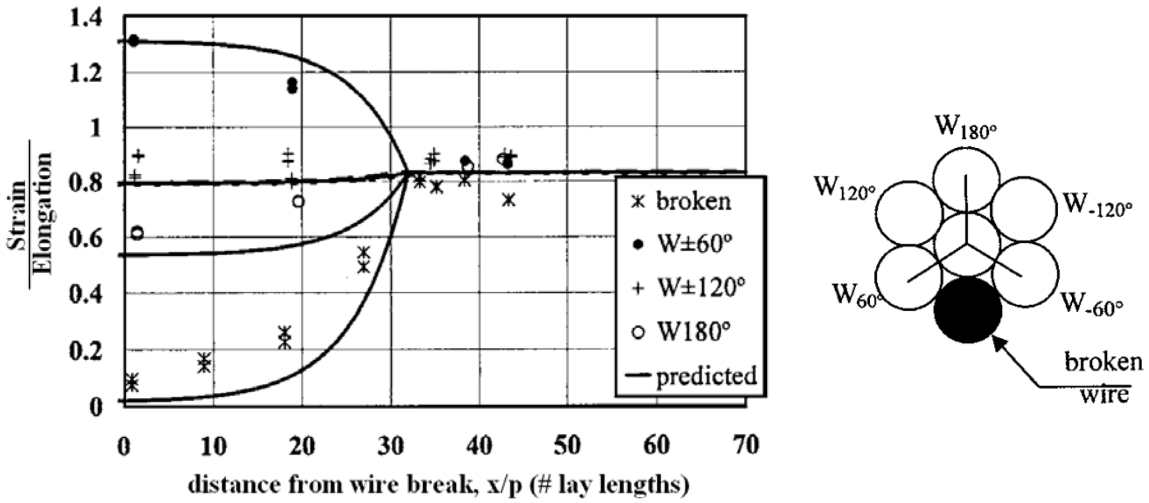

Figure 2.1: Predicted and Measured Outer Wire Strain, 0.6-in Diameter Strand (MacDougall and Bartlett, 2006)

The calculated strains are generally consistent with the measured values. The model indicates that after an outer wire breaks in a strand, tensile forces are redistributed among the wires in the immediate vicinity of the wire break. The tensile force increases in the two outer wires adjacent to the broken wire, while the tensile force in the

remaining three wires decreases. At a distance of approximately 32 lay lengths from the wire break, the strains in all six outer wires (intact and fractured) converge to the same value.

The ability of a broken wire to regain capacity is a result of internal friction between the individual wires in a strand. Because of the spiral configuration, a considerable amount of friction exists between the individual wires in the strand, which allows load to be transferred. Therefore, a broken wire is capable of supporting its total share of the load beyond the recovery distance from the fracture. Also, a loss of one wire (one-seventh of the cross-sectional area of the strand) does not correspond to a one-seventh reduction in the prestress force. The residual prestress force is attributed to inter-wire friction.

2.1.2 Stress Redistribution through Grout

Localized damage (multiple wire breaks over a short length) will reduce the tensile force in the tendon. As discussed in Section 2.1.1, stress redistribution is possible among wires in a strand for ungrouted systems. Additional stress redistribution among strands in a tendon is also possible for grouted systems. The grout even allows a completely fractured strand to carry load at a short distance away from the fracture.

Wood et al. (2008) investigated the susceptibility of full-scale, grouted stay cables to bending fatigue damage. An acoustic monitoring system provided a reliable means of detecting wire breaks in the specimens. The acoustic sensors detected a total of one hundred and fifty wire breaks during the fatigue tests on the grouted tendons specimens during the fatigue tests.

Each specimen had a clear length of 32 ft – 8 in and was constructed using 0.6-in. diameter, seven-wire strands stressed to 40% GUTS. The wire breaks were concentrated in three areas along the specimen: at both ends and at the mid-span (the location of the applied transverse load).

Figure 2.2 shows the distribution of wire breaks among the nineteen strands at each of these three locations for Specimen 12. Damage was concentrated in the strands in the

top and bottom rows of the cross-section. All seven wires fractured in four of these strands (boxed) at two locations, and all seven wires fractured in the middle strand in the top row (circled) at all three locations along the length of the specimen.

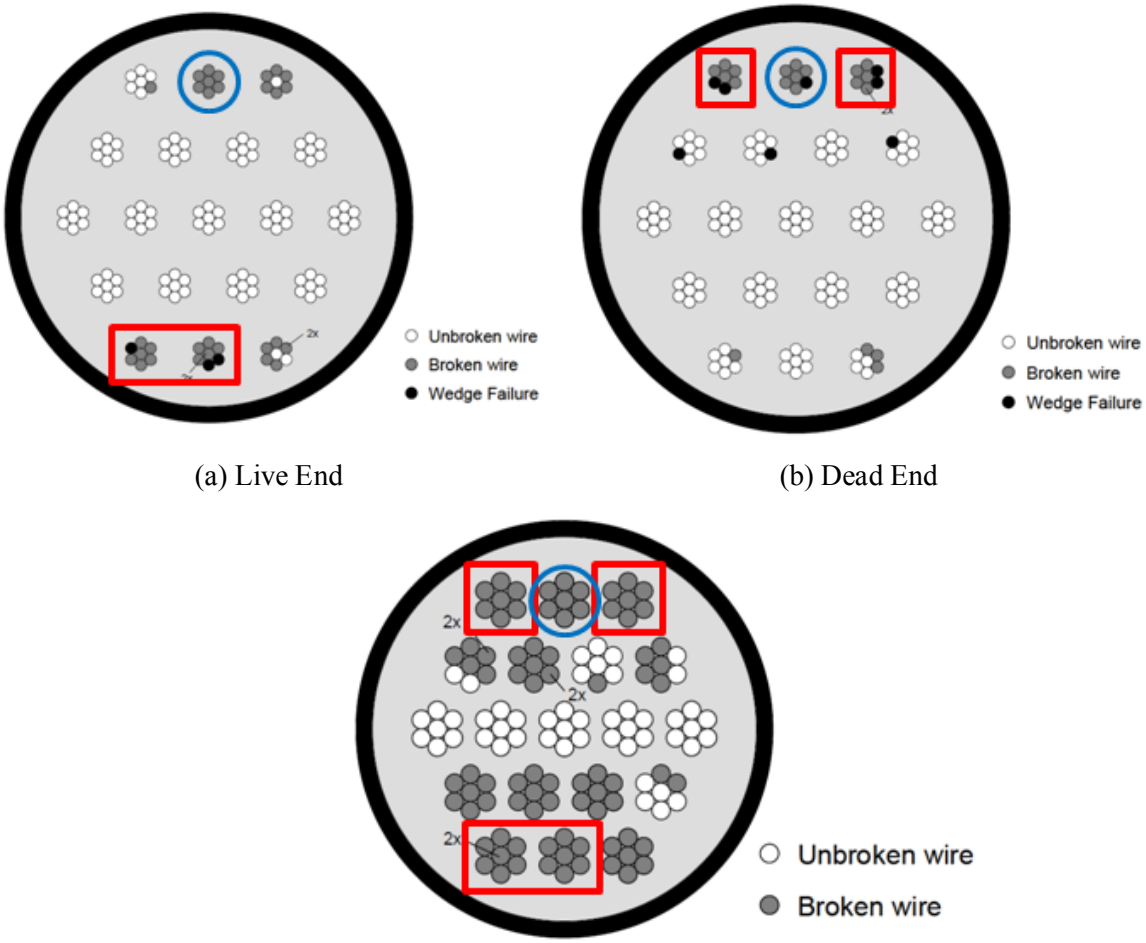

(a) Live End

(b) Dead End

(c) Mid-span

Figure 2.2: Distribution of Wire Breaks (Wood et al, 2008)

The observed damage pattern can only be explained by assuming that the tensile force in a damaged strand is redistributed through the grout. The two sections of the fractured strand behave essentially as a non-contact lap splice in a reinforced concrete member, where the tensile stresses are transferred from one bar to another through the concrete. Therefore, the grout plays an important role in the redundancy of the post-tensioned tendon.

2.2 VIBRATION TECHNIQUE

If exposed to corrosion, or other types of degradation, the tensile force in an external post-tensioned tendon will decrease during its service life. Tracking changes in the tensile force is an important factor for monitoring the structural health of an external tendon. Vibration measurements are commonly used to approximate tendon forces in a non-destructive manner.

Vibration-based testing consists of measuring the natural frequencies of a tendon either under normal service loads or after excitation. The measured frequencies can then be used to infer the value of tensile force using geometric and material parameters. Three recent investigations at the Ferguson Structural Engineering Laboratory have correlated frequency data with the level of observed damage in grouted cable and tendon specimens.

2.2.1 Variance in Natural Frequency with Increasing Damage

In the first series of tests (Wood et al, 2008), the specimens were subjected to cyclic, transverse loads at mid-span and the damage, in the form of wire breaks, was distributed at both ends and at the mid-span. In the tests conducted by Bean (2006) and Lee (2007), the cyclic loads were applied near the quarter point of the specimen and the damage was concentrated at the end closest to the applied load. Acoustic sensors were used to detect wire breaks during all three test series, but the actual distribution of damage was only known at the conclusion of the test when the specimens were disassembled.

2.2.1.1 Large-Scale Stay Cables

Wood et al. (2008) tested nine, grouted, stay-cable specimens, which were constructed with 0.6-in. strand and stressed to 40% GUTS (Table 2.2a). The fundamental frequency was measured at the beginning and conclusion of most of the fatigue tests. The ratio of the final to initial frequency is plotted as a function of the percent reduction in cross-sectional area of the strand at the location of highest damage in Figure 2.3. The fundamental frequency was not sensitive to the wire breaks induced during the bending

fatigue tests: 20 to 40% reductions in cross-sectional area were observed for 10% reductions in natural frequency.

2.2.1.2 Small-Scale Stay Cables

Bean (2006) and Lee (2007) tested three, grouted, stay-cables which were constructed with 0.6-in. strand and stressed to 50% GUTS. The measured frequency responses of two of the specimens are summarized in Table 2.2b. Natural frequencies were measured several times during these tests. Once again, a 10% reduction in natural frequency corresponded to approximately 40% reduction in cross-sectional area (Figure 2.4).

2.2.1.3 External Tendon

Lee (2007) also subjected one, grouted tendon specimen to bending fatigue loads. The specimen was also constructed with 0.6-in. strand and was stressed to 60% GUTS (Table 2.2c). At the conclusion of the fatigue test, this specimen experienced a 30% reduction in cross-sectional area of the strands, and the fundamental frequency decreased by 8% (Figure 2.4).

Table 2.2: Vibration Testing at FSEL - Summary of Test Specimens

(a) Large-Scale, Stay Cable Specimens

Specimen	# of Strands	Clear Length (ft)	Initial Prestress (% GUTS)	Initial Frequency (Hz)	Final Frequency (Hz)	Frequency Ratio	% Loss of Cross-Sectional Area at Critical Location
1	19	33.57	40	-	12.0	-	0.105
2	19	33.57	40	12.5	11.5	0.920	0.391
3	19	33.57	40	-	-	-	0.414
4	19	33.57	40	-	-	-	0.211
6	13	33.23	40	11.5	11.0	0.957	0.187
7	19	33.23	40	13.3	11.1	0.835	0.474
9	19	33.23	40	12.5	10.5	0.840	0.459
10	19	33.23	40	13.0	11.8	0.908	0.173
12	19	33.23	40	13.1	10.0	0.763	0.624

(b) Small-Scale, Stay Cable Specimens

Specimen	# of Strands	Clear Length (ft)	Initial Prestress (% GUTS)	Initial Frequency (Hz)	Final Frequency (Hz)	Frequency Ratio	% Loss of Cross-Sectional Area at Critical Location
2	2	49	50	4.4	3.9	0.886	0.500
3	2	49	50	4.3	3.5	0.814	0.714

(c) Tendon Specimen

Specimen	# of Strands	Clear Length (ft)	Initial Prestress (% GUTS)	Initial Frequency (Hz)	Final Frequency (Hz)	Frequency Ratio	% Loss of Cross-Sectional Area at Critical Location
1	12	31.96	60	15.4	14.2	0.922	0.298

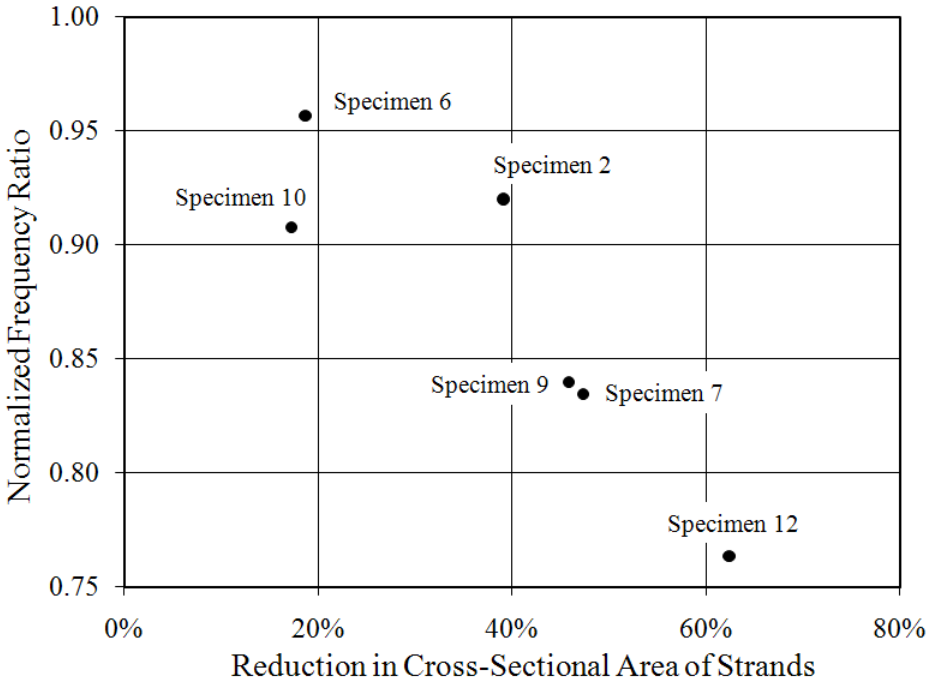

Figure 2.3: Specimens with Distributed Damage

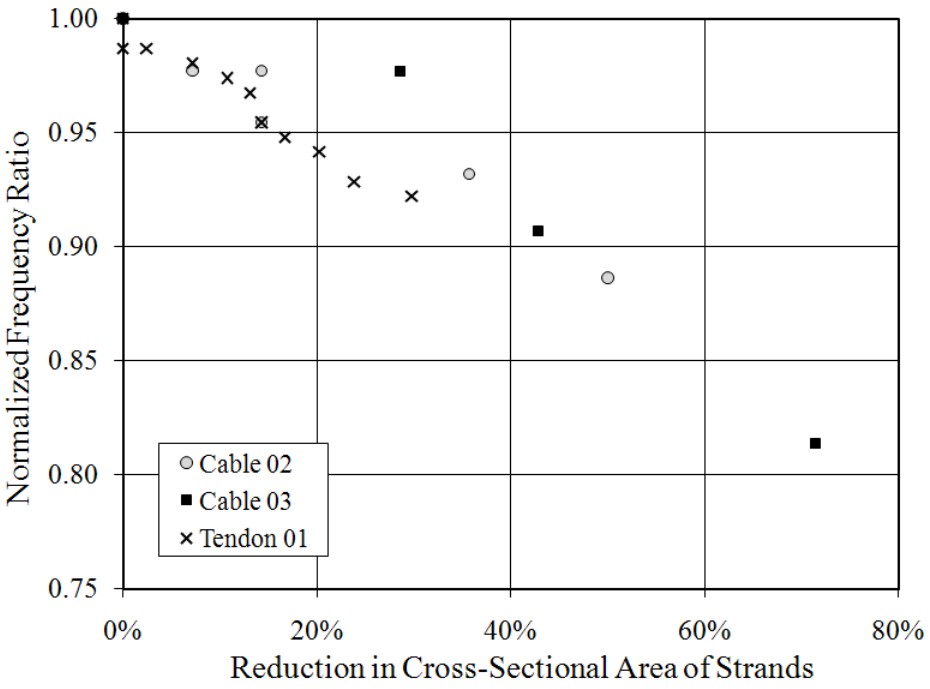

Figure 2.4: Specimens with Concentrated Damage

2.2.1.4 Summary

In general, as the number of wire breaks increased the natural frequencies of each specimen reduced. However, the natural frequencies were not sensitive to losses in cross-sectional area.

2.2.2 Double Peaks

Both Sagues (2006) and Lee (2007) observed a presence of double peaks in the frequency spectra from free-vibration tests (Figure 2.5). The separation between the peaks varies from 0.01-0.1 of their average frequency, and the separation increased with higher modes. For a given pair of frequency peaks, nearly the same tensile force value was calculated, but different flexural stiffness values were calculated (Sagues, 2006).

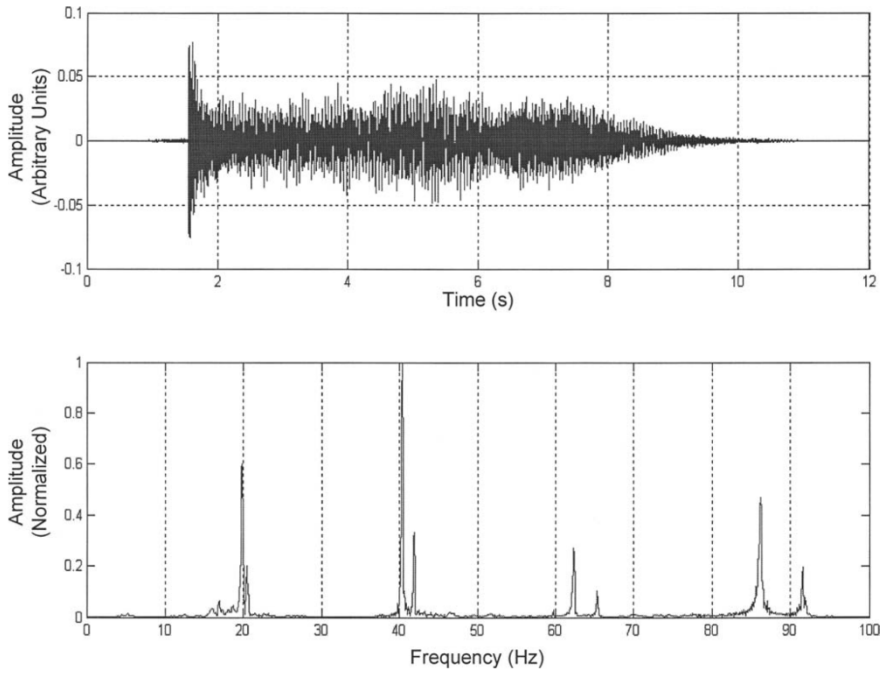

Figure 2.5: Time Domain Signal and Frequency Spectrum with Double Peaks (Sagues, 2006)

The presence of double peaks is believed to be caused by a non-uniform arrangement of strand within the cross-section. The strands are held in place at the ends by the anchor head, but shift within the cross-section along the length. At the location of

deviators, the strands tend to crowd toward the top of the duct (Figure 2.6). Because the position of the strands influences the moment of inertia differently in the horizontal and vertical directions, the frequency pairs are believed to correspond to natural frequencies for a given mode in the vertical and horizontal directions.

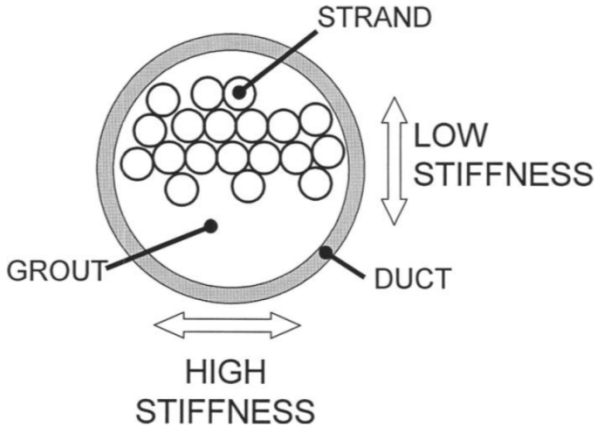

Figure 2.6: Non-Uniform Strand Arrangement (Sagues, 2006)

2.3 VIBRATION MODELS

2.3.1 Classification

Vibration models have been classified into four categories by Kim and Park (2007), depending on whether cable sag and bending stiffness are considered (Table 2.3).

Table 2.3: Considerations of Different Vibration Models

Method	Sag-Extensibility	Bending Stiffness
Taut String Model	Neglects	Neglects
Russell et al. (1998)	Considers	Neglects
Stiff String Model	Neglects	Considers
Zui et al. (1996)	Considers	Considers

The taut string model neglects both sag-extensibility and bending stiffness. While this method is the most straightforward, its applicability is limited to flat, long, slender cables.

The model formulated by Russell et al. (1998) takes into account sag and becomes slightly more complex. The approach requires solving a non-linear formula through trial-and-error, requiring additional information that is not often available in practice.

The stiff string model considers bending stiffness while neglecting sag. The process involves measuring the natural frequency and applying linear regression procedures to solve for the tension force and flexural stiffness simultaneously. Because of its simplicity, this approach is preferred by field engineers.

The last category, developed by Zui et al. (1996), takes into account both factors. This method becomes very difficult to solve because it involves many variables, many of which are unknown and/or hard to formulate.

2.3.2 Stiff String Model

When dealing with external tendons, flexural stiffness cannot be ignored. Sagues (2006) noted that the effect of stiffness is to increase the fundamental frequency compared to a string with no stiffness. This effect becomes more substantial for higher modes. Accordingly, bending stiffness must be taken into account to estimate the tensile force from the frequency data. Sag-extensibility is more significant in stay cables, which are much longer relative to external tendons. Consequently, the effects of sag can be ignored in the formulation of tendons (Sagues, 2006). Therefore, the stiff string model is considered to be appropriate for representing vibrating external, post-tensioned tendon.

The governing differential equation for the stiff string model:

$$EI\frac{\partial^4 w(x,t)}{\partial x^4} - T\frac{\partial^2 w(x,t)}{\partial x^2} + m\frac{\partial^2 w(x,t)}{\partial t^2} = 0 \qquad \text{(Equation 2.1)}$$

where x defines the longitudinal axis of the tendon, $w(x,t)$ represents the transverse deflection, T is the axial tension, EI is the flexural stiffness, and m is the mass per unit length. As shown in Equation 2.1, the flexural stiffness, tension, and mass are independent of the location along the tendon. Therefore, the values of length, mass, and flexural stiffness are assumed to remain constant throughout the length of the specimen.

Morse (1948) derived an expression (Equation 2.2) to approximate the natural frequencies of a stiff string with fixed boundary conditions at both ends:

$$f_n \cong \frac{n}{2L}\sqrt{\frac{T}{m}}\left[1+\frac{2}{L}\sqrt{\frac{EI}{T}}+\left(4+\frac{n^2\pi^2}{2}\right)\frac{EI}{TL^2}\right] \qquad \text{(Equation 2.2)}$$

where f_n is the frequency of mode n in Hz, L is the length of the specimen, T is the tensile force, m is the mass per unit length, and EI is the flexural stiffness.

The unit mass of the system is calculated based on the geometry of the specimen and material densities. The density of the grout can vary appreciably, depending on mixture proportions and water loss due to evaporation during construction. Based on grout samples collected from bridges in Florida, (Sagues, 2006) estimated the density of grout to be 100 to 115 lb/ft^3.

The calculation of the flexural stiffness depends on both the cross sectional geometry of the tendon and the modulus of elasticity of each material. As discussed in Section 2.2.2, the arrangement of the strands about the axis of bending dominates the moment of inertia term.

The specimen length can be easily measured, but uncertainty exists regarding the appropriate length. Tendons often emerge at an angle from the concrete surface. In addition, the concrete end blocks and deviators may not be rigid.

2.4 BRIDGE TESTING

Between August 2000 and July 2001, the Florida Department of Transportation performed a thorough investigation of the Mid-Bay Bridge in Okaloosa County, Florida. The discovery of multiple failed, external, post-tensioned tendons led to the development of rigorous inspections techniques and tests to catalog the level of damage. Inspection methods are generally designed to detect the presence of two major deficiencies: wire breaks and grout voids. In addition to vibration testing, the following tests were performed: sound testing for voids, borescope inspections of anchors, visual void inspections, magnetic-flux testing, grouting mock-up tests, and other corrosion related tests. The scope of this section will focus on the findings from the vibration testing.

Vibration testing was performed during October 2007 on 140 spans, each containing six tendons. The layout of the Mid-Bay Bridge tendons in a typical span is shown in Figure 2.7.

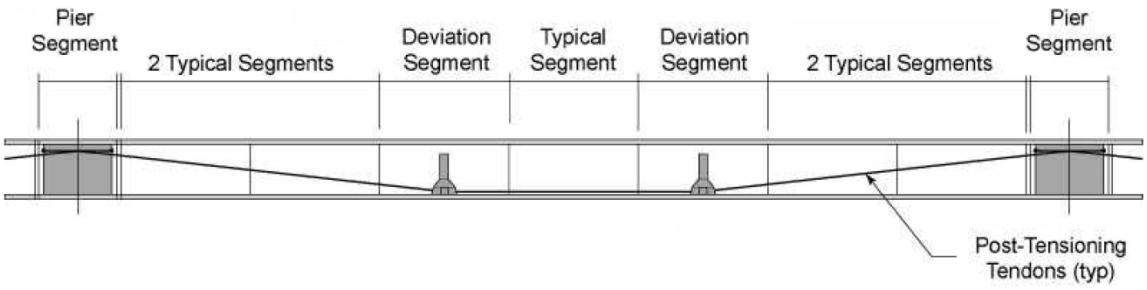

Figure 2.7: Mid-Bay Bridge Tendon Profile (Corven, 2001)

Vibrations were induced by striking each free length of the tendon at a distance L/6 from the anchor or deviator block. Accelerometers in the direction of the impact were measured L/3 from the same end.

For each tendon, the results of the three free lengths were compared against one another. In the absence of any damage, the calculated tension in the three individual segments was expected to be equal. Slight variations existed in the calculated tension, and variations of ±6% were interpreted to mean that no significant damage had occurred within the tendon. The results are plotted in Figure 2.8. Differences of ±25% were observed in one tendon (Figure 2.9), and upon further investigation, inspectors determined that the tendon had experienced severe corrosion and multiple wire breaks.

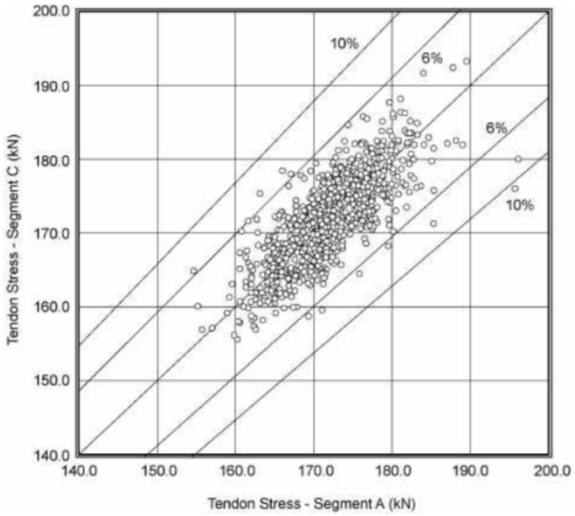

Figure 2.8: Comparative Tendons Forces from Vibration Testing of the Mid-Bay Bridge (Corven, 2001)

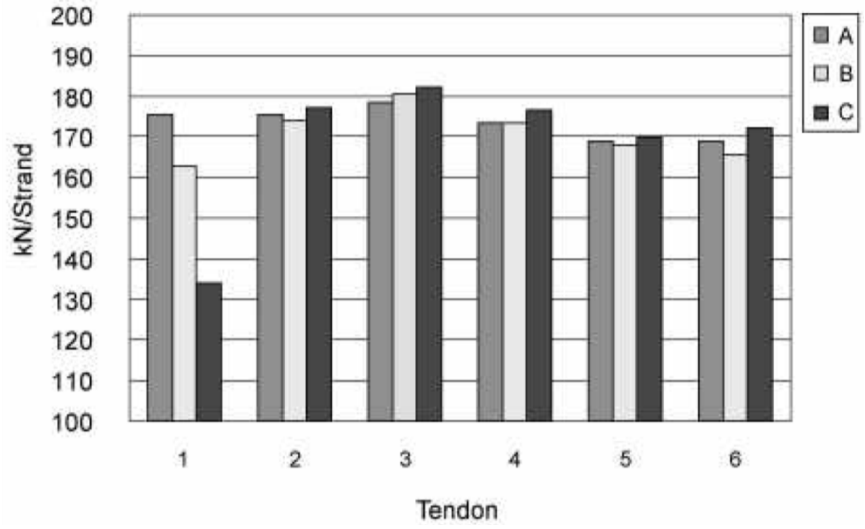

Figure 2.9: Vibration Results for Span 9 of the Mid-Bay Bridge (Corven, 2001)

While the vibration testing successfully located tendons that experienced significant levels of damage, distinct limitations in the method were also identified. Concerns were raised that vibration testing may not be sufficient to detect damage within the anchor region. In addition, the stiff string model used to extract the tendon forces assumes fixed boundary conditions and uniform distributions of mass and flexural

stiffness along the length of the tendon (Sagues, 2006). Actual tendons may differ considerably from these assumptions.

The results from the Mid-Bay Bridge inspection show that the vibration testing is most appropriately used in comparing the relative differences between equally stressed segments of a particular tendon (Corven, 2001).

CHAPTER 3

Construction of Specimens and Test Procedures

3.1 OVERVIEW

The post-tensioned tendons in this investigation were designed to simulate one section of an external tendon between two deviators in a post-tensioned bridge. Five specimens were constructed and four were tested during the project. Each specimen was grouted and contained seven, 0.6-in. diameter, seven-wire strands. The configuration of the anchorage blocks and the level of initial stressing were the two primary experimental parameters (Table 3.1).

Table 3.1: Configuration of Test Specimens

Specimen ID	Anchorage Block	Initial Prestress
1*	Concrete	15% GUTS
2	Steel	40% GUTS
3	Concrete	40% GUTS
4	Steel	70% GUTS
5	Concrete	70% GUTS

NOTE: *Specimen 1 was not tested

The concrete anchorage blocks were similar to those designed by Lee (2007) and included commercial, post-tensioning hardware. The boundary conditions provided by the concrete blocks were representative of conditions where an external tendon is anchored in a concrete deviator. The steel anchor blocks were fabricated specifically for this project and were designed to accommodate the commercial anchor heads used for the concrete anchor blocks. Different end conditions were selected to determine the effective length of the tendons corresponding to the clear distance between concrete anchor blocks or the overall distance between the anchorage hardware.

The target stress levels for the tendons were 40% and 70% of the guaranteed ultimate tensile strength (GUTS) of the strands. However, due to a construction error,

Specimen 1 was only stressed to 15% GUTS. Specimen 1 was disassembled after identifying the error and the measured response of that specimen is not discussed in this report.

A corrosion technique, which rapidly corrodes one wire in a strand at a time until a fracture occurs, was used to induce damage in the specimens. After every wire break, the natural frequencies and the tension force in the specimen were measured. The construction procedures and test methods are discussed in this chapter. Measured data are summarized in Chapter 4 and evaluated in Chapter 5.

3.2 CONSTRUCTION OF TENDON SPECIMENS

The materials and procedures used to assemble the tendons are summarized in this section.

3.2.1 Reaction Frame

Two, 32-ft steel reaction frames were used to resist the prestressing force in the post-tensioned tendons. Information of the design of the frames can be found in Poser's thesis on full-scale bending fatigue tests of grouted stay cables (2001). The frames (Figure 3.1) are made of two longitudinal W14X90 columns with built up cross beams at both ends. Slight modifications were made to each frame to accommodate the anchorage blocks used for this research. Steel plates with a 3.25" diameter opening in the center were welded to one end of the frame used to test specimens with the concrete anchorage blocks and both ends of the frame used to test specimens with the steel anchorage blocks. The plates reduced the size of the openings at the ends of the frame to ensure that each specimen had adequate bearing area.

Figure 3.1: Reaction Frames

3.2.2 Anchorage Blocks

3.2.2.1 Concrete Anchorage Blocks

Concrete anchor blocks were constructed to enclose the commercial post-tensioning hardware. All hardware was purchased from VSL. Type ECI 6-7 anchor heads, which can accommodate seven, 0.6-in. strands, were used to construct all specimens.

Each concrete block measured 18” by 18” in cross section and 24” in length. The design compressive strength of the concrete was 3500 psi. Reinforcement in the concrete blocks was designed to resist the prestressing forces, local bursting, and side-face blowout stresses. Longitudinal, transverse, and VSL-specified spiral reinforcement were provided. VSL type ECI 6-7 stressing bearing plates, along with the reinforcement, were placed inside the formwork of the concrete blocks as shown in Figure 3.2. A diagram of the concrete anchor block is shown in Figure 3.3 and the finished concrete anchor block is shown in Figure 3.4. A 1-in. steel plate was bonded to the inside face of the anchor block with hydro-stone to provide a smooth surface and alignment pocket for the center-hole load cell.

Figure 3.2: Reinforcement in Concrete Anchor Block

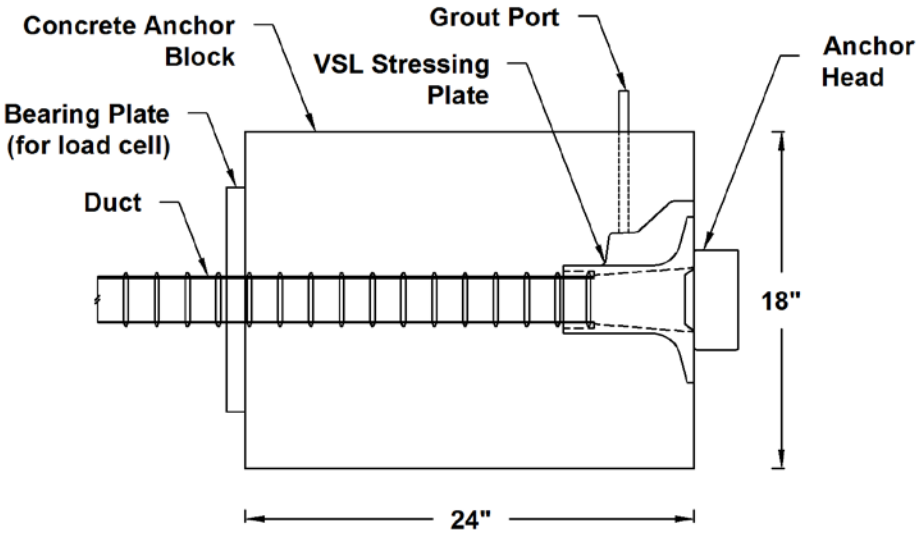

Figure 3.3: Detail of Concrete Anchor Block

(a) Bearing Plate, Duct Exiting Anchor Block

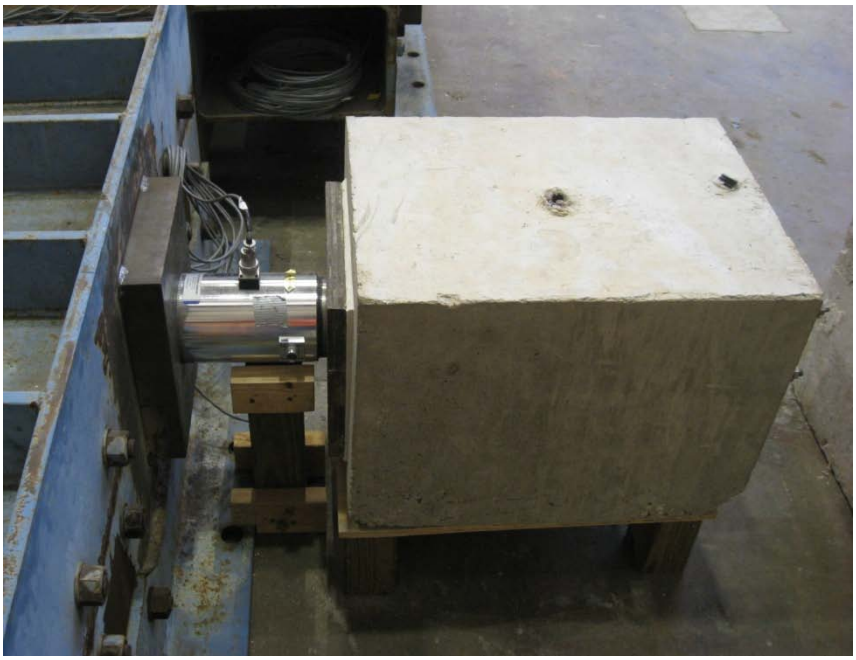

(b) South End Anchor Region

Figure 3.4: Concrete Anchor Block

The final dimensions of the specimens with concrete anchor blocks are shown in Figure 3.5. The overall length of 37' – 0" was measured from the outside faces of the concrete blocks. The clear length of 33' – 0" was measured from the inside faces of the concrete blocks.

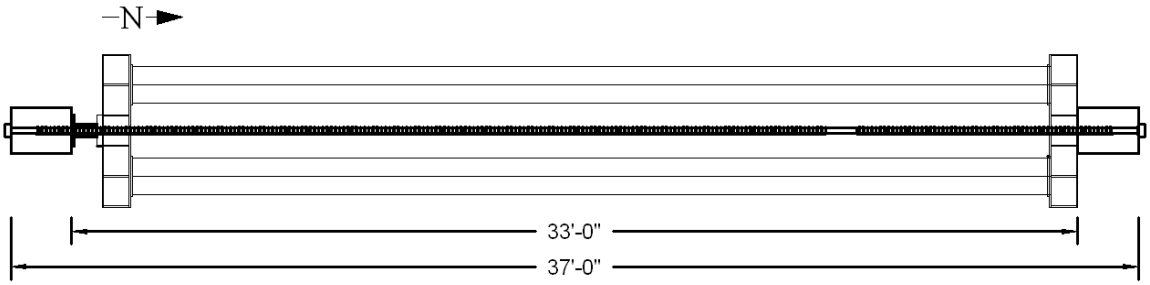

Figure 3.5: Dimensions of Specimens with Concrete Anchor Blocks (Plan View)

3.2.2.2 Steel Anchorage Blocks

In order to anchor the tendons without using concrete anchor blocks, special – purpose steel blocks were machined at Ferguson Lab. The anchors were intended to replicate the functionality of the VSL anchor system and were designed to allow the use of the VSL anchor heads.

The steel anchor blocks held the anchor heads securely when stressed and resisted the transverse forces induced by the splaying of the strands. The strand spacing at the anchor head is larger than the strand spacing along the free length. Therefore, the center hole in the steel anchorage blocks had a conical profile (Figure 3.6). Ports were also machined in the top of the steel anchorage blocks for grouting. Two ports were machined at the north end of the specimen and one at the south end. This provided one inlet at the north end and a vent at each end of the specimen. The steel anchor block is shown in Figure 3.7.

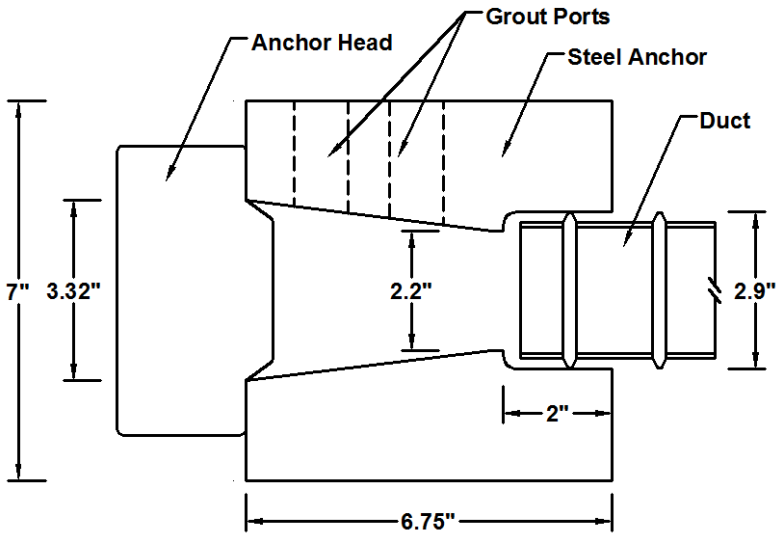

Figure 3.6: Detail of Steel Anchor Block

(a) Duct Exiting Anchor Block (north end)

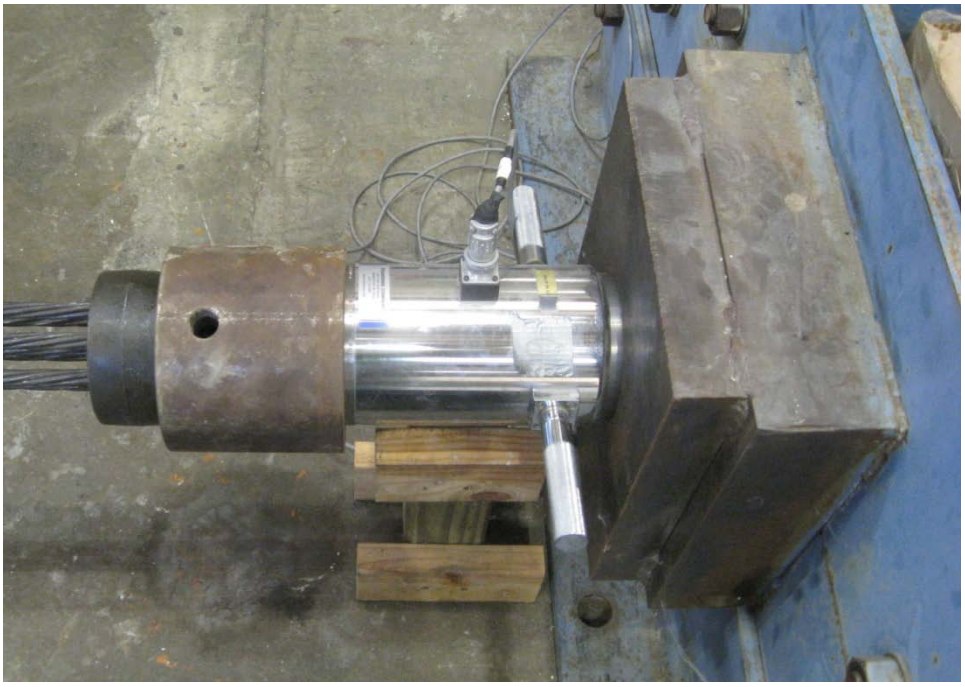

(b) South End Anchor Region

Figure 3.7: Steel Anchor Block

The final dimension of the constructed steel anchored specimen is shown in Figure 3.8. The overall length of 34' – 10" was measured from the outside faces of the steel blocks. The clear length of 33' – 9" was measured from the inside faces of the steel blocks.

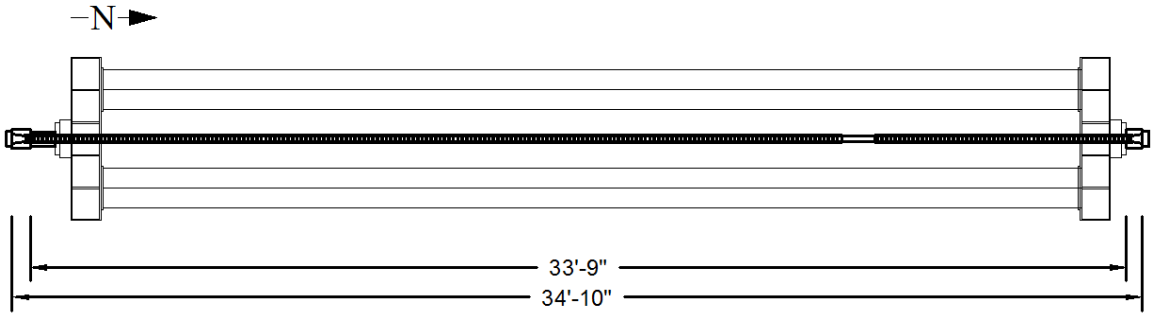

Figure 3.8: Dimensions of Specimens with Steel Anchor Blocks (Plan View)

3.2.3 Assembly Procedure

Specimen construction began by pulling seven, 45-ft sections of strand through the length of the frame, as shown in Figure 3.9. All seven strands were pulled at the same time. The strands were longer than the overall length of the specimens, because additional length was required for the stressing process. Once the strands were in place, strain gages were applied to every strand. This procedure is discussed in Section 3.4.2.1.

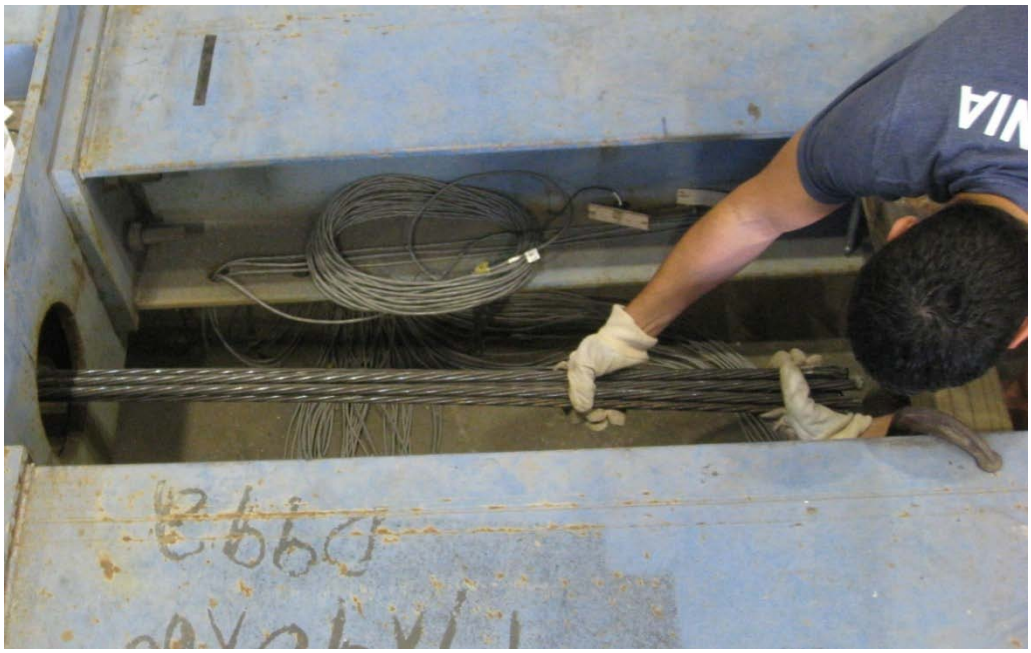

Figure 3.9: Pulling Strands Through Frame

Once the strain gages were installed, the strands were bundled in the same pattern as the anchor head. It was imperative that each of the seven strands be at the same location at each end of the specimen, and that the strands not cross along the length. Zip ties were used every four feet to ensure that each strand remained in its correct location. Once the strands were in place, high density polyethylene (HDPE) duct was pulled over the strands to enclose them. The duct had an inside diameter of 2.28-in. and a thickness of 0.1-in. Although each specimen could have been assembled using a single section of HDPE duct, multiple sections were used. Plastic couplers were used to join the sections and provide a water-tight seal during grouting. The couplers provided a convenient

means of routing the strain gage wires to the outside of the specimen (Figure 3.10) and creating a 1-ft section where the duct and grout could be easily removed to expose the strand for accelerated corrosion testing.

Figure 3.10: Coupler for HDPE Duct

After the strands and duct were in place, the load cell was placed over the south end of the specimen and the concrete or steel anchor blocks were installed at each end of the reaction frame. The ECI 6-7 anchor heads and post-tensioning wedges were then put in position for stressing.

3.2.4 Prestressing Procedure

A hydraulic, center-hole ram was used to stress the tendons. All seven strands were pulled simultaneously during stressing. The stressing ram was positioned between the outside face of the "live end" anchor head (north anchor head) and the inside face of an additional anchor head, which was used only for the stressing operation (Figure 3.11). Figure 3.12 shows the ram and the pneumatic pump during the stressing operation.

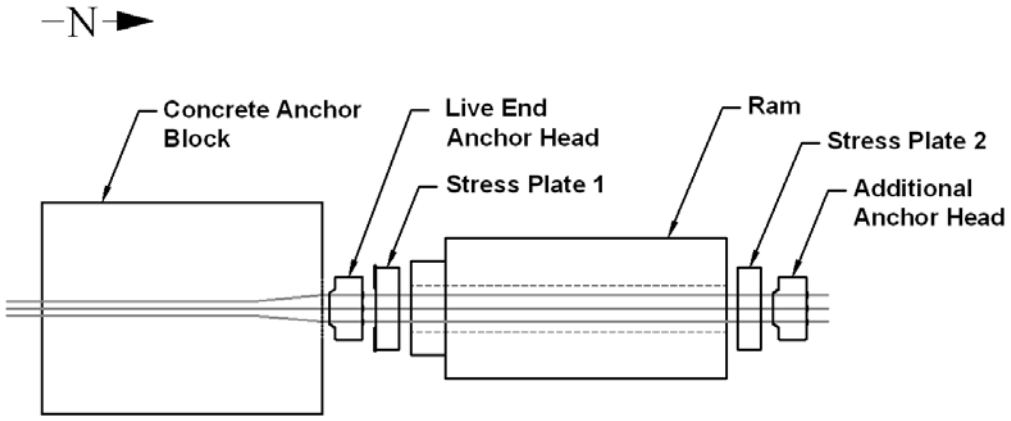

Figure 3.11: Live-End Stressing Setup

Figure 3.12: Tendon Stressing

Two steel plates were machined with seven holes, replicating the strand pattern at the anchor head, for use during the stressing operation. The plates are shown in Figure 3.13. The purpose of the plates was to provide a bearing surface for the stressing ram against the anchor heads. One of the plates was retro-fitted with 1/8-in. thick washers that were welded around the strand pattern. The washers were placed in such a manner to allow the stress plate to bear against the anchor head at the live end of the specimen, but prevent the stress plate from bearing against the individual wedges.

Figure 3.13: Steel Plates Used During Stressing

Each specimen was stressed to a level slightly greater than the target stress, in order to account for the 1/8-in. seating loss from the washers once the ram was retracted. During stressing, the applied tension was measured using three types of instrumentation: (1) pressure gage that measured the hydraulic pressure in the ram, (2) strain gages on each strand, and (3) a 500-kip load cell at the dead end of the specimen. The load cell provided the most reliable means of measuring the tension force in the strands, but the data from the three sources were consistent.

3.2.5 Grouting

A combined grout mixer and pump was used to grout the test specimens. The grout mixture consisted of prepackaged grout and tap water. The grout used was Masterflow 1205, which was manufactured by BASF and approved by VSL.

The amount of water was measured and added to the grout mixer. With the mixer turning, dry grout material was slowly added. Once all the grout had been added, the components were mixed approximately ten minutes in the disc mixer before being released into the storage trough. From there, the grout was pumped into the inlet at the north end of the specimen. The grout mixer is shown in Figure 3.14.

Figure 3.14: Grouting

Vents were provided at both anchor ends to minimize grout voids and allow air to escape. Once roughly a gallon of grout had escaped from the north air vent, it was sealed. The grouting process continued until grout had escaped from the south air vent, which was then sealed. After both vents were sealed, the valve between the mixer and specimen entrance was closed. The grout was allowed to cure for seven days before beginning any tests.

3.2.6 Accelerated Corrosion Zone

In order for the corrosion to take place, a section of strand had to be exposed. When installing the duct over the strands, a 1-ft gap was intentionally left open. This gap was covered with two half-sections of duct that were duct-taped together (Figure 3.15a). This made it easier to remove the duct after the grouting process. The region was also covered with heat shrink material in order to provide a watertight seal (Figure 3.15b). Once the grout hardened for 24 hours, the heat shrink, duct tape, and duct were removed, and the grout was chipped away with a hammer and chisel. Full removal of the grout is

shown in (Figure 3.15c). The wires protruding from the duct in Figure 3.15c were attached to the individual strands before grouting to provide an electrical connection during the corrosion phase of the experiment. Specimen 2 is shown here, but a less tedious method of attaching the wires to the strands was used for Specimens 3, 4, and 5. After the strands were exposed, a copper wire was wrapped around the entire stand in those specimens, which provided the same level of electrical connectivity as the method used for Specimen 2.

(a) with Duct Tape

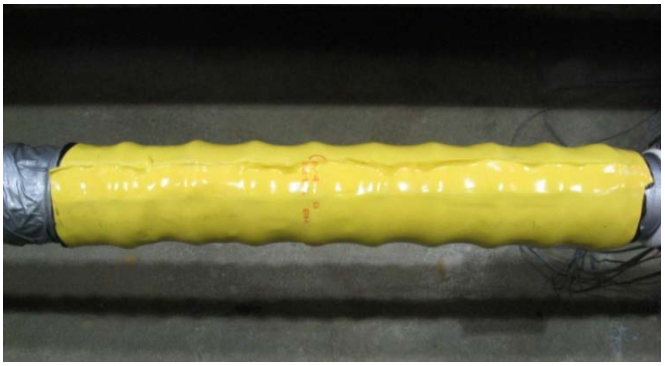

(b) with Heat-Shrink Wrap

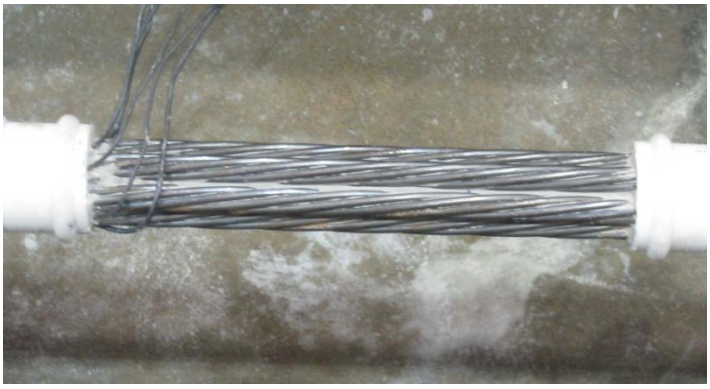

(c) with Exposed Strands

Figure 3.15: Damage Location

3.3 PROCEDURE FOR INDUCING CORROSION

The objective of the experiments was to induce damage in the test specimens in a controlled manner and monitor the changes in the prestress force and the natural frequencies.

Damage was induced in the specimen by creating an electrochemical, galvanic corrosion cell. A galvanic corrosion cell works by having two dissimilar metals in contact with an electrolyte solution. The less noble metal (anode) will transfer electrons to the metal with the higher potential (cathode). As a result, the anode will corrode. The addition of electrical current greatly accelerates the rate of corrosion at the anode.

The cell was created using a 12-V automobile battery, an 87-Ω resistor, a 3/4 –in. stainless steel tube, an electrolyte solution containing 10% sodium chloride and 20% hydrochloric acid by weight, and the prestressing strand (Figure 3.16).

Electric current flowed from the negative terminal of the battery through the resistor and into the stainless steel bar, which was submerged in the electrolyte solution. The stainless steel bar acted as the cathode in the corrosion cell. A tip from a highlighter marker was partially submerged in the electrolyte solution and extended up to the bottom of the prestressing strand. The electrolyte solution was wicked through the highlighter tip to the strand. Corrosion only occurred at the location of the tip where the strand was in direct contact with the electrolyte solution. In order to maintain contact with the strand

during corrosion, the electrolyte solution was supported on several low-stiffness springs and the entire apparatus was wedged below the strands. As the area of each wire decreased due to corrosion, the springs would decompress and contact between the highlighter tip and the strand was maintained.

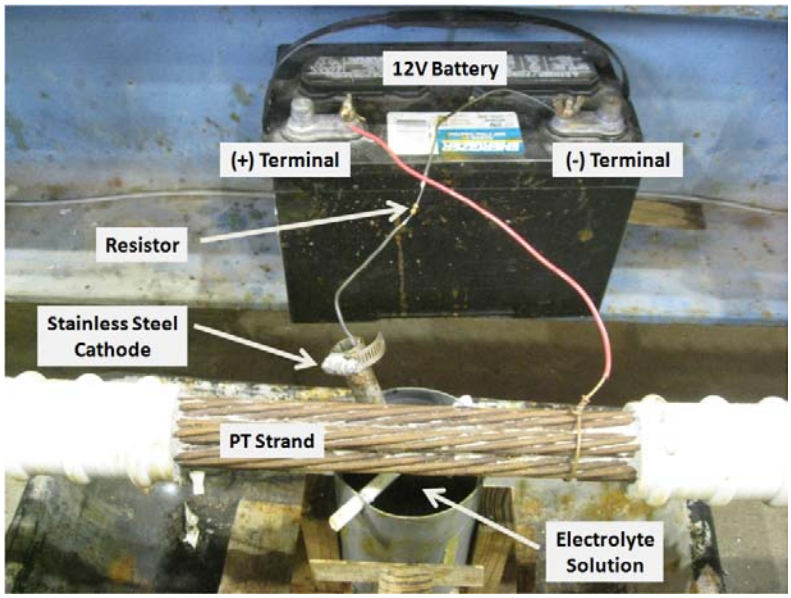

(a) View 1

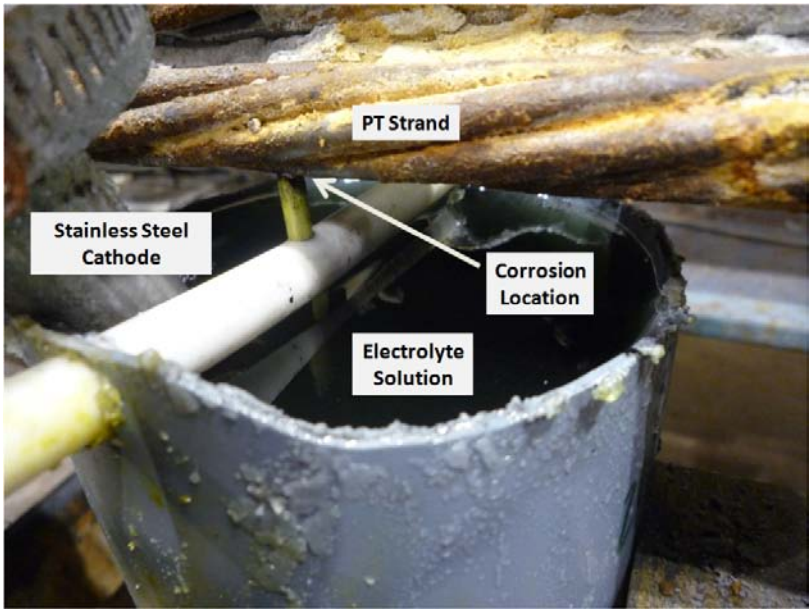

(b) View 2

Figure 3.16: Corrosion Cell

After several preliminary tests, it was determined that the most effective method to corrode the specimen was to position the wick such that it was in contact with only one wire in a strand at a time. Because the specimen was under tension, an individual wire would fracture once enough wire area had been corroded that the tensile stress exceeded the strength of the wire. Figure 3.17 shows a strand at various stages along the corrosion process.

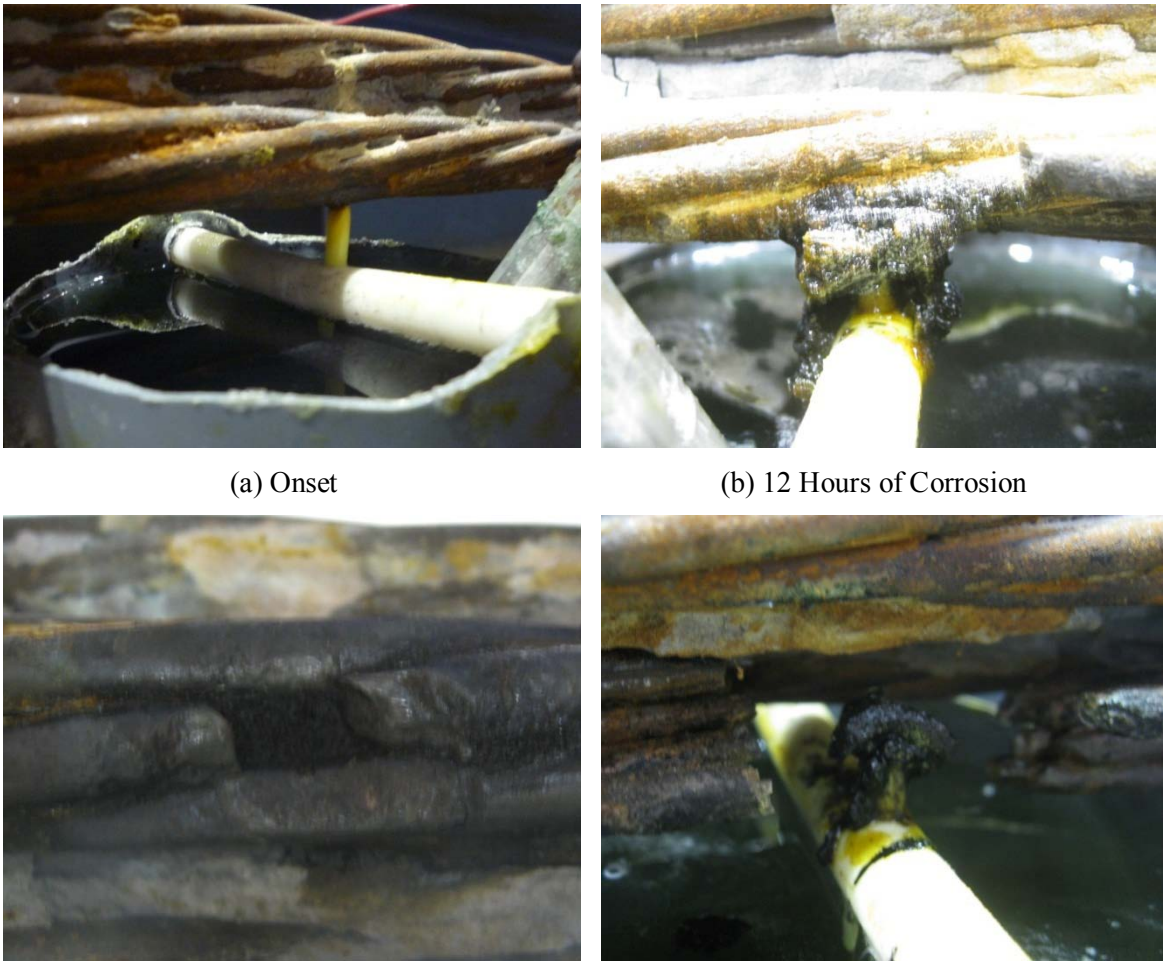

(a) Onset (b) 12 Hours of Corrosion

(c) Wire Fracture (d) Complete Strand Fracture

Figure 3.17: Accelerated Corrosion (Specimen 4)

The time to corrode a wire was largely dependent on the amount of prestress in each wire. On average, it took approximately 24 hours to corrode a wire of the specimens

stressed to 40% GUTS. For the specimens stressed to 70% GUTS, it took approximately 18 hours.

3.4 INSTRUMENTATION FOR LONG-TERM MONITORING

The tensile strains in each strand and the total tensile force in the specimen were monitored throughout the accelerated corrosion tests. Readings were taken once every five minutes in order to capture changes that occurred due to wire fractures.

3.4.1 Strain Gages

In order to monitor the distribution of stress among the different strands in a tendon, strain gages were attached to every strand. Type FLA 6-11 strain gages were used.

The process of installing the strain gages is summarized below:

1. Clean strands with sandpaper, acid solution, and base solution. (Figure 3.18a)
2. Bond strain gage to strand with cyanoacrylate adhesive glue (Figure 3.18b)
3. Apply water-proofing and coating tape (Figure 3.18c)
4. Zip-tie wire to provide stress relief
5. Apply final water-proofing (Figure 3.18d)

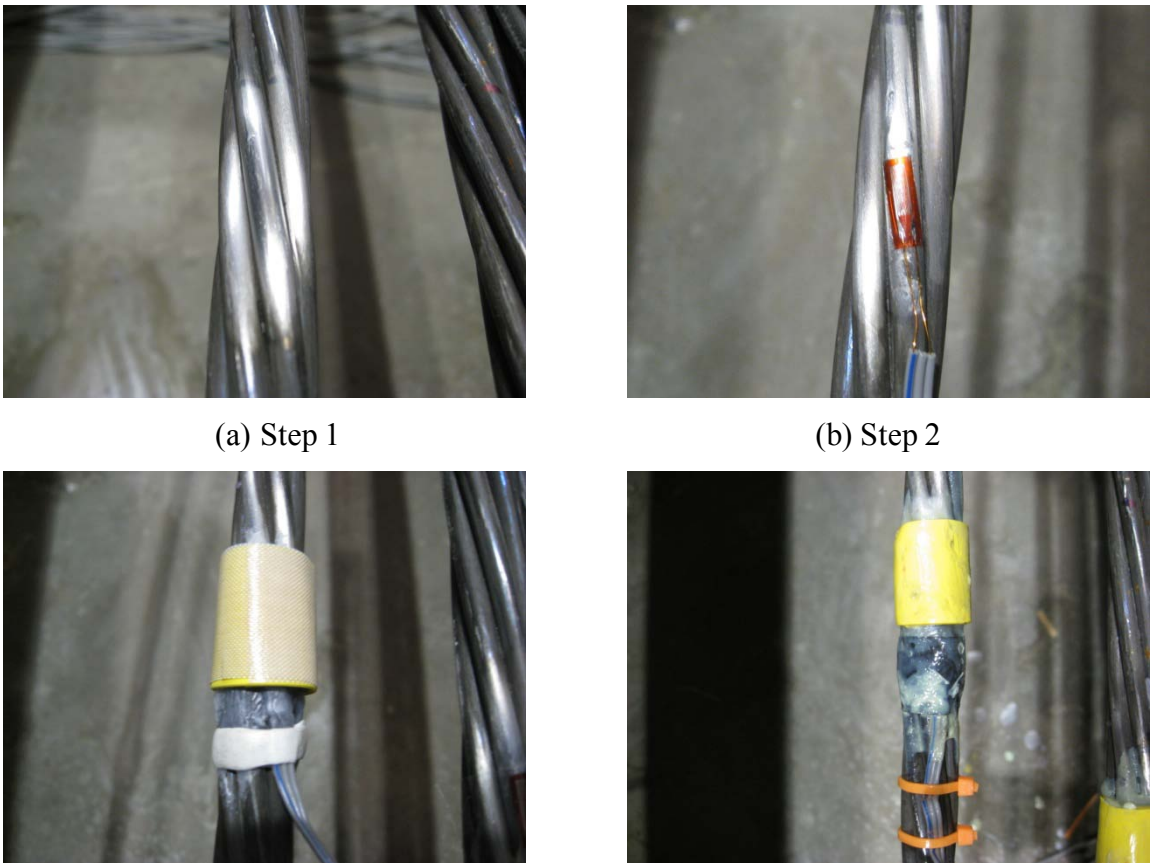

(a) Step 1 (b) Step 2

(c) Step 3 (d) Step 5

Figure 3.18: Strain Gage Process

For Specimens 2 and 3, two strain gages were attached to each strand at the south end of the specimen, for a total of fourteen gages. The two strain gages were placed on different wires within a strand, approximately one foot apart. The strain gages proved to be a reliable method for monitoring changes in the stress levels in each strand as wire breaks accumulated.

For Specimens 4 and 5, additional strain gages were used. A total of twenty-eight gages were attached to these two specimens. The additional gages were intended to monitor how the load redistributed among the strands at different distances from the corrosion location. However, for the specimens stressed to 70% GUTS, the strain gages proved to be unreliable.

3.4.2 Load Cell

Each load cell had a 3 ¼-in. diameter hole, which was large enough for the duct to pass through. The 500-kip load cell was positioned at the south end of each specimen and provided a stable measure of the variation in tension force throughout the life of the specimen.

3.5 INSTRUMENTATION FOR DYNAMIC TESTS

After each wire break, dynamic tests were conducted to measure the natural frequencies of the specimen. An impact hammer was used to induce vibrations, and four accelerometers measured the response along the length of the specimen.

3.5.1.1 Accelerometers

Four accelerometers manufactured by Crossbow were placed along the length of the specimen. The accelerometers were one-dimensional, only having the capacity to pick up motion in one direction.

3.5.1.2 Impact Hammer

An impact force hammer manufactured by PCB Piezotronics was used to excite the specimens.

3.6 DISASSEMBLY

When the residual prestress force dropped below 60% of the initial prestress, testing was discontinued. At this point, the specimen could be disassembled. Using a circular saw, the strands were slowly cut at one location of the specimen, as shown in Figure 3.19. Multiple cross-sectional cuts along the length of the specimen were made, each showing no evidence of grout voids.

Figure 3.19: Cutting Specimen

Disassembling the specimens allowed for the grout caps to be removed, which exposed the anchor heads. This gave a good idea of how well the specimen was grouted. Figure 3.20 shows both anchor heads of Specimen #3. The north end anchor was located where the grout was pumped into the specimen. The north end filled with grout while the south end only partially filled up with grout. Grout began to escape from the south vent before the south cap could fill completely.

(a) North Anchor (b) South Anchor

Figure 3.20: Specimen 3 – Anchor Heads After Grout Cap Removal

CHAPTER 4

Measured Response

The primary objective of this section is to present the measured response of the test specimens. In Section 4.1, the order of damage by means of accelerated corrosion is detailed for each specimen. The method for measuring the natural frequencies of the external tendons is presented in Section 4.2. The classification and occurrence of multiple peaks in the measured frequency response of the tendons is discussed in Section 4.3. The observed variation in tension and frequency with increasing damage is detailed in Section 4.4 and Section 4.5, respectively. The effect of the accumulation of damage on the natural frequency and tension force is summarized in Section 0. The observed stress redistribution behavior of the specimens is discussed in Section 4.7.

4.1 ACCELERATED CORROSION TESTS

Five external post-tensioned tendon specimens were constructed and damaged by means of accelerated corrosion. Due to a construction error, the first specimen was not stressed properly. Therefore, this test was terminated before appreciable damage occurred and no results are reported. Two specimens were stressed to approximately 40% GUTS (guaranteed ultimate tensile strength) and designated as Specimens 2 and 3. The primary difference between the test specimens was the type of anchorage block. Specimens 4 and 5 were stressed to 70% GUTS. Table 4.1 provides a summary of the specimens.

Table 4.1: Summary of Test Specimens

Specimen	Anchor Block	Initiation of Corrosion	Conclusion of Corrosion	Number of Strands Corroded
1	Concrete	8/6/2009	-	-
2	Steel	8/13/2009	10/6/2009	5
3	Concrete	9/10/2009	11/2/2009	4
4	Steel	10/26/2009	12/13/2009	5
5	Concrete	11/16/2009	12/15/2009	5

For each specimen, the accelerated corrosion tests were run continuously. After a wire had fractured, the test was interrupted and a vibration test was performed on the specimen. The corrosion cell apparatus was moved to allow the tendon to freely vibrate. At the conclusion of the vibration test, the corrosion test proceeded.

Due to geometry constraints of the accelerated corrosion test, the wires of a strand could only be corroded on the underside of the tendon. Once all seven wires in the bottom two strands had fractured, the strands were cut a few inches from fracture in order to gain access to the middle layer of strands. The grout between the middle and bottom layers was also removed. Shims were placed under the corrosion cell such that the wick was in contact with the strand, and the corrosion test continued. The location of damage in the specimens with steel anchor blocks is shown in Figure 4.1, while Figure 4.3 shows the location for the specimens with concrete anchor blocks. The order in which the strands were corroded in each specimen is shown in Figure 4.2 for Specimens 2 and 4 and in Figure 4.4 for Specimens 3 and 5.

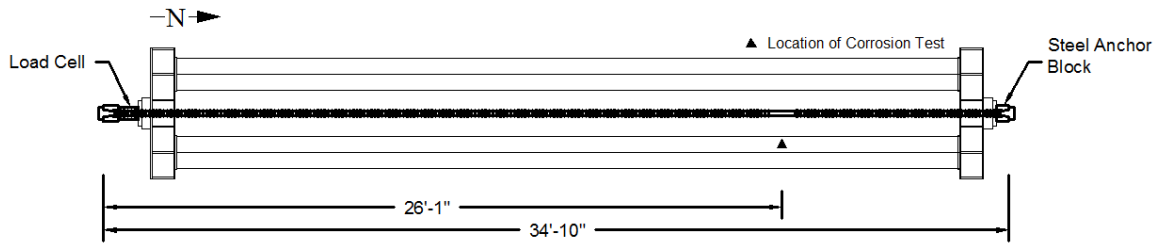

Figure 4.1: Location of Corrosion Damage for Specimens with Steel Anchor Blocks

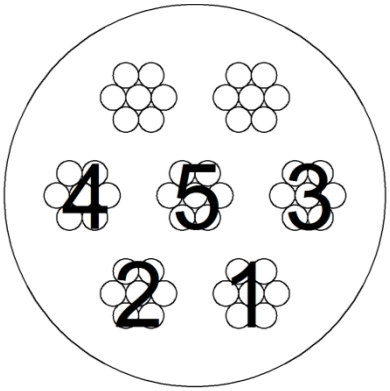

Figure 4.2: Order of Strands Subjected to Corrosion Damage for Specimens 2 and 4 (looking south)

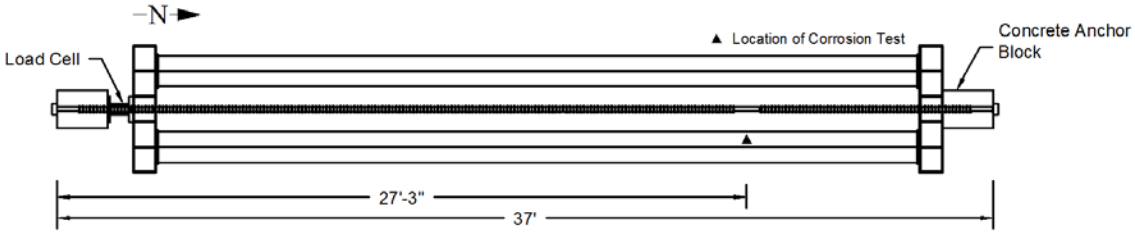

Figure 4.3: Location of Damage for Specimens with Concrete Anchor Blocks

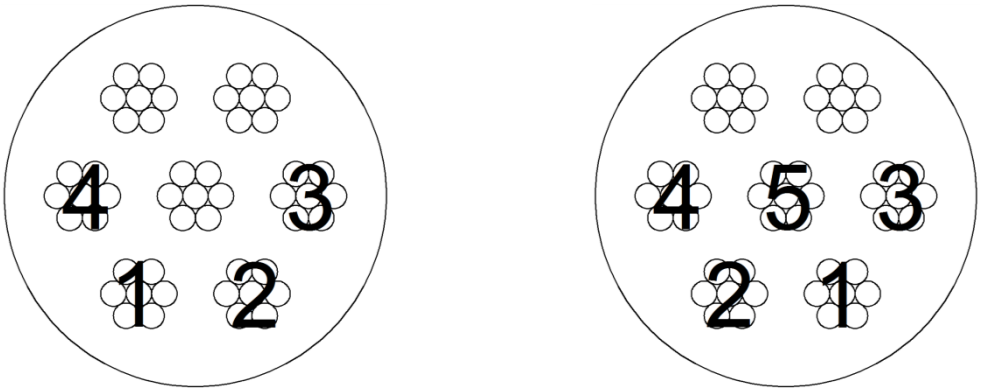

(a) Specimen 3 (b) Specimen 5

Figure 4.4: Order of Strands Subjected to Corrosion Damage for Specimens 3 and 5 (looking south)

4.2 MEASURED NATURAL FREQUENCY

Free vibrations were induced in the test specimens using an impact hammer (Figure 4.5). The acceleration response was measured at several locations along the specimen.

Figure 4.5: Vibration Test

Data from the impact hammer and accelerometers were captured at 2000 Hz during each free-vibration test. A triggered acquisition mode was used such that 20 seconds of data were recorded, with 0.5 seconds before the impact.

For most tests, accelerometers recorded the vertical motions of the test specimens. As discussed in Section 4.2.2, both horizontal and vertical accelerations were recorded for some tests of Specimens 4 and 5.

4.2.1 Standard Approach

Four accelerometers were placed symmetrically along the length of the test specimens (Figure 4.6). The accelerometers for the specimens with concrete anchors were at a distance L/6 and L/3.5 from each end, where L is the overall length of the specimens. For the specimens with steel anchors, the accelerometers were at a distance L/5.2 and L/3.2 from each end.

Twelve dynamic tests were performed after each wire break. The top surface of the specimens was struck adjacent to each accelerometer three times (Table 4.2).

Table 4.2: Summary of Standard Vibration Tests

Test	Location of Hit	Orientation of Acc at Hit Location	Direction of Hit
1 - 3	acc 0 / acc 4	Vertical	Vertical
4 - 6	acc 1 / acc 5	Vertical	Vertical
7 - 9	acc 2 / acc 6	Vertical	Vertical
10 - 12	acc 3 / acc 7	Vertical	Vertical

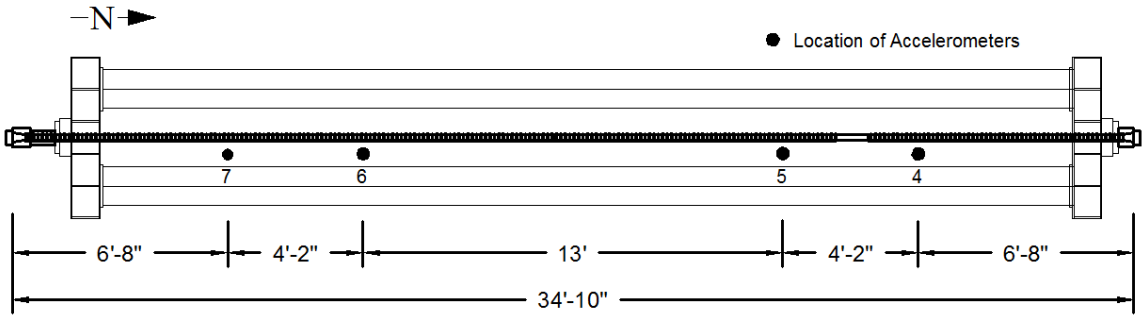

(a) Steel Anchor Specimens

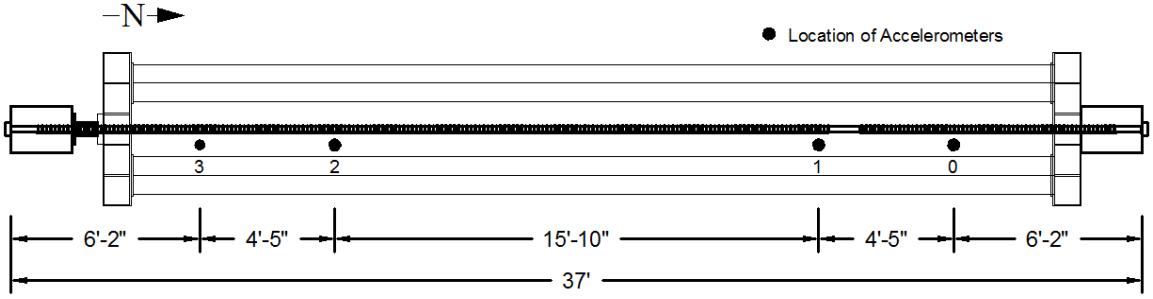

(b) Concrete Anchor Specimens

Figure 4.6: Location of Accelerometers

The response of the four accelerometers for a dynamic test on Specimen 2 is shown in Figure 4.7. The data acquisition system used the Fast Fourier Transform (FFT) algorithm to compute the frequency spectra shown in Figure 4.8. The plot in the frequency domain indicates that each of the accelerometers exhibited the same frequency response, regardless of location along the specimen. This gives adequate confirmation that there is no local variation in the measured natural frequencies of the accelerometers at varying lengths along the specimen.

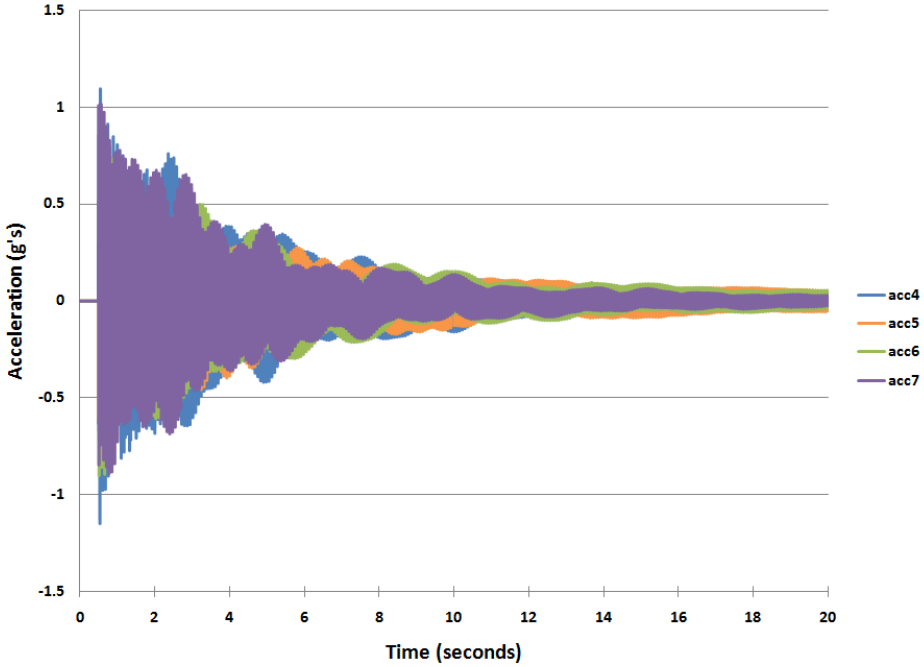

Figure 4.7: Vibration Test – Time Domain

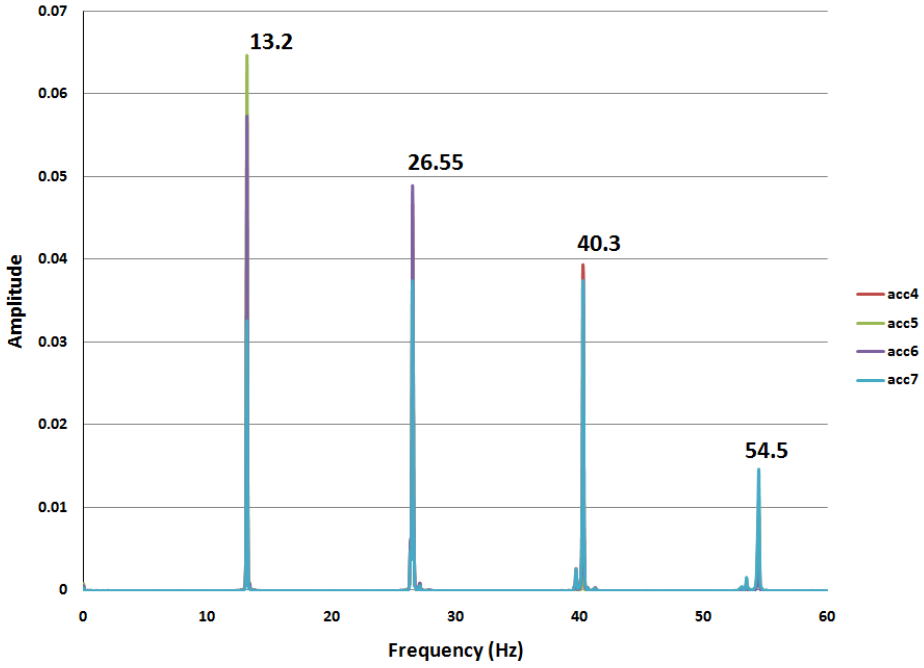

Figure 4.8: Vibration Test – Frequency Domain

4.2.2 Modified Approach

The vibration technique was modified during the tests of Specimens 4 and 5 to further investigate the effect of the flexural stiffness on the natural frequency. The following section describes the changes made in the vibration technique.

In an ideal environment, the cross section of the strands in a tendon would be symmetrical about the horizontal and vertical longitudinal axis. After Specimens 2 and 3 were disassembled, it was observed that the strands (Figure 4.9) were not symmetrically placed within the cross section. As a result, the flexural stiffness may not be the same in the horizontal and vertical directions.

Figure 4.9: Tendon Cross Section - Specimen 3 (near south anchor end)

In order to understand the influence of the flexural stiffness on the measured natural frequencies, the orientation of two of the accelerometers were rotated. For Specimen 4, accelerometers 1 and 3 were oriented horizontally (Figure 4.10). For Specimen 5, accelerometers 5 and 7 were rotated in the same fashion.

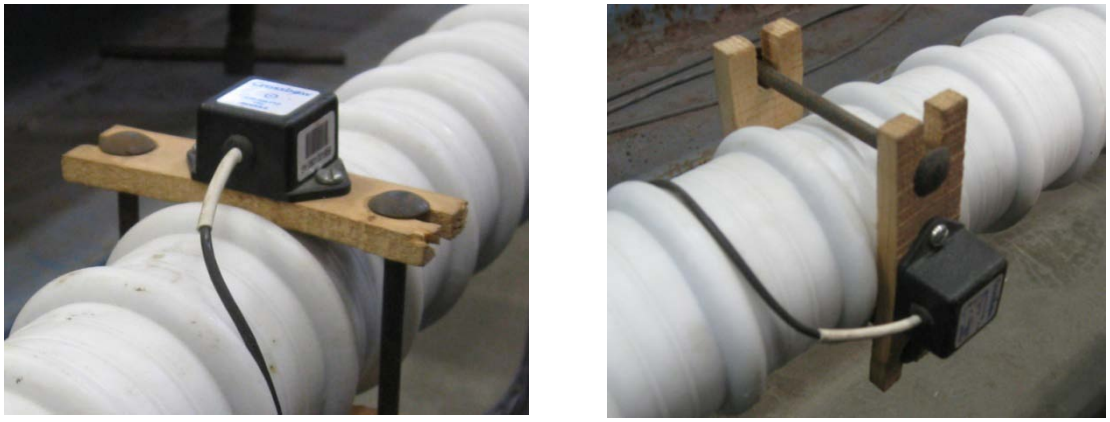

(a) Vertical (b) Horizontal

Figure 4.10: Orientation of Accelerometers

The modified plan for the free-vibration tests for Specimens 4 and 5 is summarized in Table 4.3.

Table 4.3: Summary of Modified Vibration Tests

Test	Location of Hit	Orientation of Acc at Hit Location	Direction of Hit
1 - 3	acc 0 / acc 4	Vertical	Vertical
4 - 6	acc 1 / acc 5	Horizontal	Horizontal
7 - 9	acc 2 / acc 6	Vertical	Vertical
10 - 12	acc 3 / acc 7	Horizontal	Horizontal

The frequency response of Specimen 5 when excited vertically is shown in Figure 4.11a and when excited horizontally is shown in Figure 4.11b. The frequencies are slightly different for the first, second, and third modes of vibration. For the fourth mode of vibration, two peaks may be observed in both plots, but the relative amplitude of the peaks is reversed. The presence of multiple peaks is addressed in the next section.

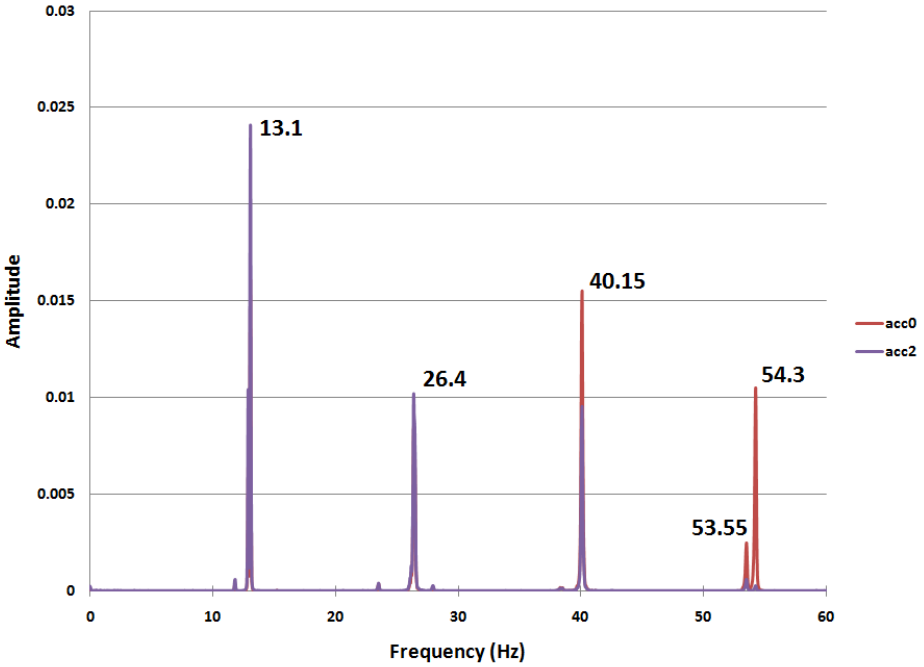

(a) Vertical Excitation

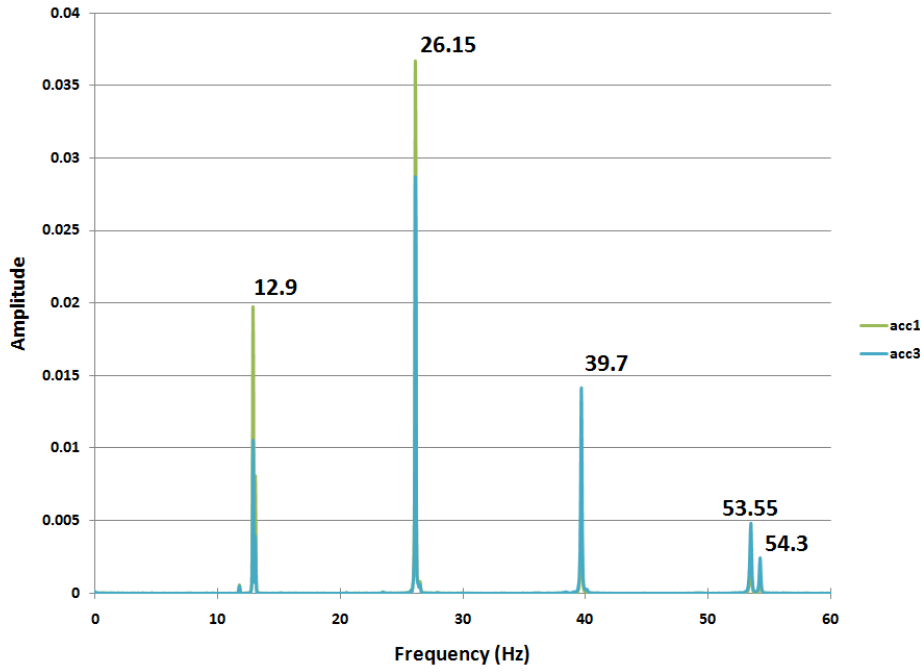

(b) Horizontal Excitation

Figure 4.11: Frequency Response – Specimen 5

Because the length, tension, and mass per unit length are the same for both tests, the only difference is the flexural stiffness in the two directions. The higher measured natural frequencies in the vertical direction imply that the moment of inertia is slightly larger in the vertical direction than the horizontal direction.

4.3 MULTIPLE PEAKS

Previous work by Lee (2007) at the University of Texas and Sagues (2006) at the University of South Florida indicated the presence of dual peaks in the frequency spectrum. In the scope of this research, a dual peak is classified as two distinct peaks formed for a given mode of vibration where the lower-amplitude peak is at least 50% of the higher-amplitude peak.

While multiple peaks were common in the tests conducted by Lee and Sagues, that was not the case in this investigation. One possible explanation is that the tendons in this investigation were much smaller than the twelve and nineteen-strand specimens tested by Lee and Sagues, respectively. The observed variations in the strand patterns along the length of the specimens in this investigation were considerably less than those reported by Lee and Sagues. Therefore, detecting fewer cases of multiple peaks is not unexpected.

A total of 1596 free-vibration tests were conducted during this investigation. Of these, only 180 tests were classified as having multiple peaks (Table 4.4).

Table 4.4: Observed Occurrences of Multiple Peaks (all specimens)

Wire Break	Mode 1	Mode 2	Mode 3	Mode 4
0 - 7	0	18	30	6
8 - 14	0	0	51	0
15 - 21	0	3	21	0
22 - 28	0	3	12	24
29 - 35	6	6	0	0

The third mode experienced the greatest number of multiple peaks - 114 of the 180 cases. The first mode had the least amount of multiple peaks with only 6. The second and fourth mode both had a total of 30 multiple peaks for the four specimens. The level of

damage did not seem to influence the number of multiple peaks, but very few multiple peaks were observed when more than four strands had been corroded.

4.4 OBSERVED VARIATION OF FREQUENCY WITH INCREASING DAMAGE

The following section summarizes the variation in the natural frequencies as damage accumulated in each specimen. The four measured natural frequencies are plotted against the accumulation of wire breaks in Figure 4.12 for all four test specimens. In a few instances, multiple wire breaks occurred in a very short amount of time, which prevented dynamic tests to be performed after every wire break. This is noted by absent data points at a given level of damage, and was much more prominent in the higher stressed specimens due to the much shorter time to corrode a wire. It should be noted that wire break 32 of Specimen 2 and wire break 9 and 10 of Specimen 4 did not produce a noticeable peak for the fourth mode.

The four specimens exhibited similar trends in the natural frequencies as damage accumulated. The higher modes were slightly more sensitive to damage than the lower modes. The rate of change in the measured natural frequencies also tended to increase as the level of damage increased.

The normalized fundamental frequency response of all four specimens is compared in Figure 4.13. The fundamental frequencies for Specimens 4 and 5 were slightly more sensitive to damage than for Specimens 2 and 3, but the differences were not significant. A 20% reduction in fundamental frequency corresponds to a 60% reduction in cross-sectional area for Specimens 2 and 3, and a 50% reduction in cross-sectional area for Specimens 4 and 5.

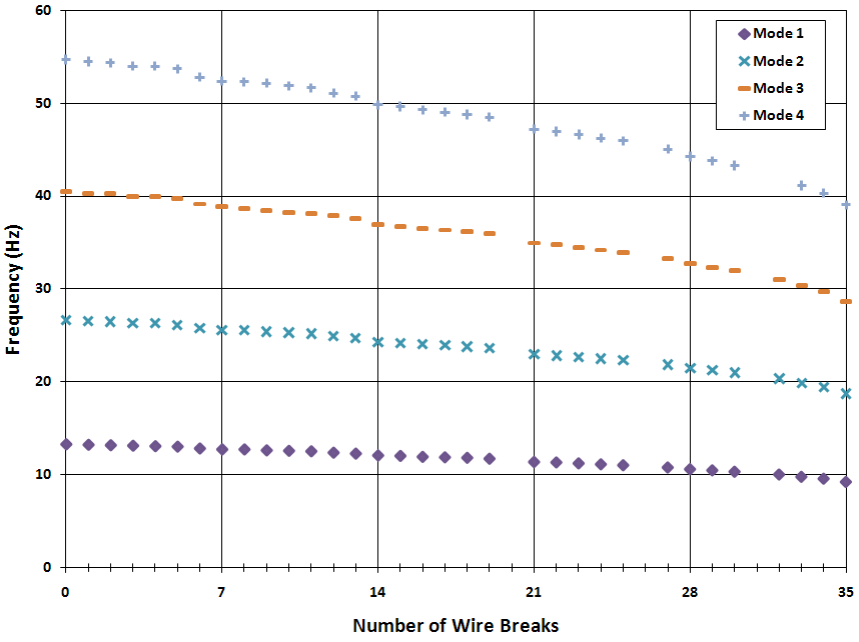

(a) Specimen 2

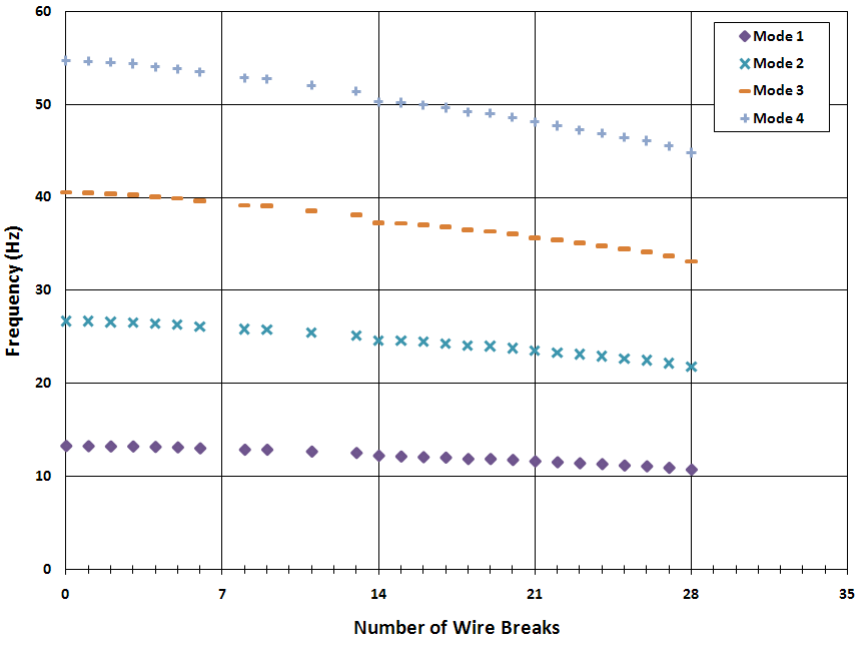

(b) Specimen 3

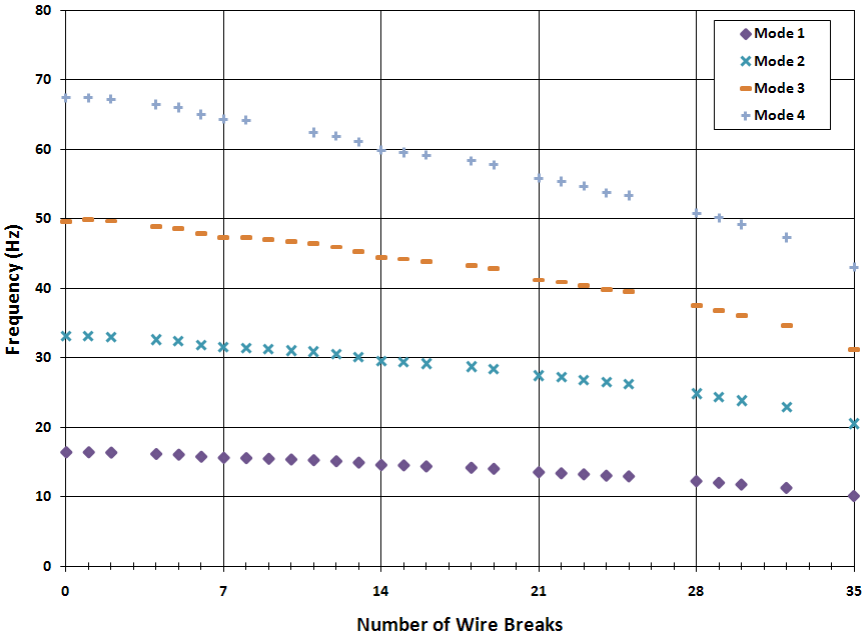

(c) Specimen 4

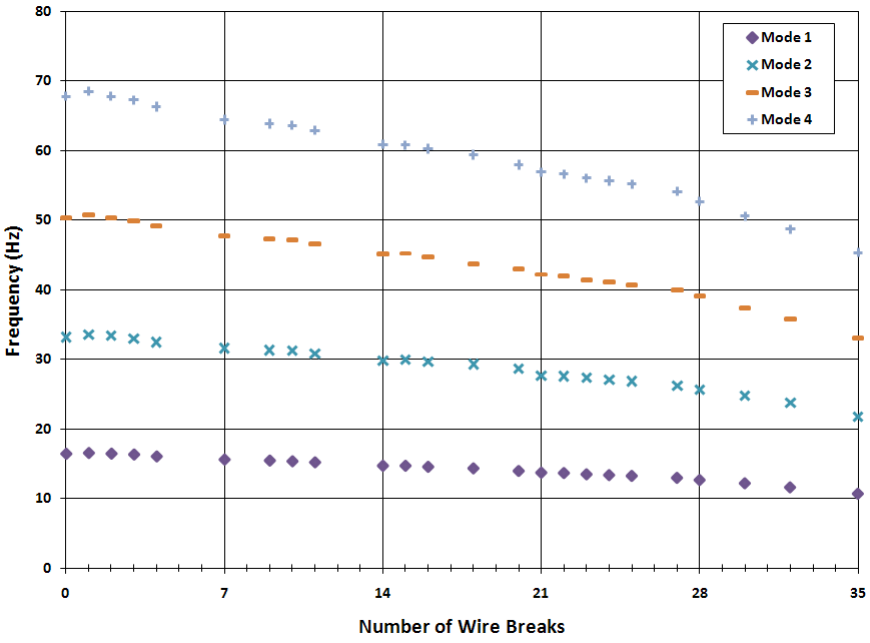

(d) Specimen 5

Figure 4.12: Frequency versus Wire Breaks (all specimens)

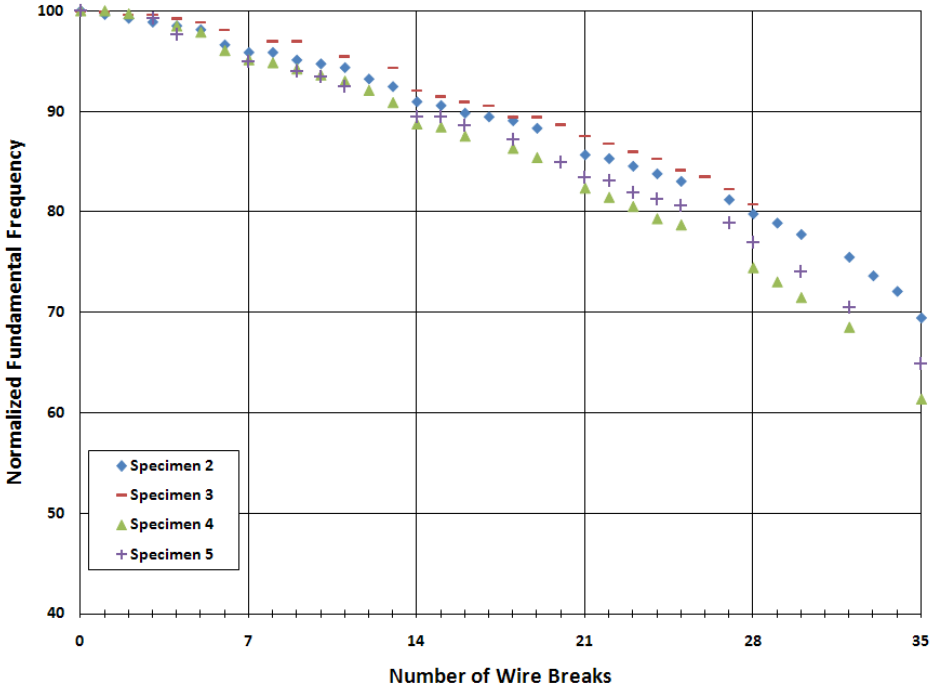

Figure 4.13: Variation of Fundamental Frequencies with Level of Damage

4.5 OBSERVED VARIATION OF TENSION WITH INCREASING DAMAGE

The load cell provided a direct measure of the tensile force in each specimen as damage increased. The initial level of tension of the specimens is summarized in Table 4.5.

Table 4.5: Summary of Initial Tension Force per Specimen

Specimen ID	Initial Tension Force (kips)	% of GUTS
2	174.2	42
3	174.8	43
4	279.2	68
5	275.2	67

The ability to measure the tension force accurately was a key aspect of the investigation. The tension force was not measured in previous investigations at the University of Texas (Lee, 2007, Wood et al, 2008).

To provide a basis for comparison, each plot of measured response also includes a line that corresponds to a linear reduction in tensile force with each wire break. This idealization corresponds to the case of zero redistribution of stress within the tendon. As will be discussed, significant stress redistribution was observed.

4.5.1 Specimens 2 and 3

The measured variations in tensile force with increasing damage are plotted in Figure 4.14 for Specimens 2 and 3. After each wire break, the tensile force in the tendon decreased. However, at all damage levels, the residual force in the specimens exceeded the idealized response corresponding to zero stress redistribution. As the number of intact wires became less than the number of fractured wires, the loss of tensile force with each wire break became larger. The loss of tension force with each wire break is summarized in Table 4.6 and Table 4.7, and plotted in Figure 4.15 and Figure 4.16.

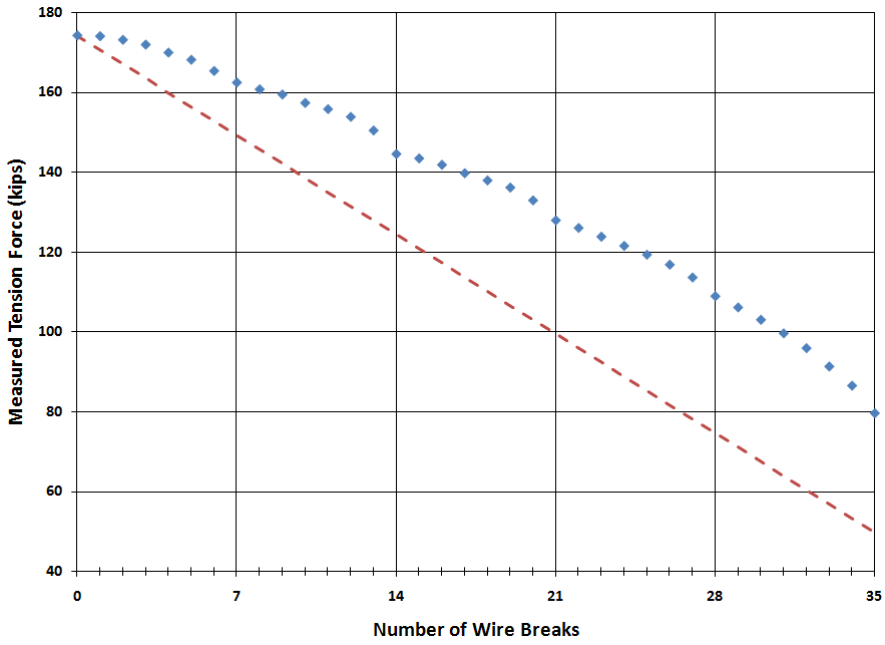

(a) Specimen 2

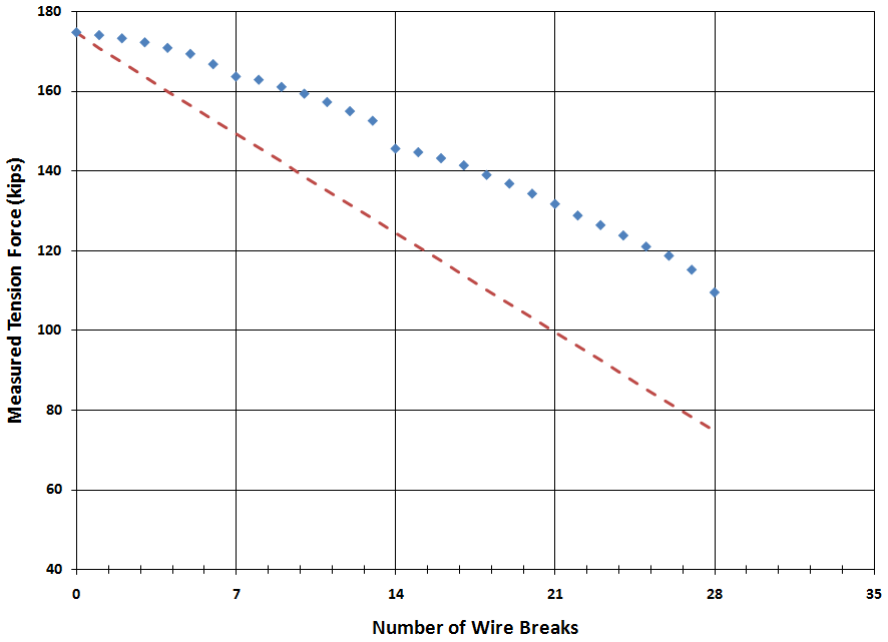

(b) Specimen 3

Figure 4.14: Observed Variation of Tensile Force with Number of Wire Breaks (Specimens Stressed to 40% GUTS)

Table 4.6: Summary of Tension Loss per Wire Break - Specimen 2

Strand 1		Strand 2		Strand 3		Strand 4		Strand 5	
Wire Break	**ΔT (kips)**	**Wire Break**	**ΔT (kips)**	**Wire Break**	**ΔT (kips)**	**Wire Break**	**ΔT (kips)**	**Wire Break**	**ΔT (kips)**
1	0.2	8	1.7	15	1.1	22	1.9	29	2.8
2	0.9	9	1.3	16	1.6	23	2.2	30	3.1
3	1.2	10	2.1	17	2.1	24	2.3	31	3.4
4	2.0	11	1.6	18	1.8	25	2.2	32	3.7
5	1.8	12	1.9	19	1.8	26	2.5	33	4.6
6	2.8	13	3.4	20	3.2	27	3.2	34	4.8
7	2.9	14	5.9	21	5.0	28	4.7	35	6.9
Total ΔT (kips)	11.8	**Total ΔT (kips)**	17.9	**Total ΔT (kips)**	16.6	**Total ΔT (kips)**	19	**Total ΔT (kips)**	29.3
Residual Tension (kips)	162.4	**Residual Tension (kips)**	144.5	**Residual Tension (kips)**	127.9	**Residual Tension (kips)**	108.9	**Residual Tension (kips)**	79.6
Residual Tension (%)	93.2	**Residual Tension (%)**	83.0	**Residual Tension (%)**	73.4	**Residual Tension (%)**	62.5	**Residual Tension (%)**	45.7

Table 4.7: Summary of Tension Loss per Wire Break - Specimen 3

Strand 1		Strand 2		Strand 3		Strand 4	
Wire Break	**ΔT (kips)**	**Wire Break**	**ΔT (kips)**	**Wire Break**	**ΔT (kips)**	**Wire Break**	**ΔT (kips)**
1	0.7	8	0.8	15	0.9	22	2.9
2	0.8	9	1.8	16	1.5	23	2.4
3	1.0	10	1.7	17	1.8	24	2.6
4	1.4	11	2.1	18	2.4	25	2.8
5	1.5	12	2.3	19	2.2	26	2.3
6	2.6	13	2.4	20	2.5	27	3.5
7	3.1	14	7.0	21	2.6	28	5.7
Total ΔT (kips)	11.1	**Total ΔT (kips)**	18.1	**Total ΔT (kips)**	13.9	**Total ΔT (kips)**	22.2
Residual Tension (kips)	163.7	**Residual Tension (kips)**	145.6	**Residual Tension (kips)**	131.7	**Residual Tension (kips)**	109.5
Residual Tension (%)	93.6	**Residual Tension (%)**	83.3	**Residual Tension (%)**	75.3	**Residual Tension (%)**	62.6

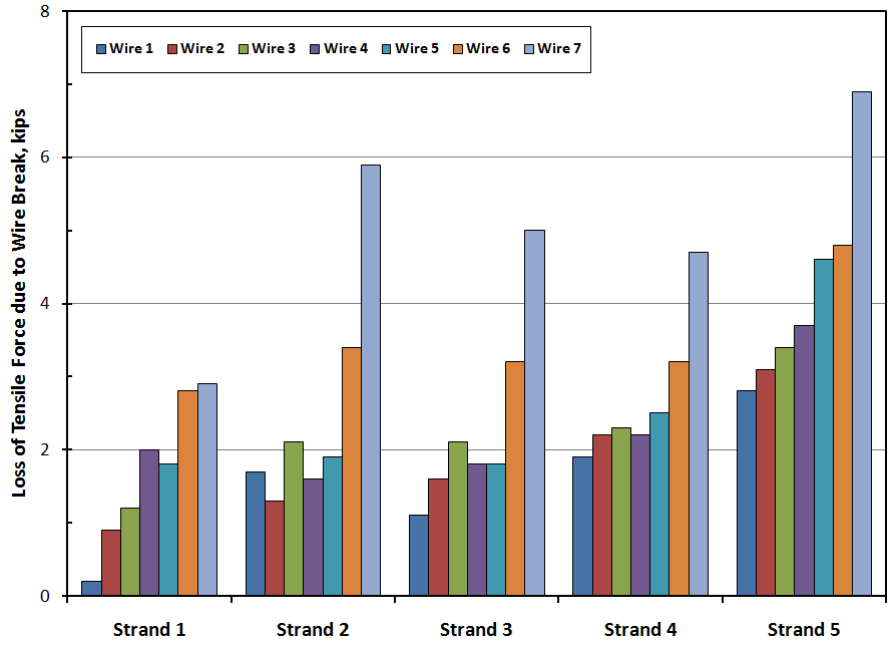

Figure 4.15: Loss of Tensile Force due to Wire Breaks - Specimen 2

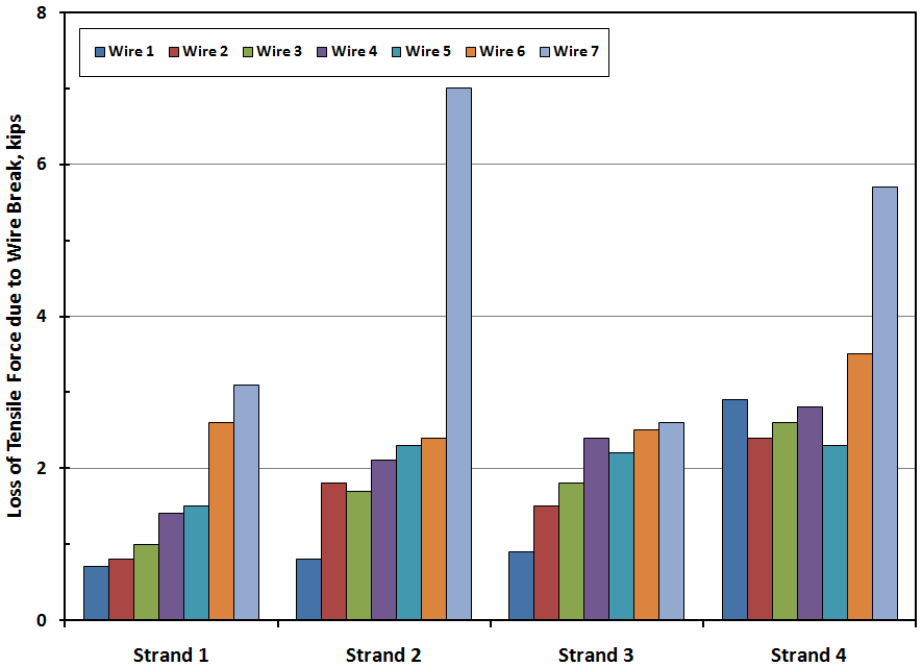

Figure 4.16: Loss of Tensile Force due to Wire Breaks - Specimen 3

4.5.2 Specimens 4 and 5

Specimens 4 and 5 exhibited similar variations in the tensile force as damage accumulated (Figure 4.17). Due to the higher stress levels of Specimen 4 and 5, simultaneous wire breaks occurred numerous times. This is noted by absent data points in Figure 4.17. In these instances, only the total loss in tensile force could be measured.

The differences between the measured and idealized responses were much less for the specimens with higher initial stress than for Specimens 2 and 3 (Figure 4.14). This indicates that the stress in an individual wire cannot be redistributed as efficiently for higher levels of prestress. Force losses due to individual wire breaks are reported in Table 4.8 and Table 4.9 and plotted in Figure 4.18 and Figure 4.19.

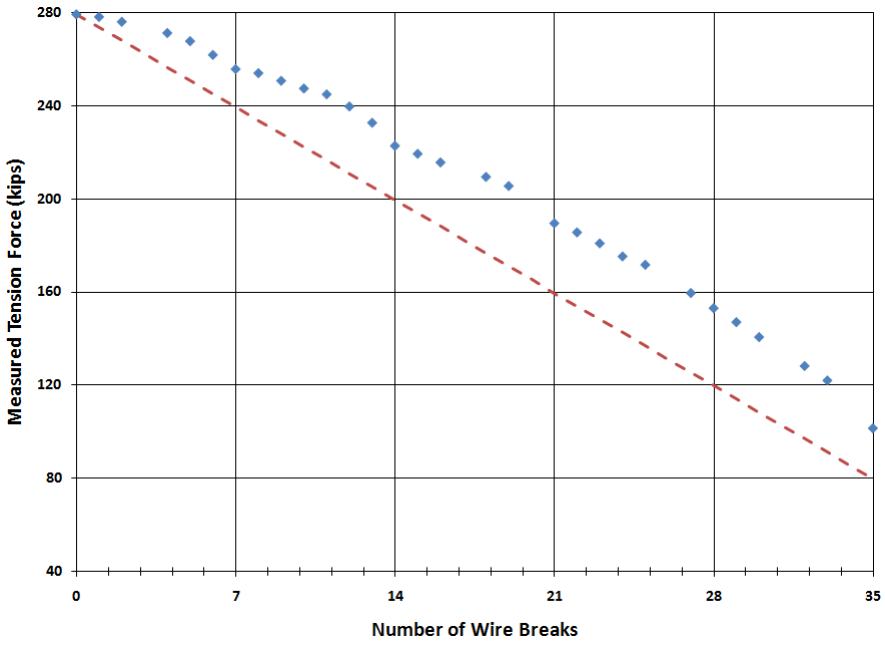

(a) Specimen 4

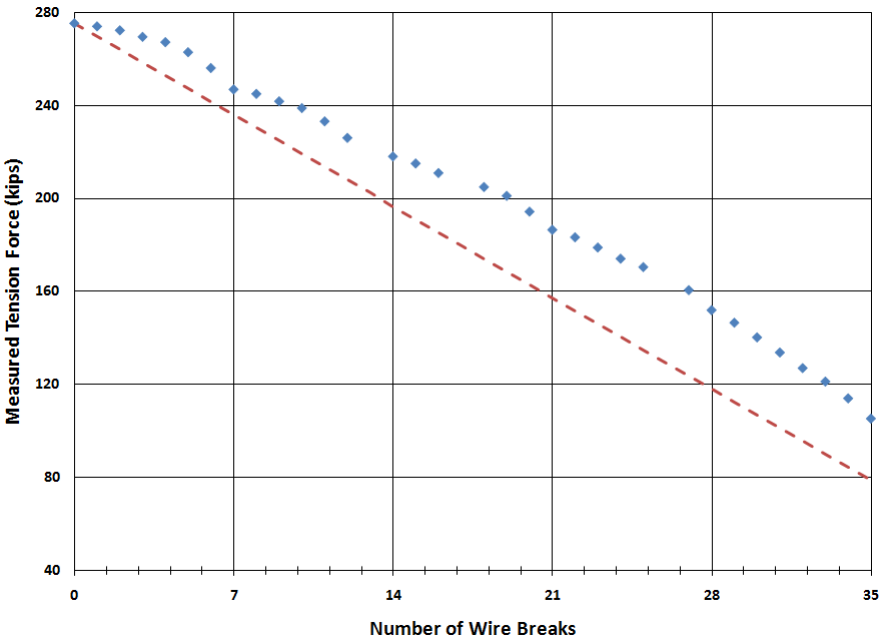

(b) Specimen 5

Figure 4.17: Observed Variation of Tensile Force with Number of Wire Breaks (Specimens Stressed to 70% GUTS)

Table 4.8: Summary of Tension Loss per Wire Break - Specimen 4

Strand 1		Strand 2		Strand 3		Strand 4		Strand 5	
Wire Break	**ΔT (kips)**	**Wire Break**	**ΔT (kips)**	**Wire Break**	**ΔT (kips)**	**Wire Break**	**ΔT (kips)**	**Wire Break**	**ΔT (kips)**
1	1.1	8	1.7	15	3.4	22	3.9	29	6.0
2	2.1	9	3.3	16	3.7	23	4.7	30	6.4
3*	2.4	10	3.3	17*	3.1	24	5.6	31*	6.2
4*	2.4	11	2.5	18*	3.1	25	3.6	32*	6.2
5	3.5	12	5.2	19	3.9	26*	6.1	33	6.2
6	5.9	13	7.0	20*	8.0	27*	6.1	34*	10.3
7	6.1	14	9.9	21*	8.0	28	6.5	35*	10.3
Total ΔT (kips)	23.5	**Total ΔT (kips)**	32.9	**Total ΔT (kips)**	33.2	**Total ΔT (kips)**	36.4	**Total ΔT (kips)**	51.5
Residual Tension (kips)	255.7	**Residual Tension (kips)**	222.8	**Residual Tension (kips)**	189.6	**Residual Tension (kips)**	153.2	**Residual Tension (kips)**	101.7
Residual Tension (%)	91.6	**Residual Tension (%)**	79.8	**Residual Tension (%)**	67.9	**Residual Tension (%)**	54.9	**Residual Tension (%)**	36.4

NOTE: Wire breaks marked with * occurred simultaneously. The total loss in tensile force was evenly distributed between the two breaks.

Table 4.9: Summary of Tension Loss per Wire Break - Specimen 5

Strand 1		Strand 2		Strand 3		Strand 4		Strand 5	
Wire Break	**ΔT (kips)**	**Wire Break**	**ΔT (kips)**	**Wire Break**	**ΔT (kips)**	**Wire Break**	**ΔT (kips)**	**Wire Break**	**ΔT (kips)**
1	1.3	8	1.9	15	3.0	22	3.2	29	5.4
2	1.7	9	3.2	16	4.1	23	4.4	30	6.3
3	2.8	10	2.9	17*	3.0	24	4.8	31	6.5
4	2.3	11	5.7	18*	3.0	25	3.6	32	6.7
5	4.3	12	7.1	19	3.8	26*	5.0	33	5.8
6	6.8	13*	4.0	20	6.8	27*	5.0	34	7.2
7	9.2	14*	4.0	21	7.8	28	8.6	35	8.7
Total ΔT (kips)	28.4	**Total ΔT (kips)**	28.8	**Total ΔT (kips)**	31.5	**Total ΔT (kips)**	34.5	**Total ΔT (kips)**	46.6
Residual Tension (kips)	246.8	**Residual Tension (kips)**	218	**Residual Tension (kips)**	186.5	**Residual Tension (kips)**	152	**Residual Tension (kips)**	105.4
Residual Tension (%)	89.7	**Residual Tension (%)**	79.2	**Residual Tension (%)**	67.8	**Residual Tension (%)**	55.2	**Residual Tension (%)**	38.3

NOTE: Wire breaks marked with * occurred simultaneously. The total loss in tensile force was evenly distributed between the two breaks.

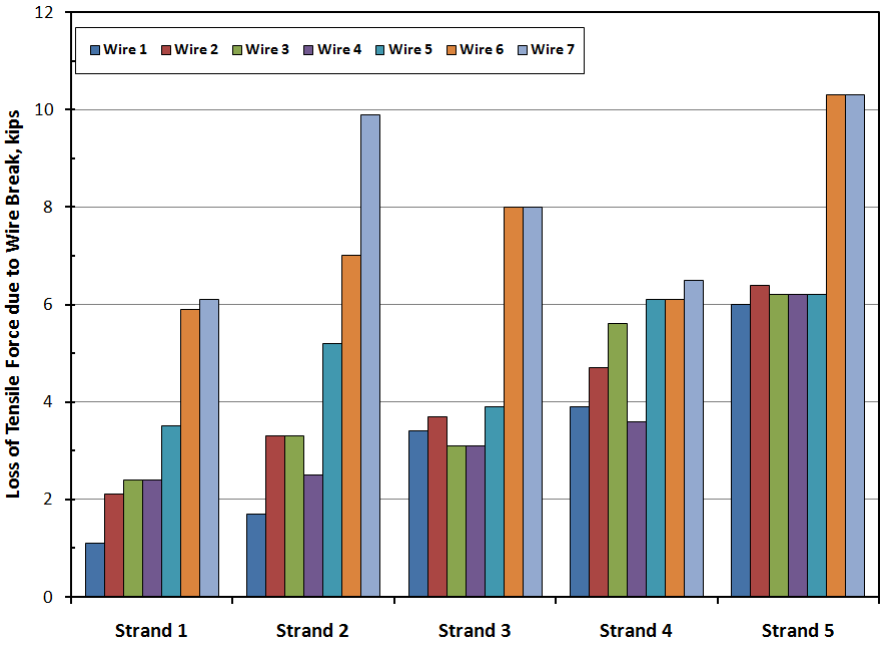

Figure 4.18: Loss of Tensile Force due to Wire Breaks - Specimen 4

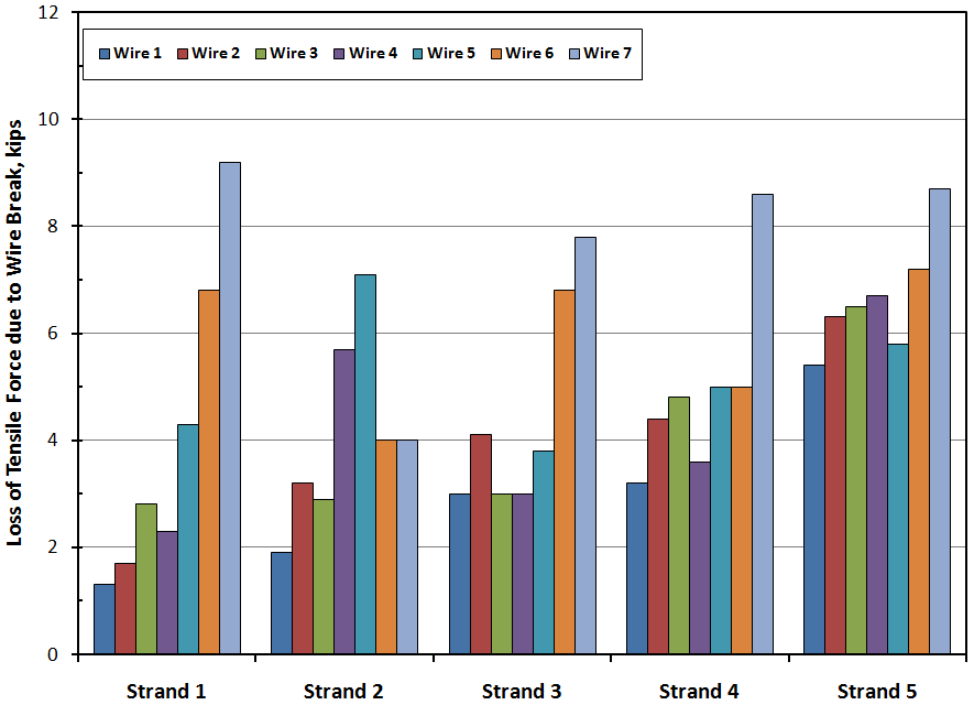

Figure 4.19: Loss of Tensile Force due to Wire Breaks - Specimen 5

4.5.3 Comparisons

The tensile response of all four specimens is compared in Figure 4.20. Similarly to the measured frequency response, the specimens with the higher initial prestress were more sensitive to localized damage. For specimens with an initial prestress of 40% GUTS, a 40% loss in cross-sectional area caused an approximately 25% reduction in tensile force. For specimens with an initial prestress of 70% GUTS, a 40% loss in cross-sectional area caused an approximately 30% loss in tensile force.

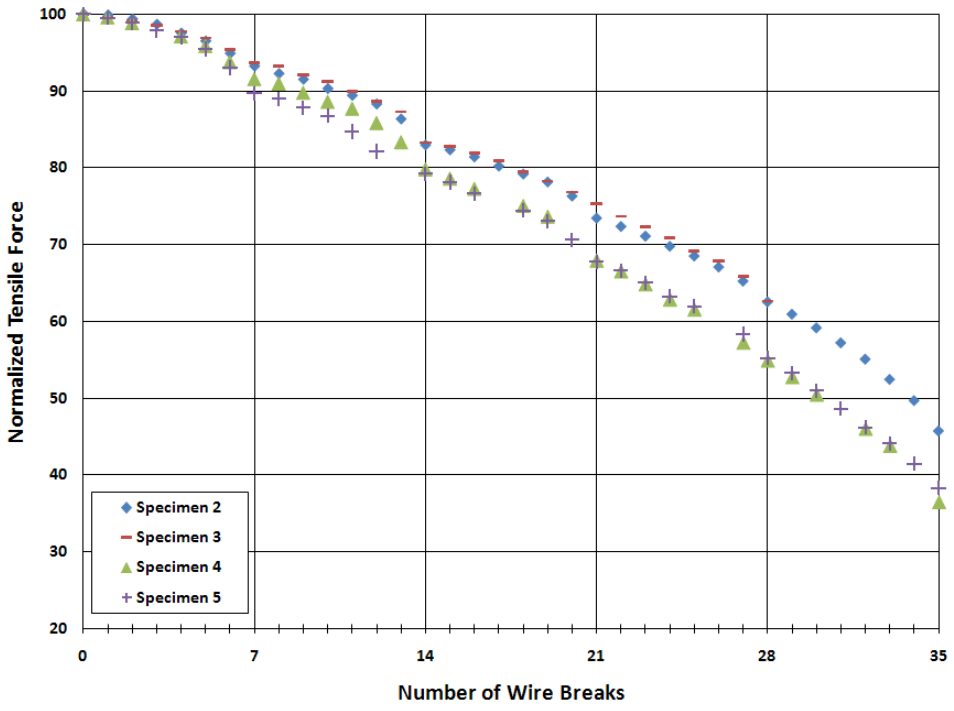

Figure 4.20: Variation of Tensile Force with Level of Damage

4.6 SENSITIVITY OF MEASURED RESPONSE TO LEVEL OF LOCAL DAMAGE

Although slight differences were attributed to the level of initial prestress, all four test specimens responded in a similar manner to increasing levels of localized damage. As shown in Figure 4.21, the variations in tensile force were more sensitive to local damage than the variations in the fundamental frequencies.

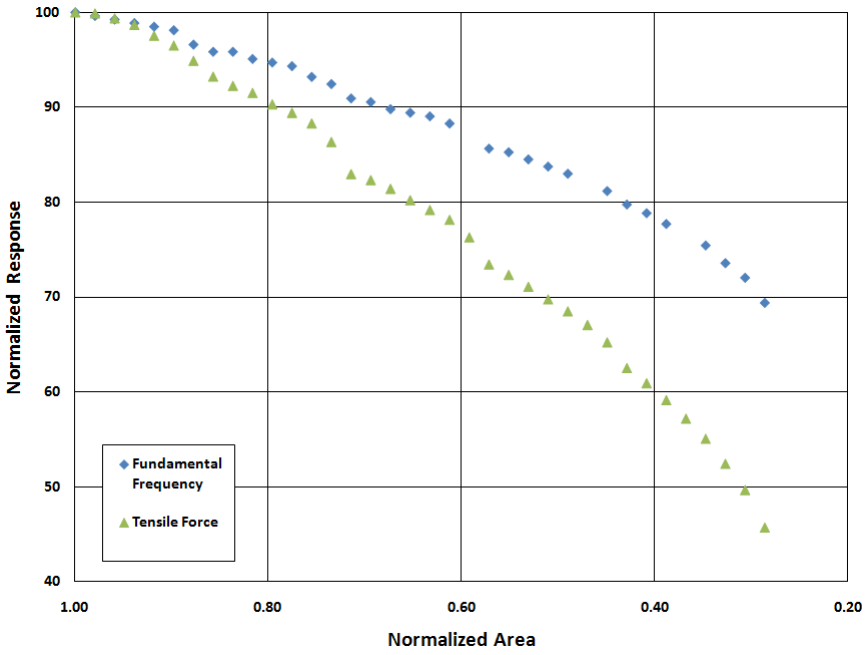

(a) Specimen 2

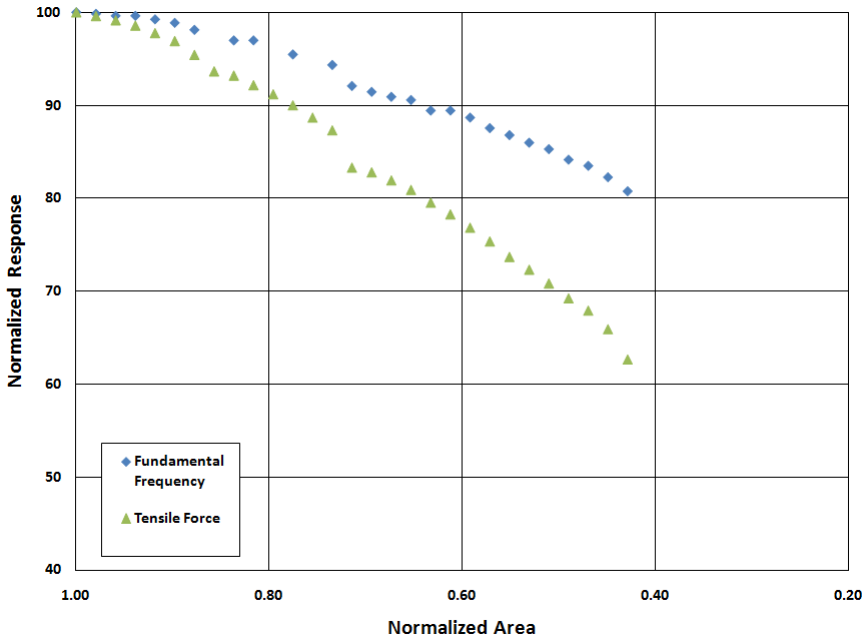

(b) Specimen 3

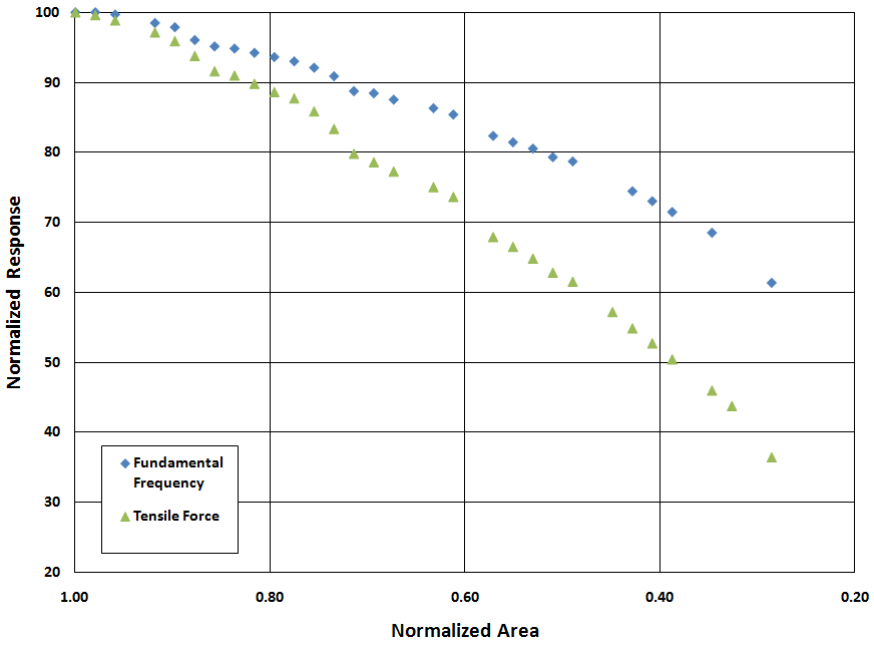

(c) Specimen 4

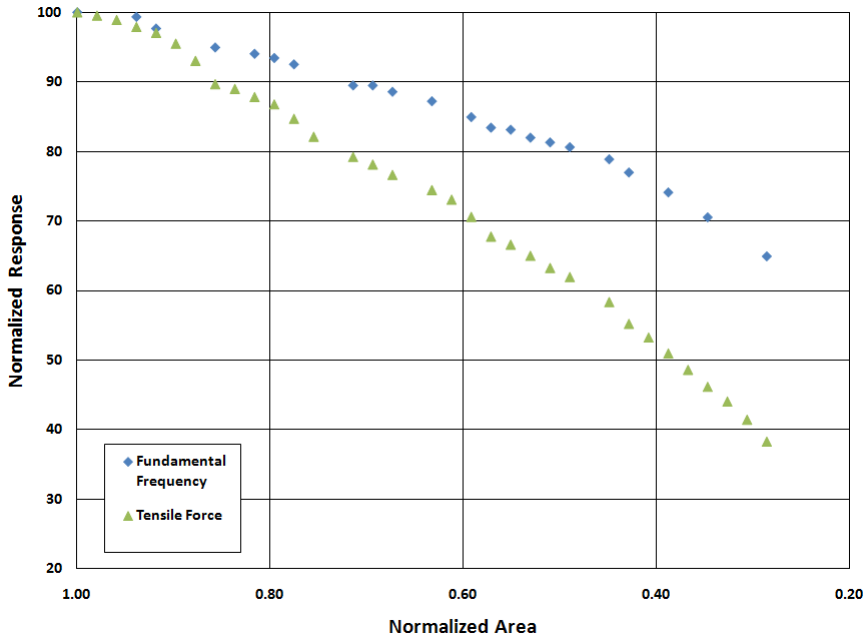

(d) Specimen 5

Figure 4.21: Variation of Fundamental Frequency and Tensile Force to Increasing Levels of Damage (all specimens)

4.7 STRESS REDISTRIBUTION

Strain gages were positioned directly on individual wires of strands in order to monitor the change in strain of each strand as damage accumulated. Because the strands remained elastic during the testing, the strain gage readings could be directly related to tensile force.

The strain gages were attached to the strands before stressing. After stressing, slight variations in the strains of each strand were observed. In order to provide a consistent baseline, all strain gages for a given specimen were set equal to the average measured strain after stressing. Variations from this average reading are reported in this section.

4.7.1 Specimen 2

Fourteen gages (two per strand) were used to monitor the response of Specimen 2. The location of the strain gages are shown in Figure 4.22 and Figure 4.23.

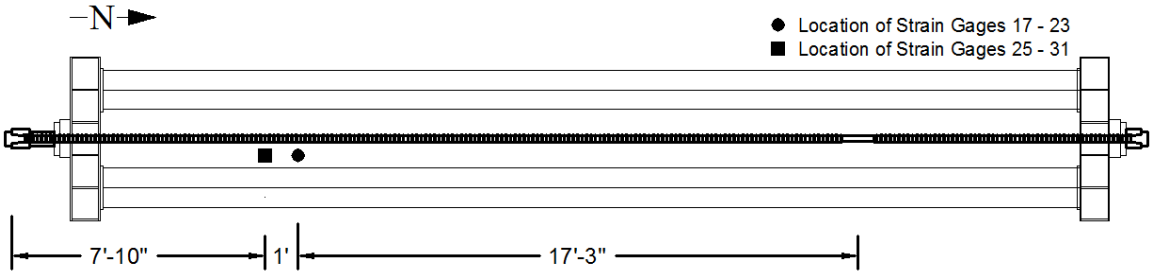

Figure 4.22: Location of Strain Gages - Specimen 2

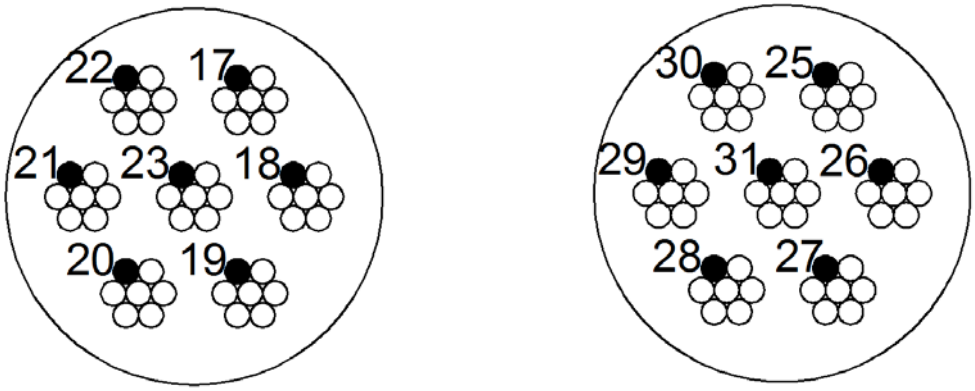

Strain Gages 17 - 23 Strain Gages 25 - 31

Figure 4.23: Location of Individual Strain Gages - Specimen 2 (looking south)

Seven of the fourteen gages provided reliable data during the entire test and are plotted in Figure 4.24. Although the gages were attached to different strands, the trends were similar. The change in strain was nearly the same in all gages after each wire break. As damage accumulated near the north end of the specimen, the strains were nearly uniformly distributed near the south end of the specimen. This indicates that tensile stresses were transferred through the grout and redistributed to other strands following fracture of the seven wires in a given strand. After all seven wires in the bottom two strands were fractured, the strain in these strands (Gages 19 and 28) were less sensitive to change. At the end of the test, these strands appeared to be carrying more load than the other strands.

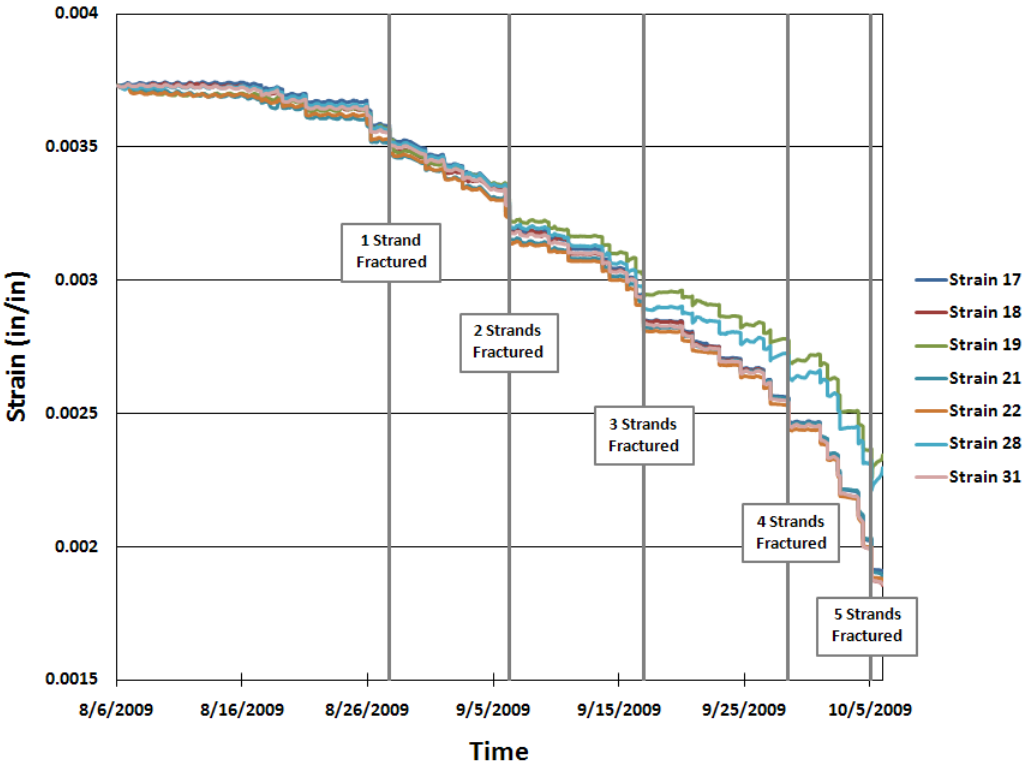

Figure 4.24: Strain Monitoring - Specimen 2

4.7.2 Specimen 3

Fourteen strain gages were also installed to monitor the response of Specimen 3. The location of the gages is shown in Figure 4.25 and Figure 4.26. Eleven gages provided reliable data throughout the test (Figure 4.27).

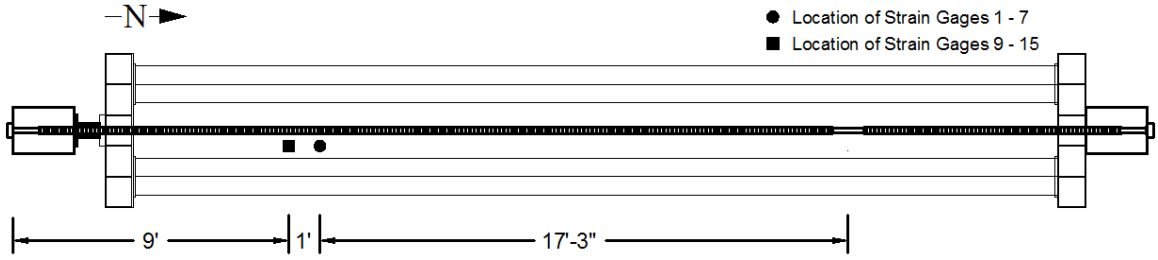

Figure 4.25: Location of Strain Gages - Specimen 3

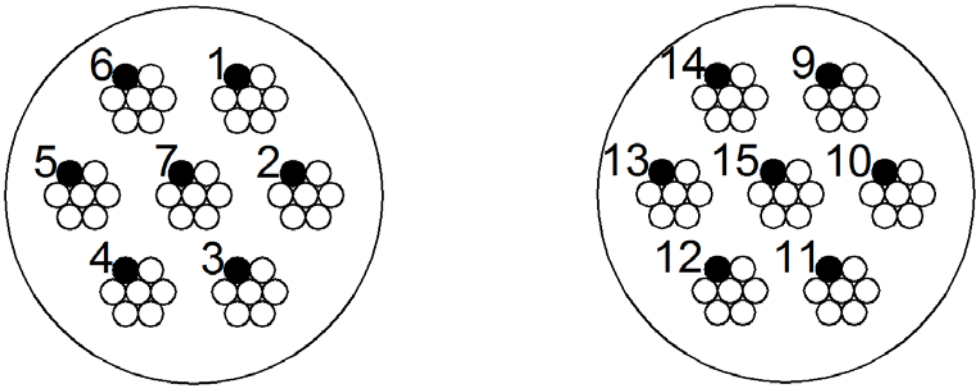

Strain Gages 1 - 7 Strain Gages 9 - 15

Figure 4.26: Location of Individual Strain Gages - Specimen 3

The strain data from Specimen 3 were similar to those from Specimen 2, although the spread in the data was slightly larger.

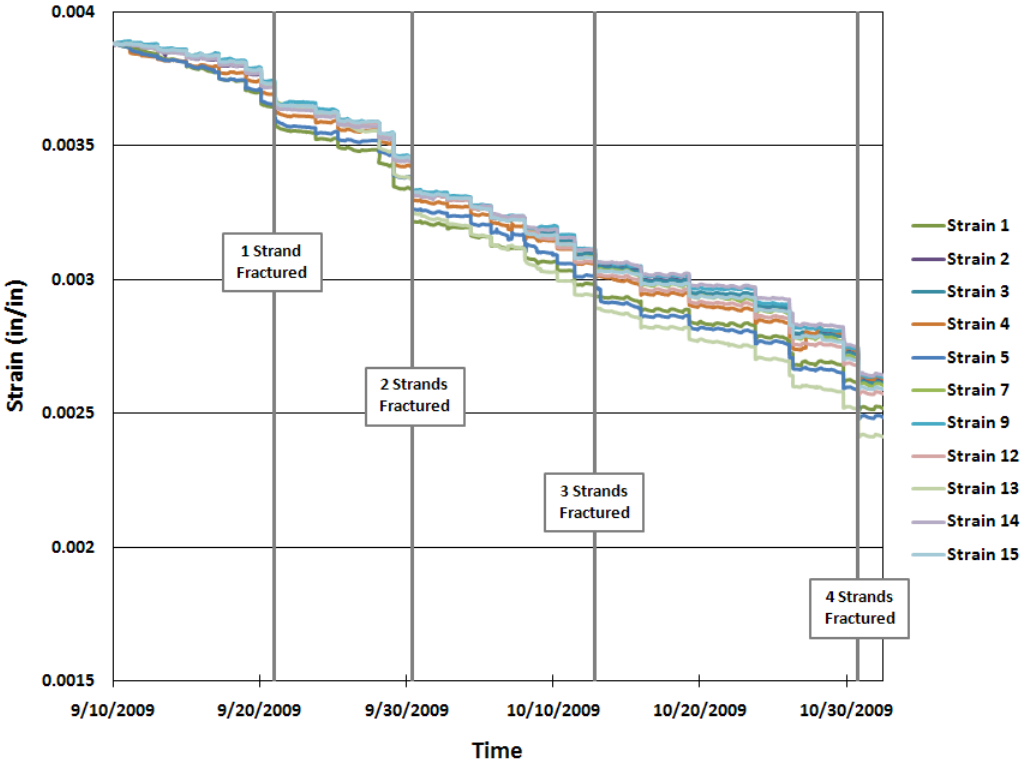

Figure 4.27: Strain Monitoring - Specimen 3

4.7.3 Specimens 4 and 5

Twenty-eight strain gages were applied to Specimens 4 and 5 in order to monitor the variance in strain distribution with distance from the location of damage. Figure 4.28 shows the location of the strain gages for Specimen 5. Unfortunately, the data from the strain gages proved to be unreliable for these specimens.

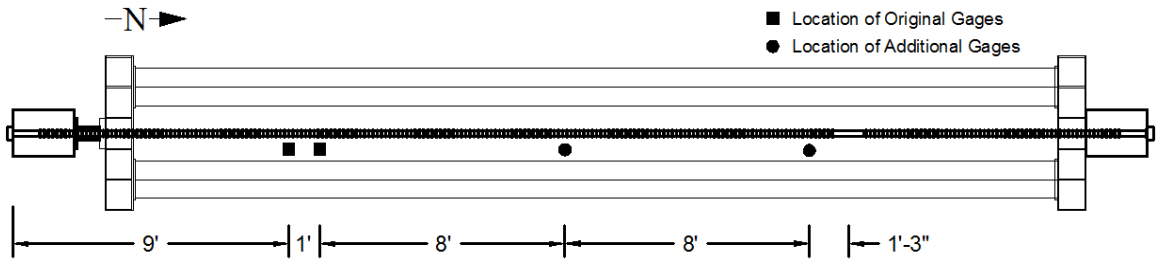

Figure 4.28: Location of Strain Gages - Specimens 5

As shown in Figure 4.29, most of the gages drifted significantly during the first week of monitoring. Therefore, all the strain data were considered to be unreliable for the specimens.

It is believed the higher stress level caused a considerable amount of drift in the strain gages of Specimen 4 and 5. The strain monitoring of Specimen 5 is illustrated in Figure 4.29. It was seen that once grouting was initiated the strain gages began to drift significantly. Due to the response of the gages, the data was deemed unreliable and is not presented.

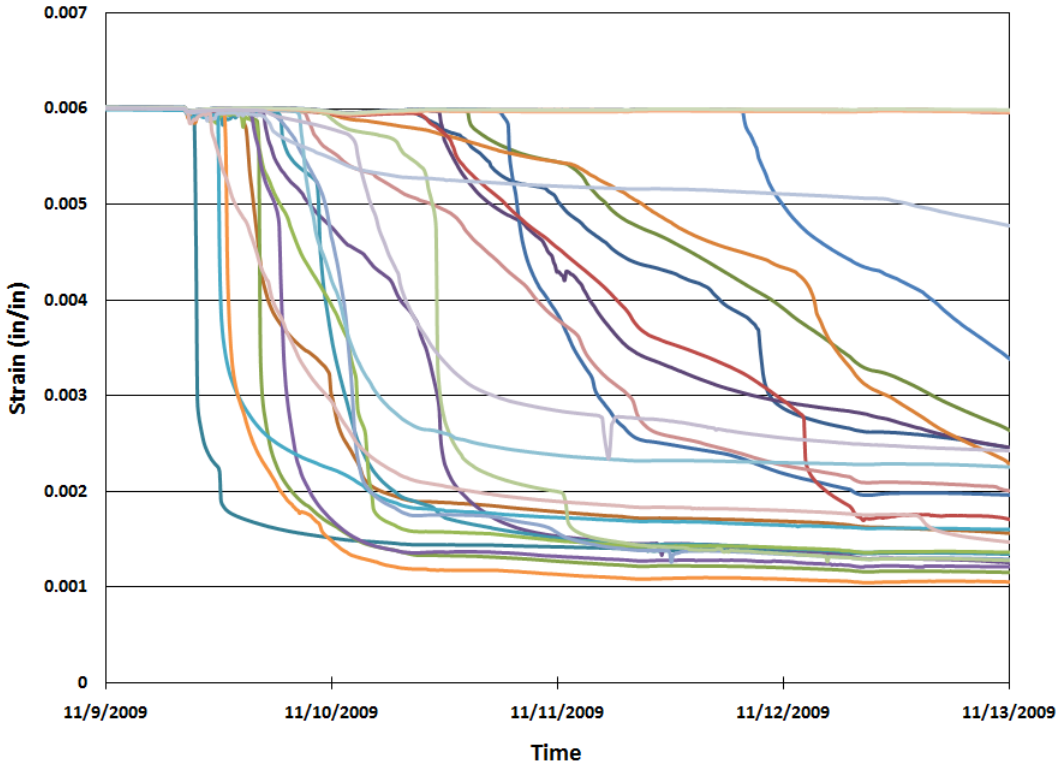

Figure 4.29: Strain Monitoring - Specimen 5

4.7.4 Residual Tensile Force

Once the specimens reached the target level of damage, the corrosion cell was removed and the tendon was disassembled. This involved cutting each specimen with a circular saw. During this process, the tensile force was monitored.

In Specimen 2, the bottom five strands in the tendon were fully fractured near the north end due to corrosion. The specimen was carefully cut near the south end so that only the top two strands fractured (Figure 4.30). At this point, none of the strands in the tendon were continuous along the entire length.

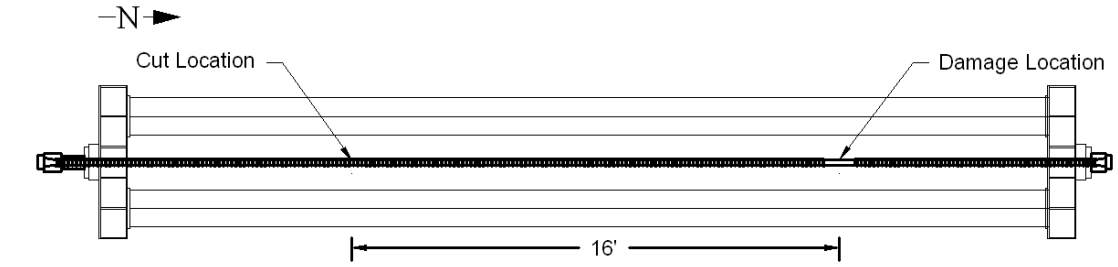

(a) Specimens with Steel Anchors

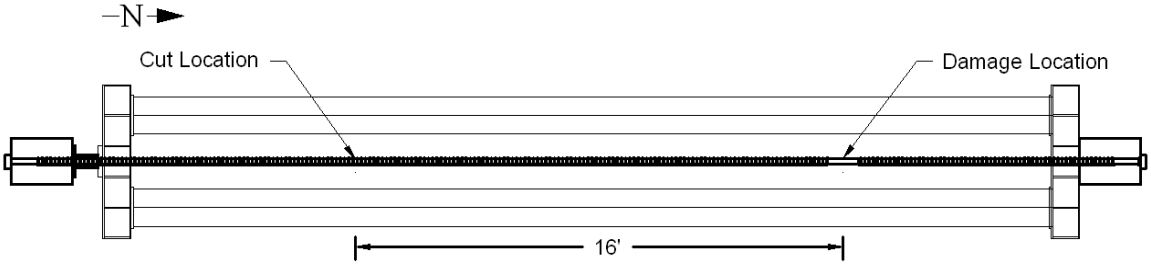

(b) Specimens with Concrete Anchors

Figure 4.30: Specimen Disassembly - Location of Cut

The variation of the tensile force during disassembly of Specimen 2 is summarized in Figure 4.31. After cutting the top two strands, a residual tensile force of approximately 50 kips was measured. Only after all strands were cut at a single location did the tensile force drop to zero. Specimens 3, 4, and 5 exhibited similar behavior (Table 4.10).

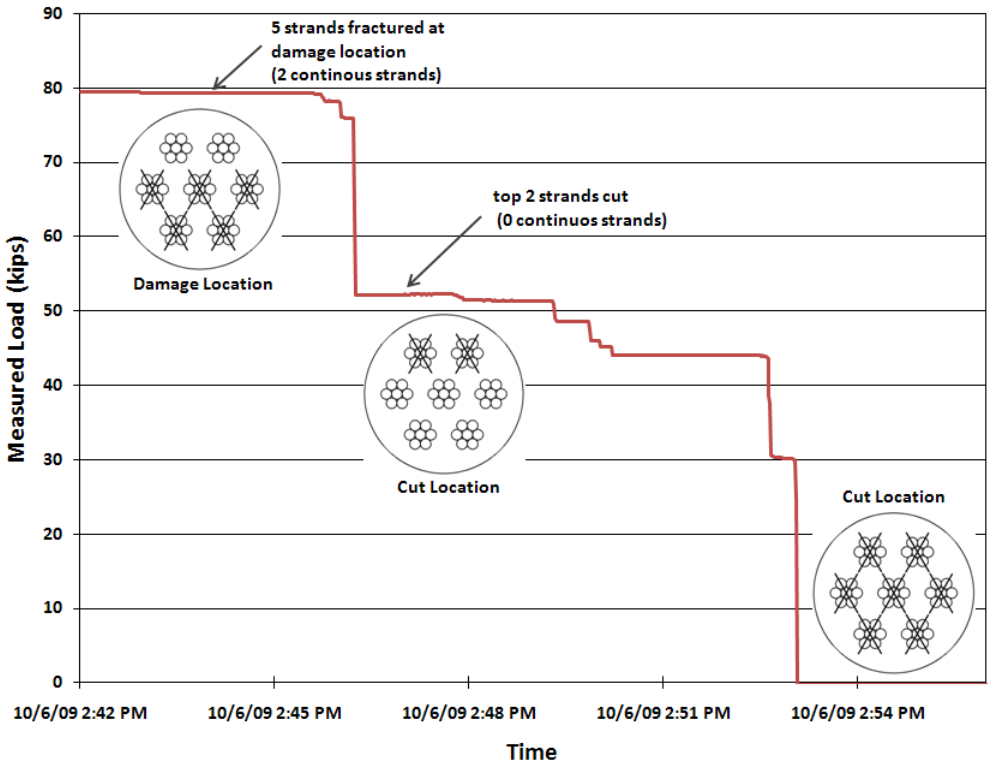

Figure 4.31: Response of Residual Tension during Disassembly - Specimen 2

Table 4.10: Summary of Residual Tension during Disassembly

Specimen ID	Number of Fractured Strands at Damage Location	Number of Fractured Strands at Cut Location	Residual Tension (kips)
2	5	0	79.3
		2	52.2
		5	44.0
		7	0.0
3	4	0	105.8
		2	61.3
		5	28.2
		7	0.0
4	5	0	101.2
		2	35.2
		5	25.5
		7	0.0
5	5	0	105.6
		2	16.8
		5	11.8
		7	0.0

4.8 SUMMARY

In this chapter, the measured variations in the tensile force and natural frequencies with increasing damage were presented.

As expected, the natural frequencies were less sensitive to the level of damage than the tensile force. Specimens with higher levels of initial prestress exhibited larger changes in both the tensile force and natural frequencies with damage than specimens with lower levels of initial prestress.

Redistribution of stress following a wire break was observed in all specimens. In all cases, the tensile force in the specimens corresponding to a given level of damage exceeded the area of intact wires times the initial level of prestress.

The loss in tensile force corresponding to every strand fracture is summarized in Figure 4.32. In general, the reduction in tensile force increased as the level of damage increased. On average, 8% of the initial prestress force was lost after the first strand fractured, where more than 17% of the initial prestress force was lost after the fifth strand fractured.

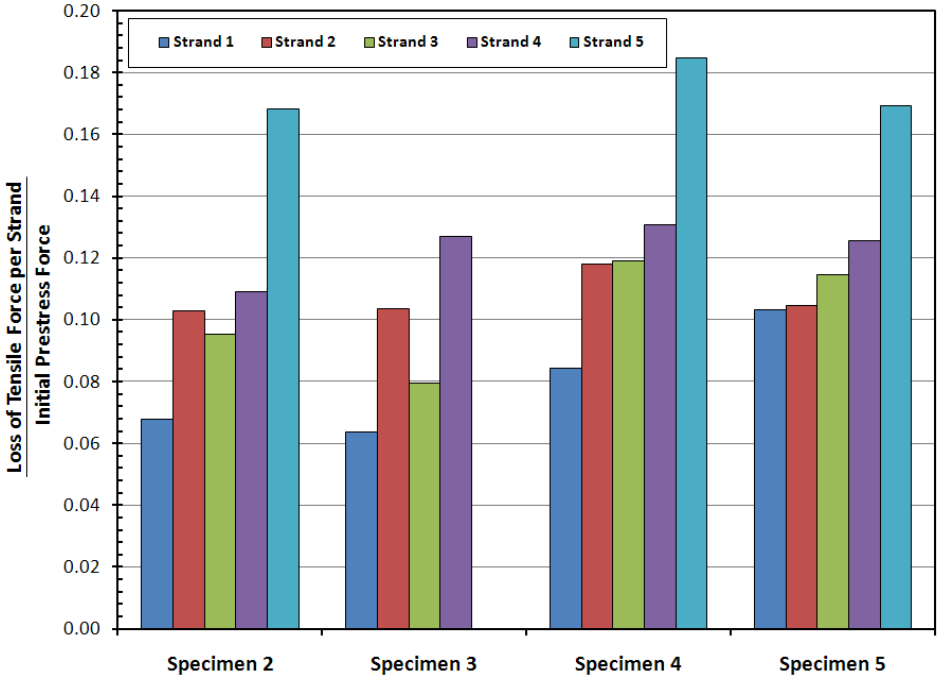

Figure 4.32: Loss of Tensile Force in Strand Break

During disassembly, the tendons were able to resist approximately 30% of the initial prestress force with no continuous strands.

CHAPTER 5

Evaluation of Measured Response

The objective of this chapter is to determine if the stiff string model is capable of reproducing the changes in response due to localized damage from the measured frequency response. The damage was induced through local accelerated corrosion, in which individual wires in a strand were corroded until they fractured. The wire breaks resulted in a loss of tensile force, causing reductions in the natural frequencies of the test specimens.

Section 5.1 summarizes the Morse approximation of the stiff string model and the associated structural parameters necessary to use the model. The initial measured natural frequencies and those calculated using the analytical model are compared in Section 5.2. The sensitivity of the frequency response to variations in the tensile force is discussed in Section 5.3.

5.1 STIFF STRING MODEL

The stiff string model is often used to represent the dynamic response of external post-tensioned tendons. The model includes the bending stiffness of the tendon, but ignores sag – the tendon is assumed to be straight. The ends of the tendon are also assumed to be restrained against rotation and displacement.

As discussed in Chapter 2, Morse (1948) developed an approximate solution for the stiff string model:

$$f_n \cong \frac{n}{2L}\sqrt{\frac{T}{m}}\left[1+\frac{2}{L}\sqrt{\frac{EI}{T}}+\left(4+\frac{n^2\pi^2}{2}\right)\frac{EI}{TL^2}\right] \qquad \text{(Equation 5.1)}$$

where f_n is the frequency of mode n in Hz, L is the length of the specimen, T is the tensile force, m is the mass per unit length, and EI is the flexural stiffness. All parameters are assumed to remain constant along the length of the specimen, therefore, local

variations in EI and m due to the induced corrosion damage are not considered in this idealization.

The method used to calculate the four parameters in Equation 5.1 is discussed in the following section. For a given level of damage, the measured tensile force was used directly in the calculations.

5.1.1 Tension

The tensile force in the specimen was directly measured with a center-hole load cell located at the south end of the specimen. The load cell provided an accurate measurement of the tensile force throughout the experiment.

5.1.2 Flexural Stiffness

The flexural stiffness is defined as the product of the transformed moment of inertia, I, and the modulus of elasticity, E. The moment of inertia was calculated considering the prestressing strands and the surrounding grout in the tendon. The values of E for the grout and the strands were not measured in the experimental program. Therefore, typical values of these properties were assumed in all calculations. The modulus of elasticity of the grout was assumed to be 3,600 ksi and the modulus elasticity of the strand was assumed to be 29,500 ksi.

A potential error exists in calculating the second moment of inertia of the specimen. A symmetric cross-sectional layout was assumed, as shown in Figure 5.1a. The arrangement of the strands will more than likely vary from the assumed position, as observed after each specimen was disassembled (Figure 5.1b). It can be seen that the relative locations of the strands closely follow the idealized section; however, the strands are not centered within the duct. Because there in nothing holding the duct in place, gravity tends to pull the duct downward, resulting in a larger area of grout below the strands than above.

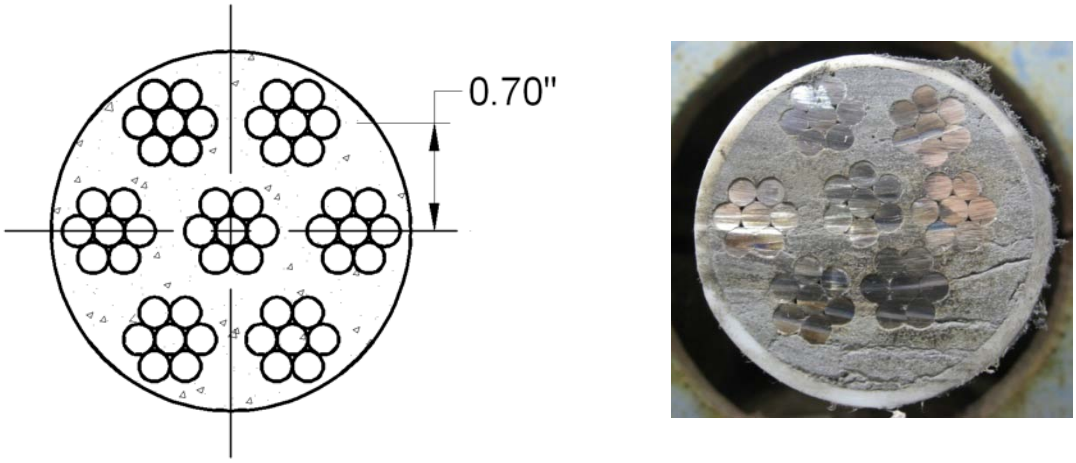

(a) Idealized Section (b) Actual Section (Sp. 3)

Figure 5.1: Specimen Cross Section – Idealized and Actual

The non-symmetrical placement of the strands within the cross-section was ignored, since it would be impossible to determine the placement of each strand in the tendon at a given location. Therefore, local variations in the flexural stiffness were neglected and the idealized layout of the strands was used in all calculations. The calculated value of 16,500 kip-in^2 (Appendix A) was used for the flexural stiffness for all specimens.

5.1.3 Mass per Unit Length

In the experimental program, the unit mass of each specimen was directly measured after the tendon was disassembled. Two, 1-ft sections were cut from opposite ends of the tendon and weighed to obtain an average unit mass. The measured values are reported in Table 5.1.

Table 5.1: Measured Mass per Unit Length

Specimen ID	Average Unit Weight (lb/ft)	Average Unit Mass (lb-sec^2/ft^2)
2	7.95	0.25
3	7.84	0.24
4	7.94	0.25
5	7.80	0.24

5.1.4 Length

The clear length of the test specimens was used in Equation 5.1. The clear length is measured between the inside faces of the anchor blocks (Figure 5.2). For specimens with steel anchor blocks, the clear length was 33 ft – 9 in. The specimens with concrete anchor blocks had a clear length of 33 ft - 0 in.

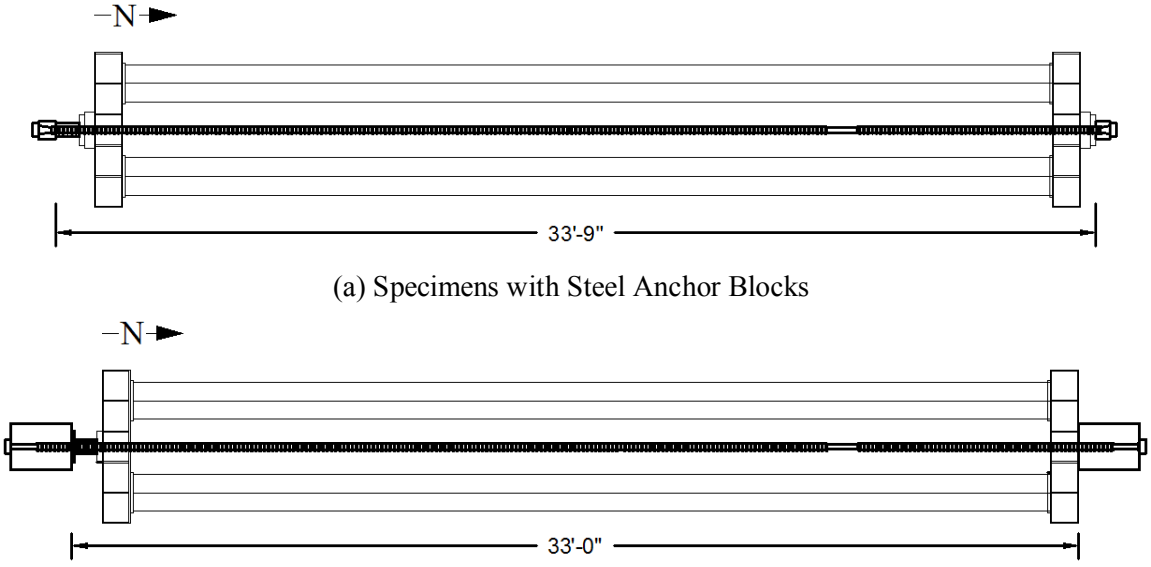

(a) Specimens with Steel Anchor Blocks

(b) Specimens with Concrete Anchor Blocks

Figure 5.2: Clear Length of Specimens

5.1.5 Verification of Tendon Behavior

In the analysis of cable structures, two dimensionless parameters are typically used to describe the geometric properties (Irvine, 1981). The expressions for γ and λ^2 are defined in Equation 5.2 and Equation 5.3.

$$\gamma = \sqrt{\frac{TL^2}{EI}} \qquad \text{(Equation 5.2)}$$

$$\lambda^2 = \left(\frac{mgL}{T}\right)^2 \cdot \frac{EA}{T} \qquad \text{(Equation 5.3)}$$

where T is the tensile force, L is the length of the cable, EI is the flexural stiffness, m is the mass per unit length, g is the gravitational acceleration, and EA is the axial stiffness.

The parameter γ indicates the relative importance of cable and beam action. For values of γ on the order of 1000, the effects of flexural rigidity are insignificant and may be ignored (Irvine, 1981). As γ approaches zero, the member behaves as a beam and the axial stiffness may be ignored. Pebley (2005) determined the cutoff value between beam and cable action to be approximately 50.

The parameter λ^2 accounts for the relative importance of elastic and geometric effects. Elastic effects include axial deformations, whereas geometric effects include cable sag (Irvine, 1981). The parameter is a measure of how taut a cable is, and its value depends on the ratio of the weight to the tensile force. Sag is typically ignored when λ^2 approaches zero.

The values of the two parameters for each specimen are summarized in Table 5.2. The values of λ^2 are essentially zero and suggest that sag can be ignored. The values of γ are approximately equal to the cutoff value proposed by Pebley (2005); therefore, both the flexural stiffness and tensile force are expected to influence the response of the specimens.

Table 5.2: Initial Values of Behavioral Parameters of Cable Structures

Specimen ID	λ^2	γ
2	0.00095	41.8
3	0.00091	40.6
4	0.00023	52.9
5	0.00023	51.3

5.2 INITIAL RESPONSE

The values of the structural parameters discussed in Section 5.1 were used with Equation 5.1 to calculate an initial set of natural frequencies. These frequencies are compared with the measured natural frequencies for Specimens 2, 3, 4, and 5 in Table 5.3 and Figure 5.3.

Table 5.3: Comparison of the Initial Set of Natural Frequencies

Specimen ID	Frequency (Hz)							
	Mode 1		Mode 2		Mode 3		Mode 4	
	Measured	Calculated	Measured	Calculated	Measured	Calculated	Measured	Calculated
2	13.25	13.10	26.68	26.40	40.48	40.13	54.71	54.49
3	13.25	13.53	26.70	27.29	40.55	41.50	54.70	56.40
4	16.45	16.40	33.11	32.97	49.60	49.88	67.40	67.28
5	16.48	16.83	33.20	33.84	50.37	51.21	67.81	69.13

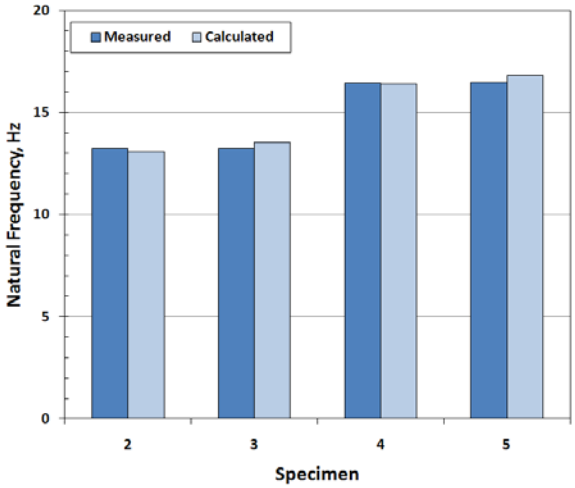

(a) Mode 1

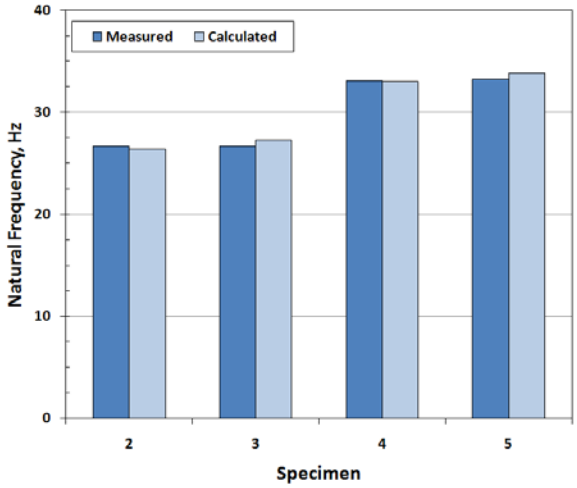

(b) Mode 2

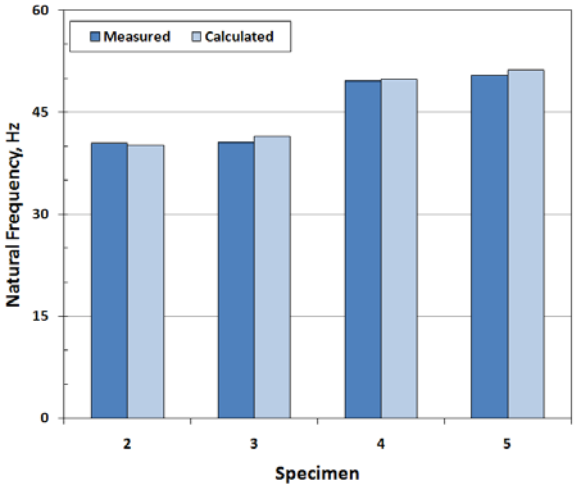

(c) Mode 3

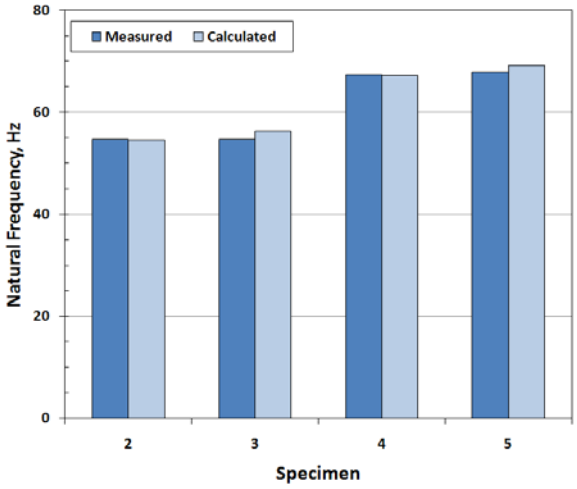

(d) Mode 4

Figure 5.3: Comparison of Measured and Calculated Natural Frequencies at Beginning of Tests

The calculated natural frequencies compared very well with the measured values for all four specimens. In specimens 3 and 4, the calculated natural frequencies were always greater than the measured, with differences not exceeding 4%. The first three modes of specimen 2 and first two modes of specimen 4 had the measured frequencies greater than the calculated, with a difference less than 1%.

5.3 SENSITIVITY OF FREQUENCY RESPONSE TO VARIATION OF TENSILE FORCE

The natural frequency and tensile force trends discussed in Chapter 4 are useful for comparing the response of the test specimens with other laboratory specimens. However, in field applications, only the frequencies can be measured directly. The tensile force and extent of cross-sectional damage are not known and can only be estimated from the measured frequencies. Therefore, it is important to evaluate the sensitivity of the measured frequencies to the measured variations in the tensile force.

The idealized response of the test specimens is shown in Figure 5.4 for the structural parameters reported in Section 5.1 and the approximate solution given in Equation 5.1. Based on these calculations, the higher modes are expected to be slightly more sensitive to changes in the tensile force.

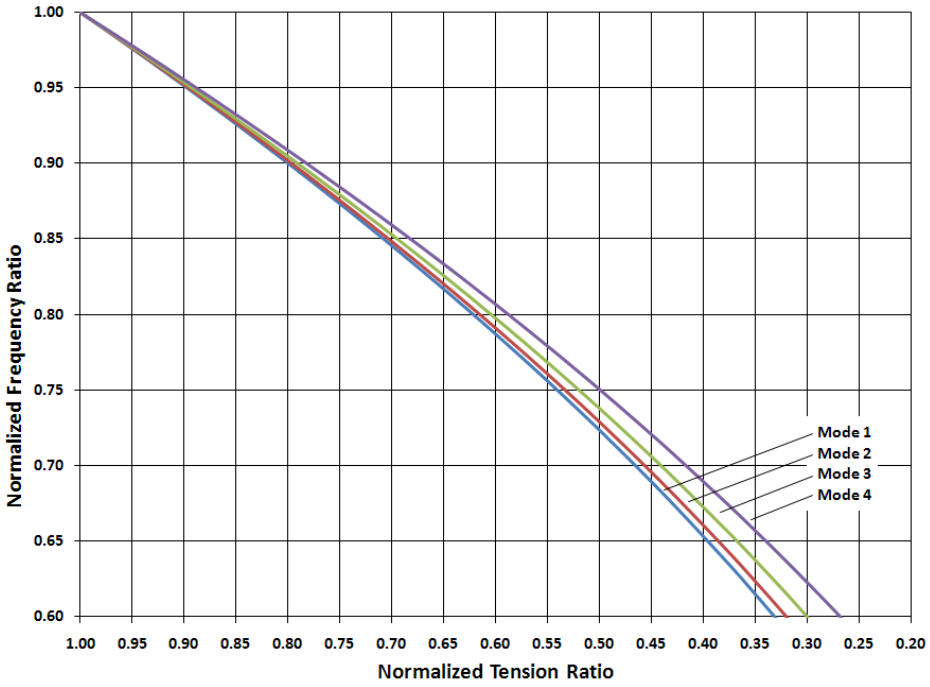

(a) Specimens with Lower Initial Prestress

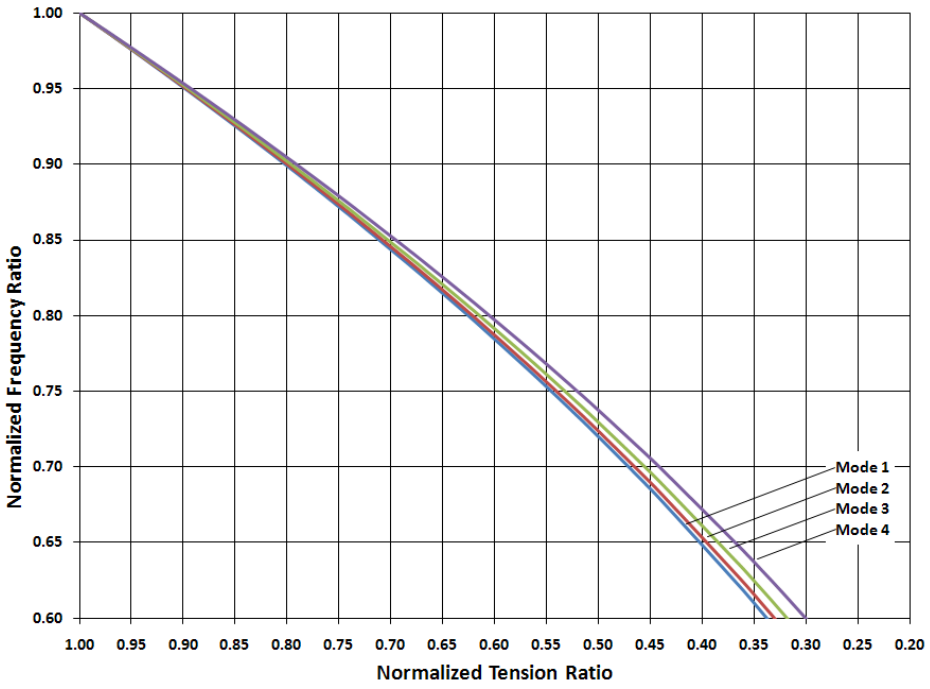

(b) Specimens with Higher Initial Prestress

Figure 5.4: Calculated Relationship between Tensile Force and Natural Frequency

The calculated relationship is essentially the same for Specimens 2 and 3 and Specimens 4 and 5. The differences between the clear lengths and measured unit mass values were insignificant and the flexural stiffness was assumed to be the same for all specimens. The measured and calculated responses of each specimen are discussed in the following sections.

5.3.1 Specimen 2

The normalized frequency ratio is plotted versus the normalized tension ratio for Specimen 2 in the four plots in Figure 5.5. The dashed line represents the relationship calculated using Equation 5.1, while the points represent the measured response.

The measured response is very similar to the calculated response, although the fourth mode exhibited the largest deviation from the calculated response. In all cases, the calculated normalized frequency ratio tended to be greater than the measured normalized frequency ratio for a given level of damage.

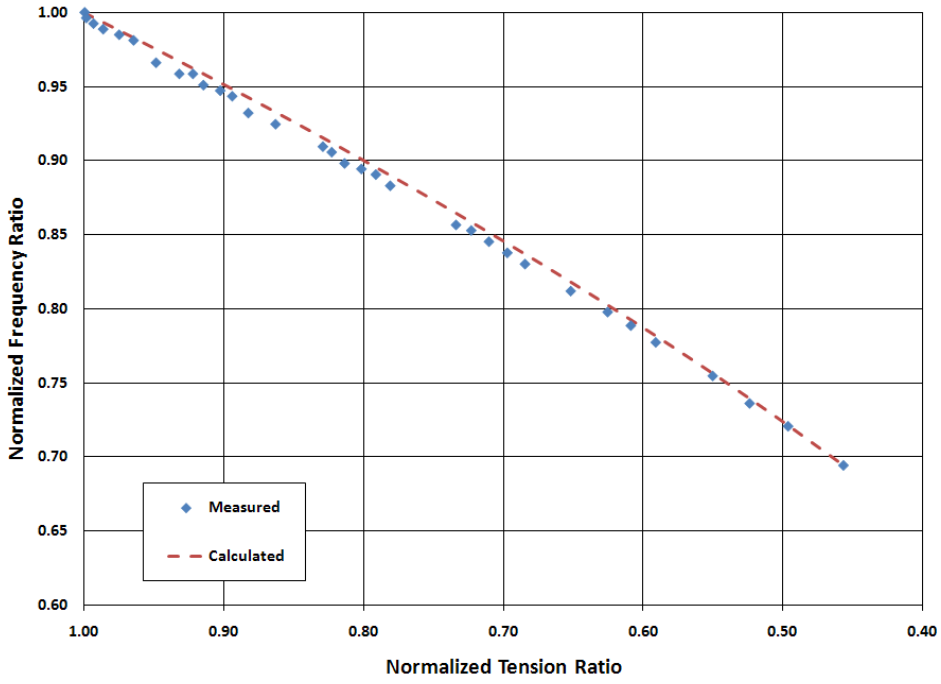

(a) Mode 1

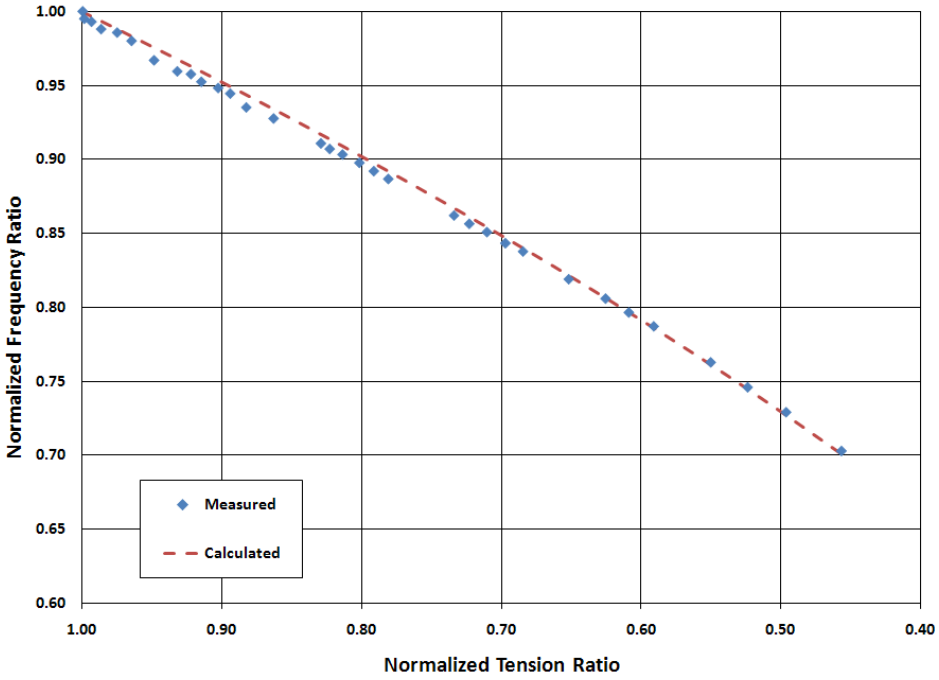

(b) Mode 2

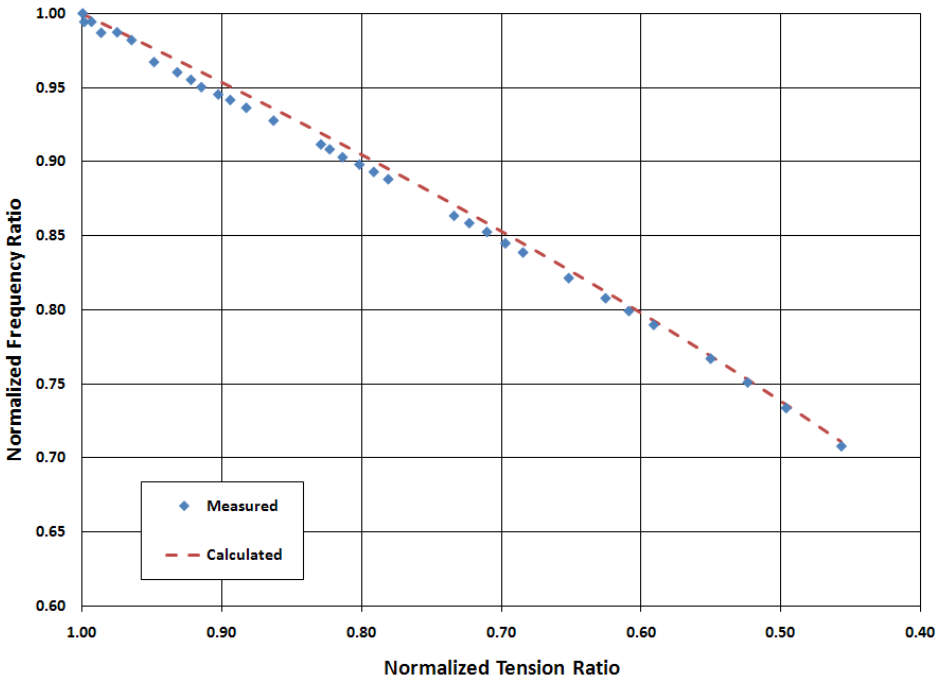

(c) Mode 3

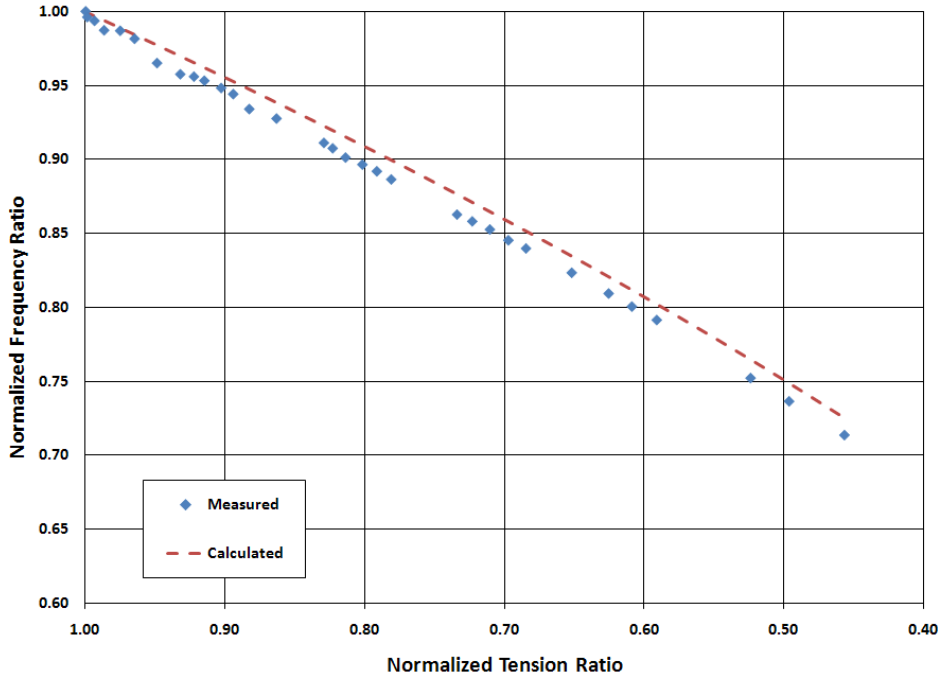

(d) Mode 4

Figure 5.5: Sensitivity of Natural Frequencies to Variation of Tensile Force – Specimen 2

The measured response for all four modes is plotted in Figure 5.6. The final tension was 45.7% of the initial tension force. The measured frequencies at the conclusion of the test ranged from 69.4% of the initial for mode 1 to 71.4% of the initial for mode 4.

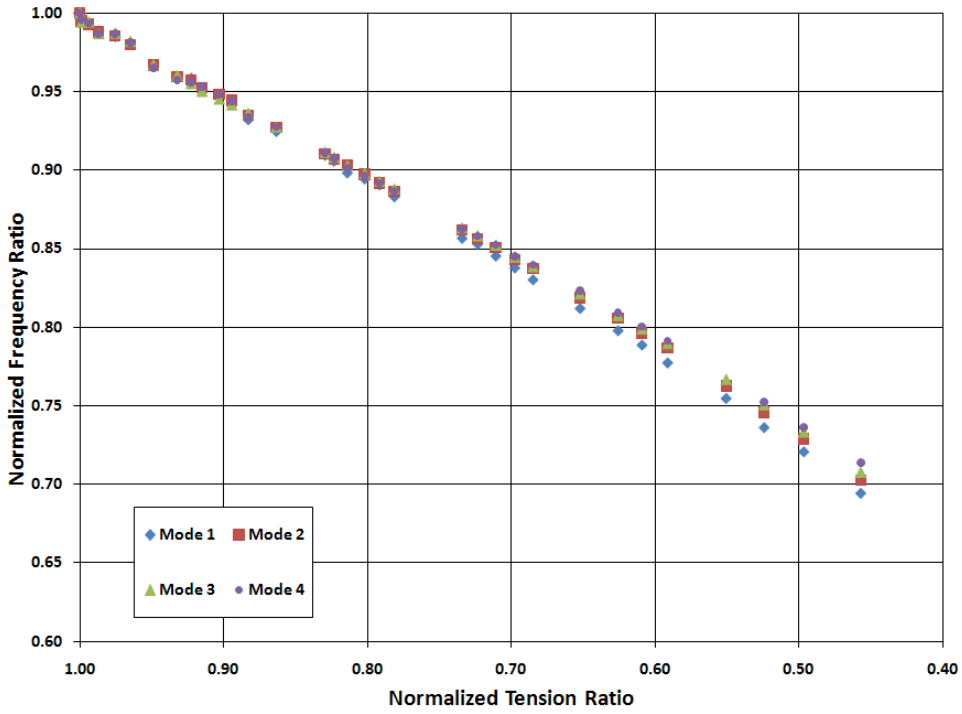

Figure 5.6: Sensitivity of Measured Natural Frequencies to Variation of Tensile Force – Specimen 2

Measured and calculated values of the fundamental natural frequency are plotted as a function of the measured tensile force in Figure 5.7. Equation 5.1 was used to determine the calculated fundamental frequency for each damage state. The data indicate that the frequencies calculated from the measured tensile force using the Morse approximation will differ from the measured fundamental frequency by -1 to 1% for each mode. This difference was independent of the level of induced damage.

When using the vibration method to evaluate a bridge, the natural frequencies will be measured and the corresponding value of tensile force will be extracted using Equation 5.1. Therefore, measured and extracted values of the tensile force are plotted as a function of the measured fundamental frequency in Figure 5.8. The data show that the tensile forces extracted from the Morse approximation differed from the measured tensile force by 0 to 3% for the first mode and -3 to 1% for the fourth mode. Again, the differences appeared to be independent of the level of induced damage.

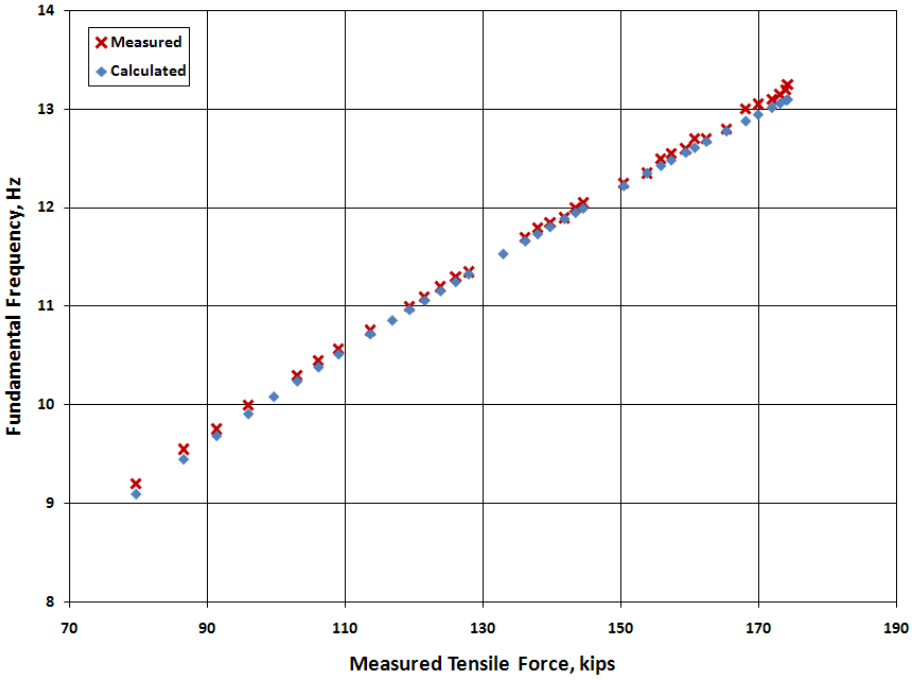

(a) Mode 1

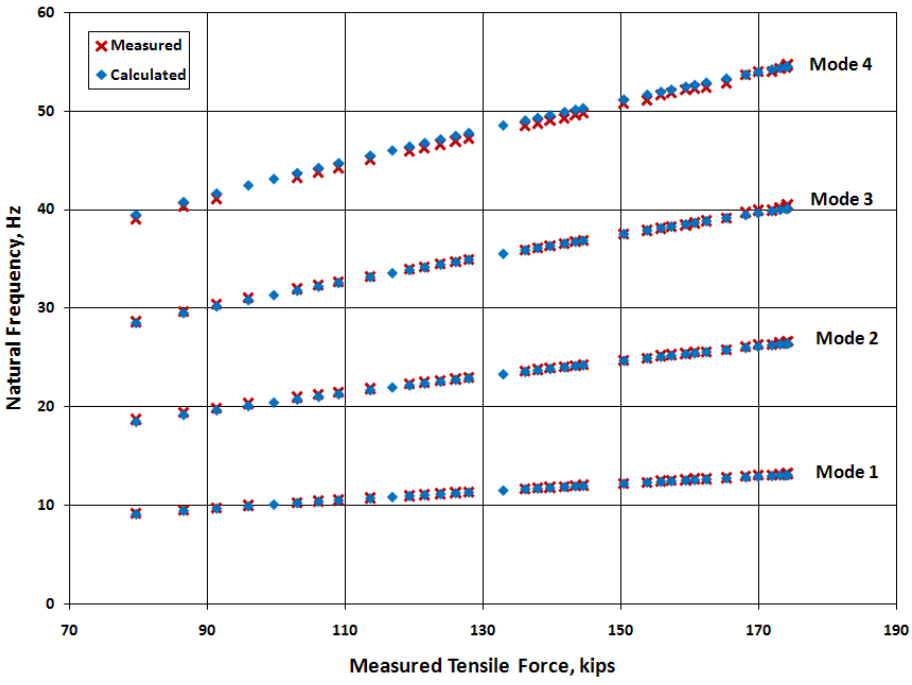

(b) All Modes

Figure 5.7: Variation in Frequency with Measured Tensile Force – Specimen 2

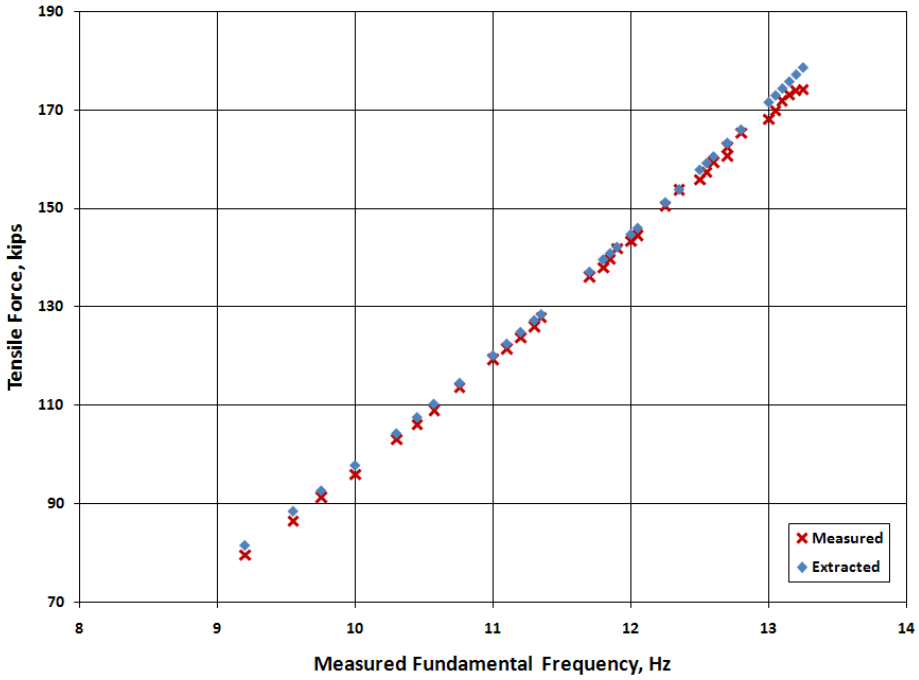

(a) Mode 1

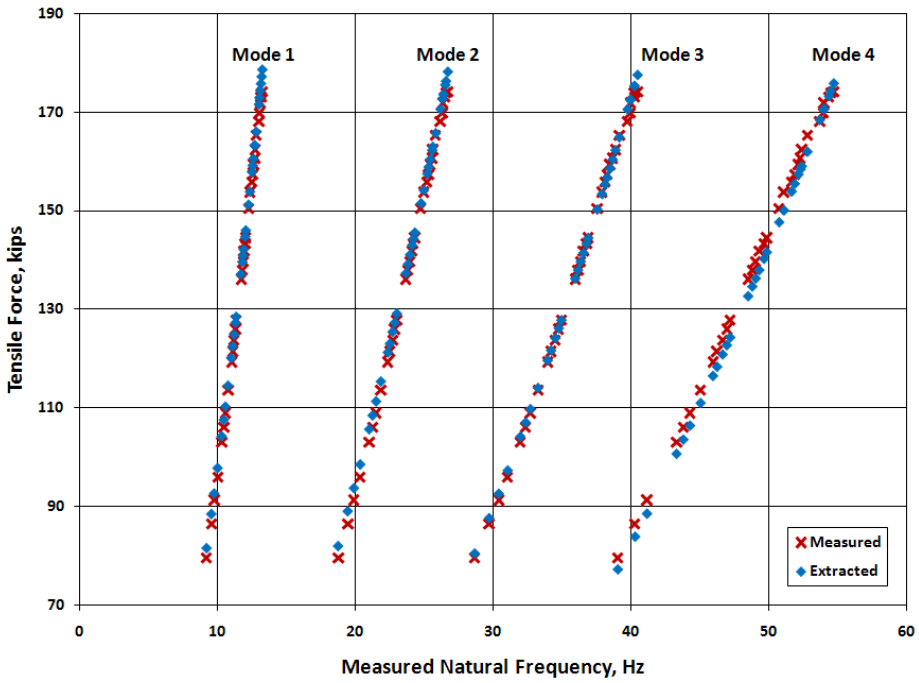

(b) All Modes

Figure 5.8: Variation in Tensile Force with Measured Frequency – Specimen 2

5.3.2 Specimen 3

The normalized frequency ratio is plotted versus the normalized tension ratio for Specimen 3 in the four plots in Figure 5.9.

The measured response is very similar to the calculated response. In the first two modes, the measured normalized frequency ratios tended to be slightly greater than the calculated normalized frequency ratios for a given level of damage. In the third and fourth modes, the measured and calculated normalized ratios were nearly identical.

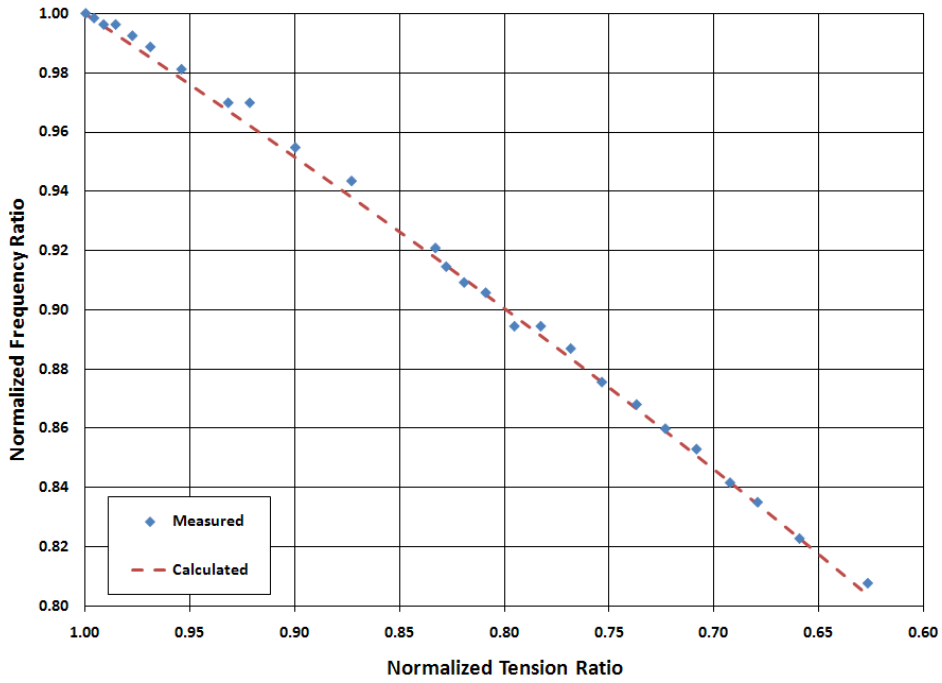

(a) Mode 1

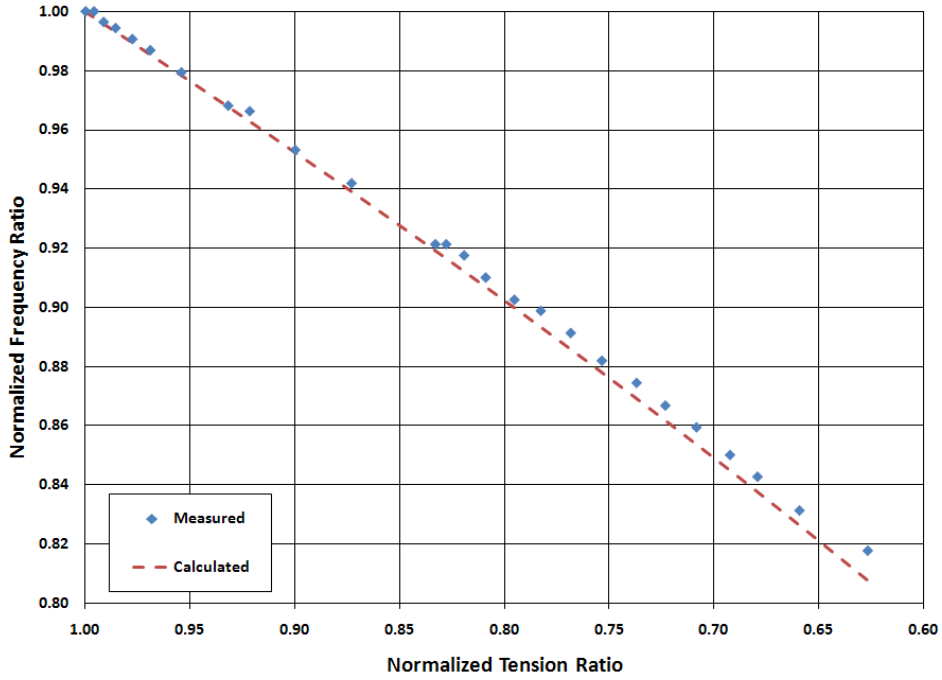

(b) Mode 2

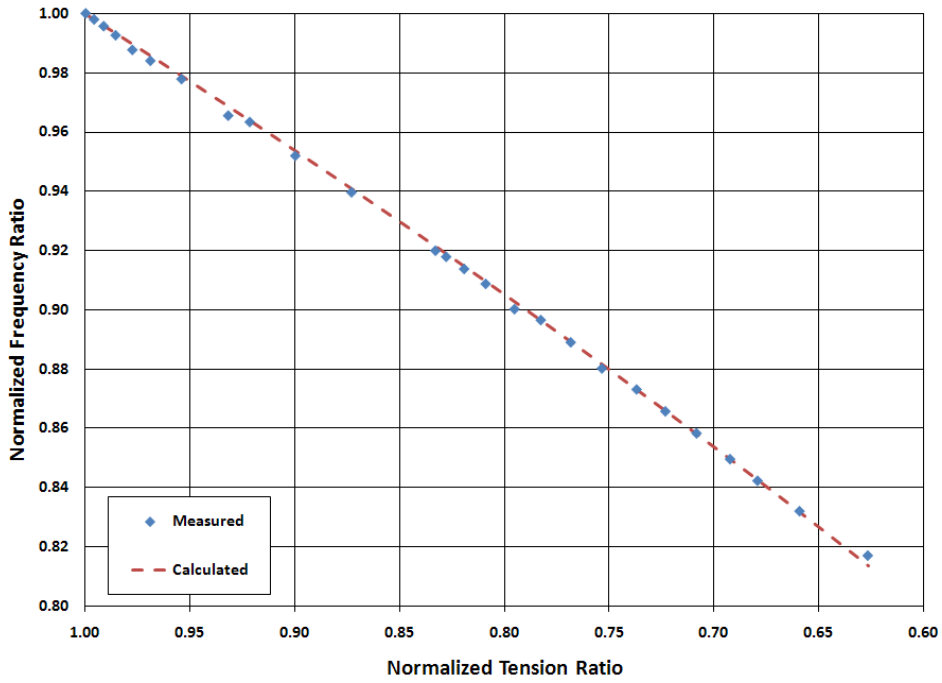

(c) Mode 3

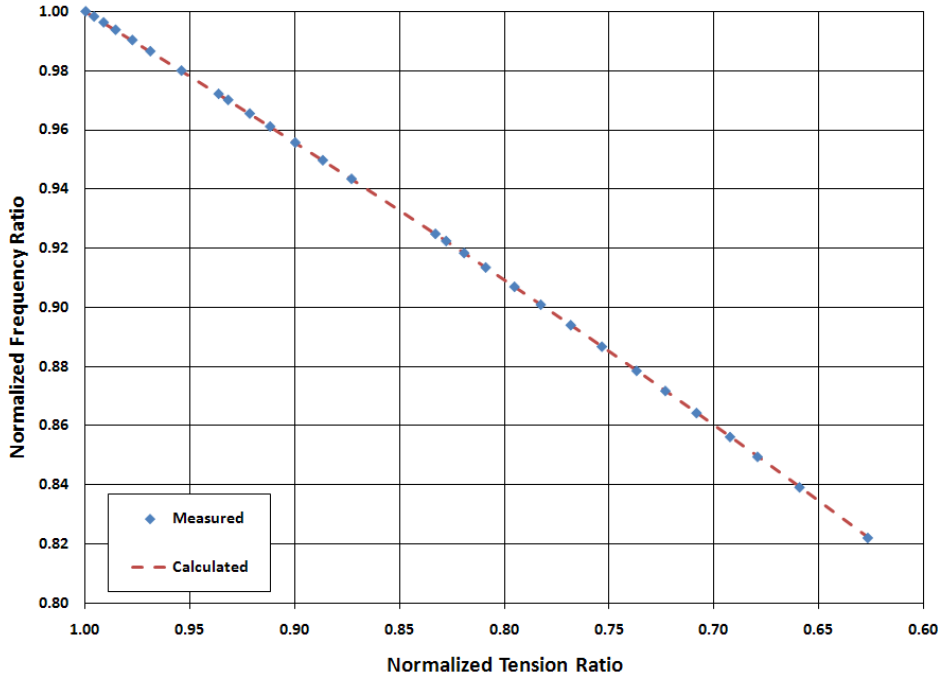

(d) Mode 4

Figure 5.9: Sensitivity of Natural Frequencies to Variation of Tensile Force – Specimen 3

The measured trends for all four modes are plotted in Figure 5.10. The final tension was 62.6% of the initial tension force. The measured frequencies at the conclusion of the test ranged from 80.8% of the initial for mode 1 to 81.9% of the initial for mode 4.

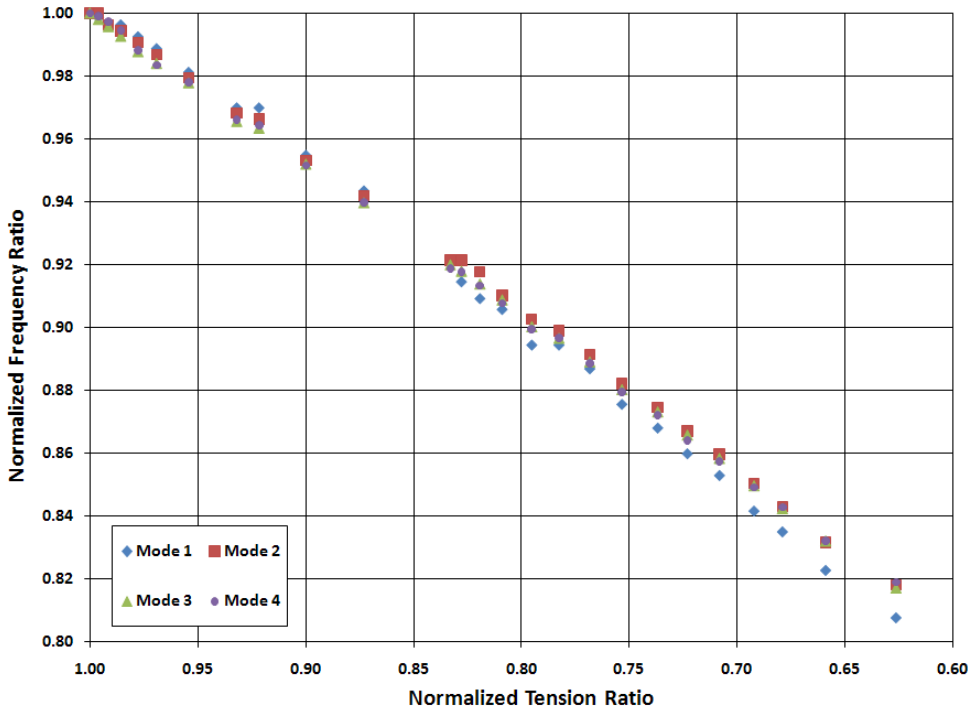

Figure 5.10: Sensitivity of Measured Natural Frequencies to Variation of Tensile Force – Specimen 3

Measured and calculated values of the fundamental natural frequency are plotted as a function of the measured tensile force in Figure 5.11. The calculated frequencies overestimated the measured natural frequencies by 1 to 3% for the first mode and 3 to 4% for the fourth mode.

Measured and extracted values of the tensile force are plotted as a function of the measured fundamental natural frequency in Figure 5.12. The extracted tensile forces underestimated the measured tensile forces by 2 to 5% for the first mode and 7 to 9% for the fourth mode.

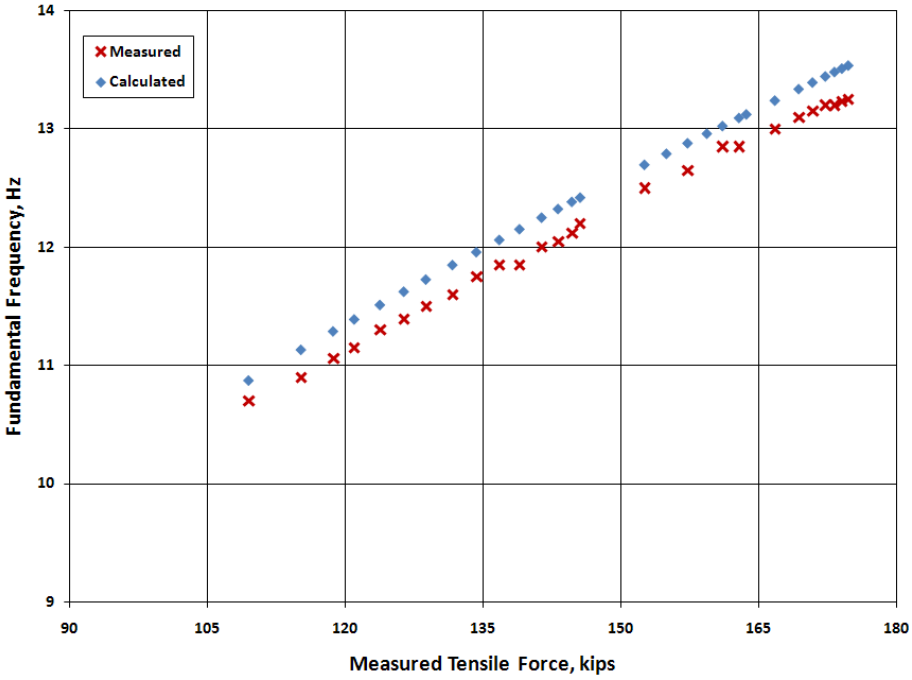

(a) Mode 1

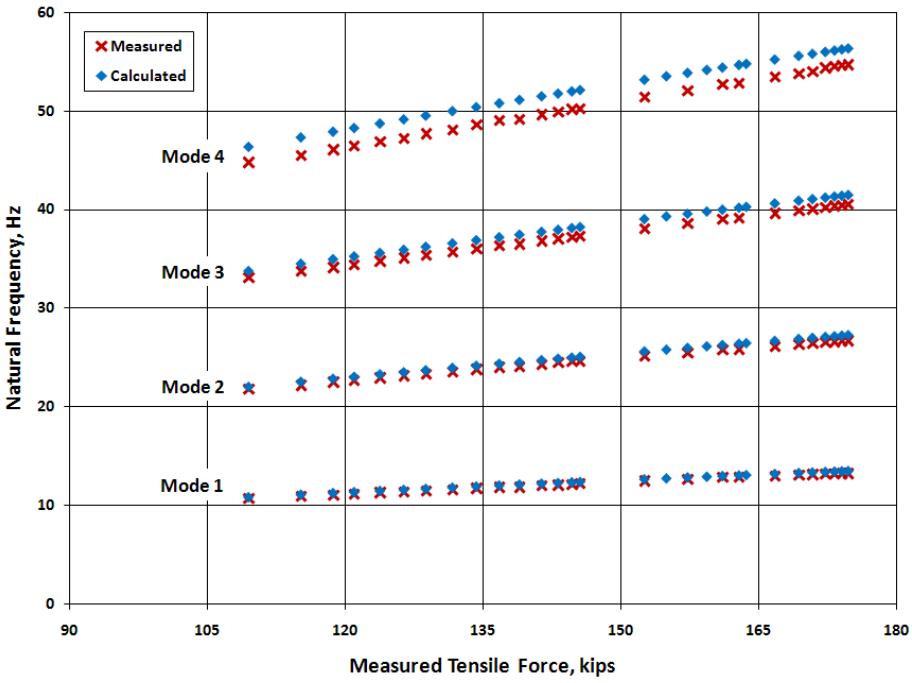

(b) All Modes

Figure 5.11: Variation in Frequency with Measured Tensile Force – Specimen 3

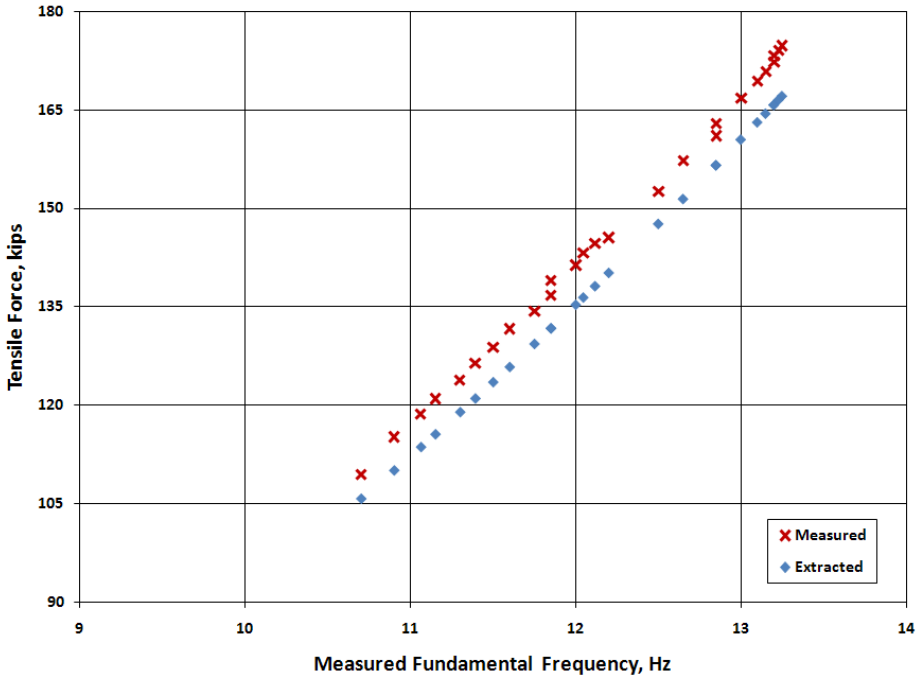

(a) Mode 1

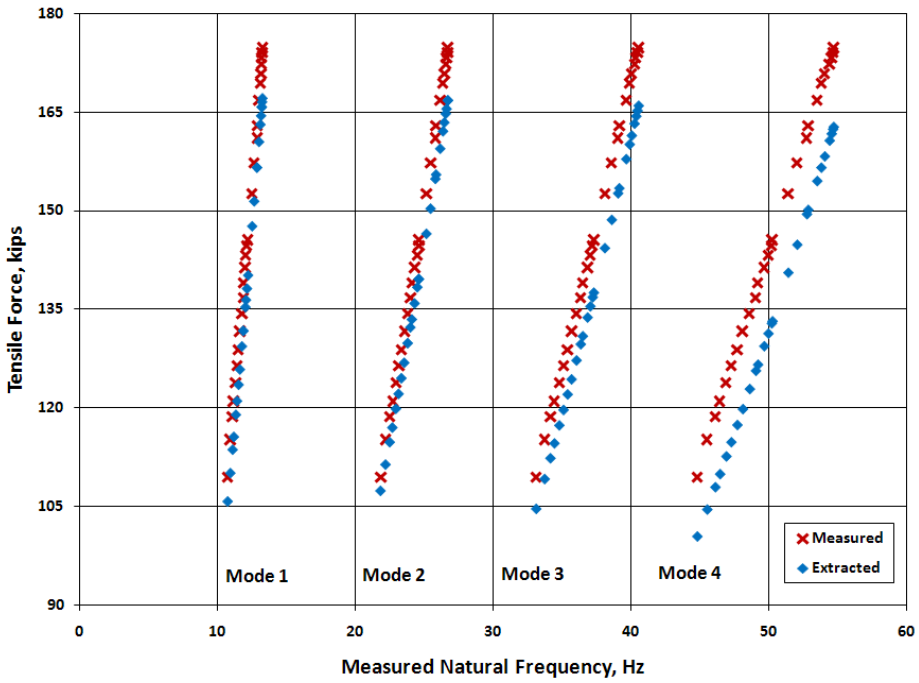

(b) All Modes

Figure 5.12: Variation in Tensile Force with Measured Frequency – Specimen 3

5.3.3 Specimen 4

The normalized frequency ratio is plotted versus the normalized tension ratio for Specimen 4 in the four plots in Figure 5.13.

The measured response is very similar to the response of Specimen 2. In all cases, the calculated normalized frequency ratios tended to be greater than the measured normalized frequency ratios for a given level of damage.

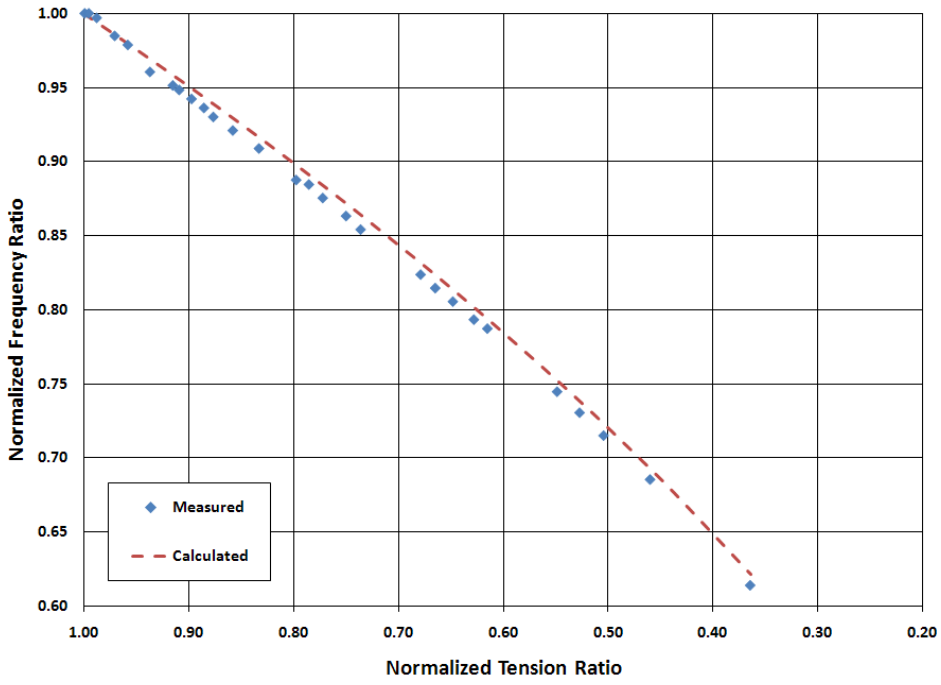

(a) Mode 1

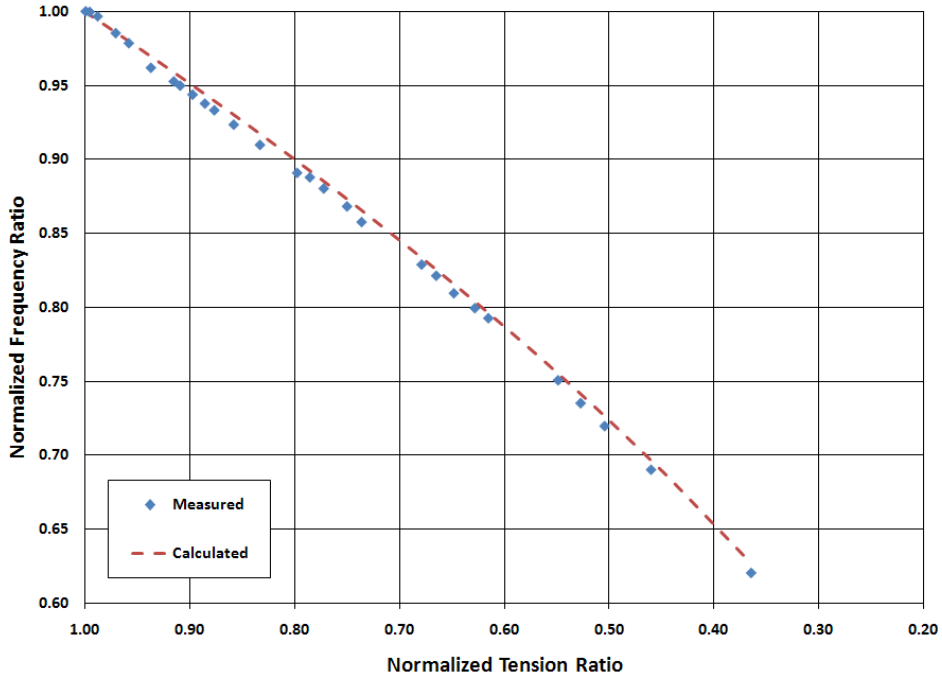

(b) Mode 2

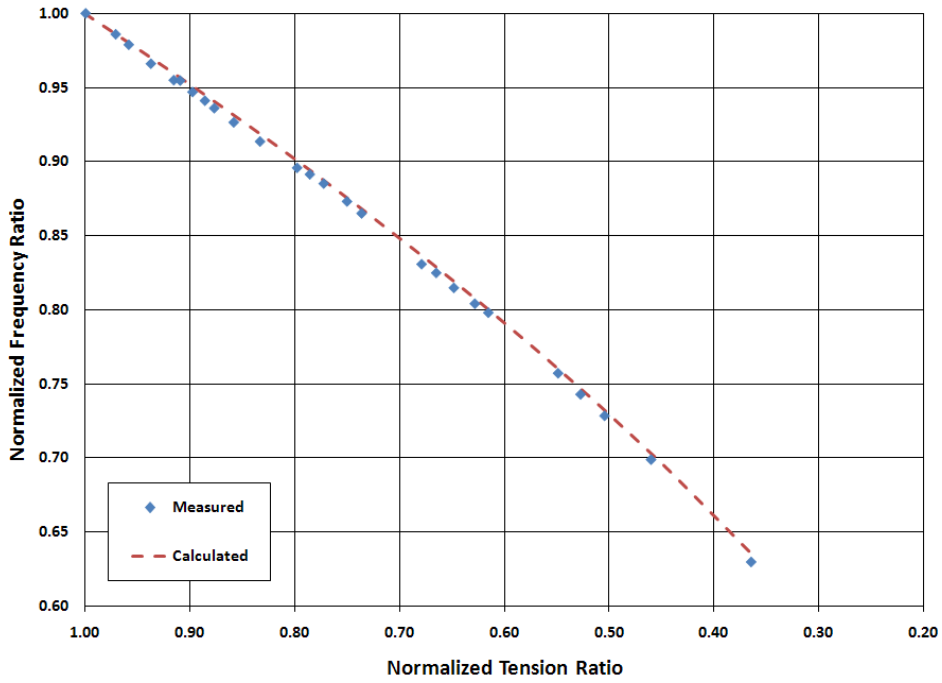

(c) Mode 3

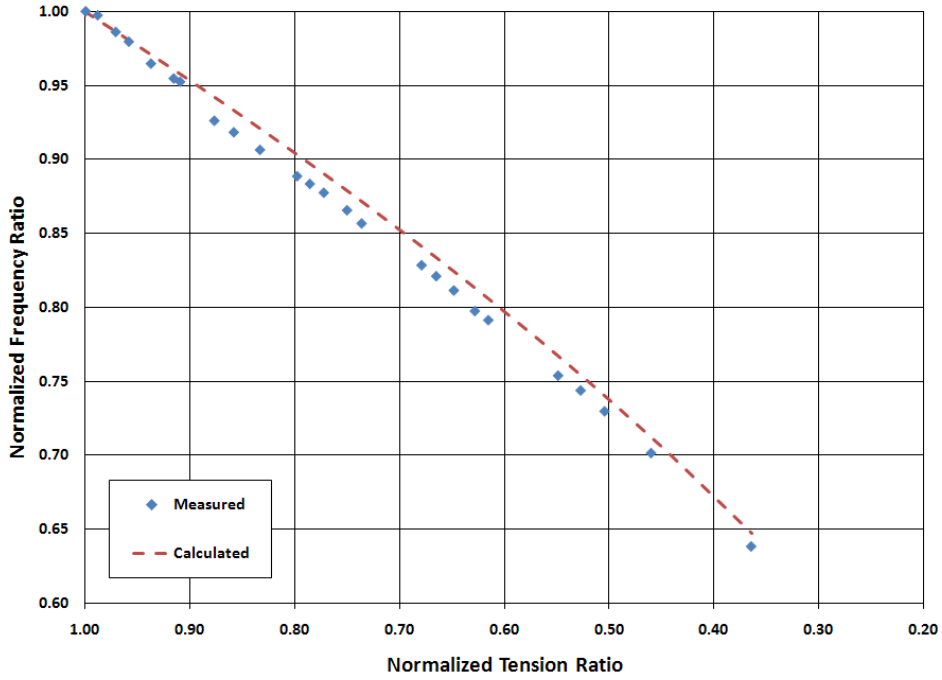

(d) Mode 4

Figure 5.13: Sensitivity of Natural Frequencies to Variation of Tensile Force – Specimen 4

The measured trends for all four modes are plotted in Figure 5.14. The final tension was 36.4% of the initial tension force. The measured frequencies at the conclusion of the test ranged from 61.4% of the initial for mode 1 to 63.9% of the initial for mode 4.

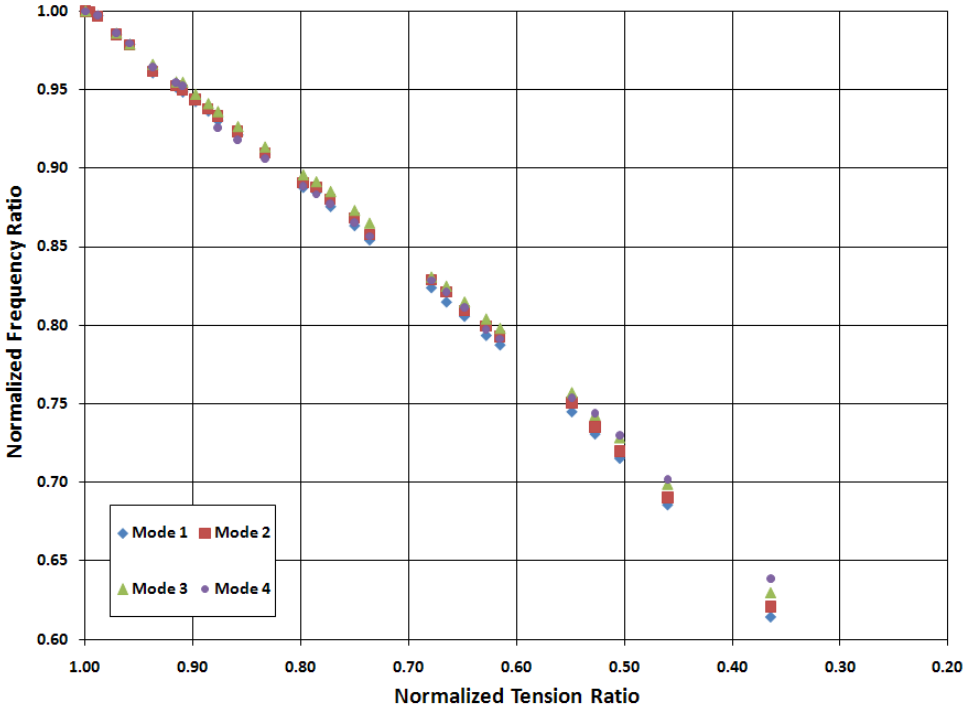

Figure 5.14: Sensitivity of Measured Natural Frequencies to Variation of Tensile Force – Specimen 4

Measured and calculated values of the fundamental natural frequency are plotted as a function of the measured tensile force in Figure 5.15. The calculated frequencies differed from the measured natural frequencies by -1 to 2% for each mode.

Measured and extracted values of the tensile force are plotted as a function of the measured fundamental natural frequency in Figure 5.16. The extracted tensile forces differed from the measured tensile forces by -2 to 1% for each mode.

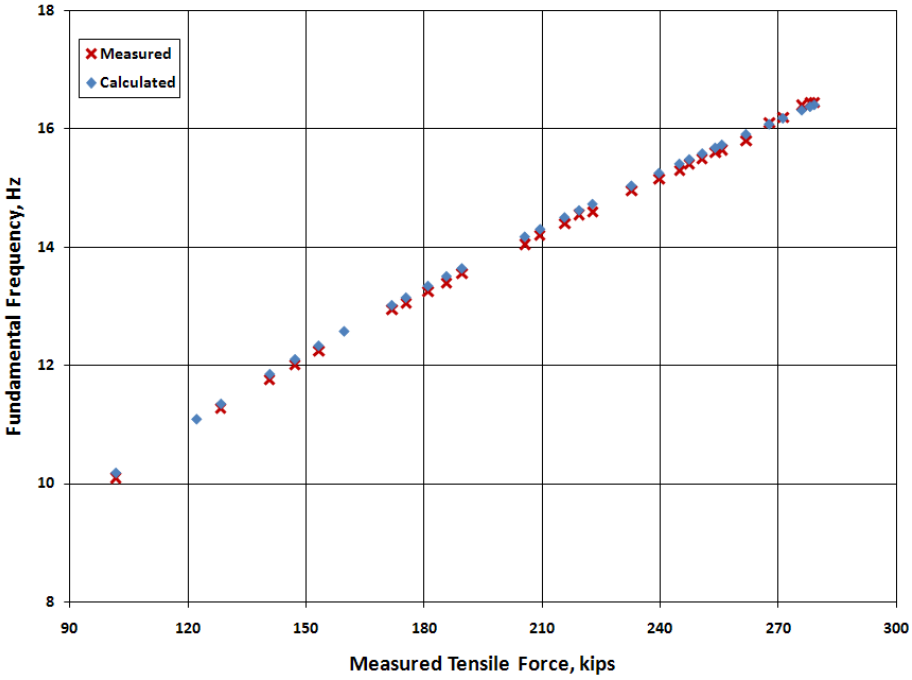

(a) Mode 1

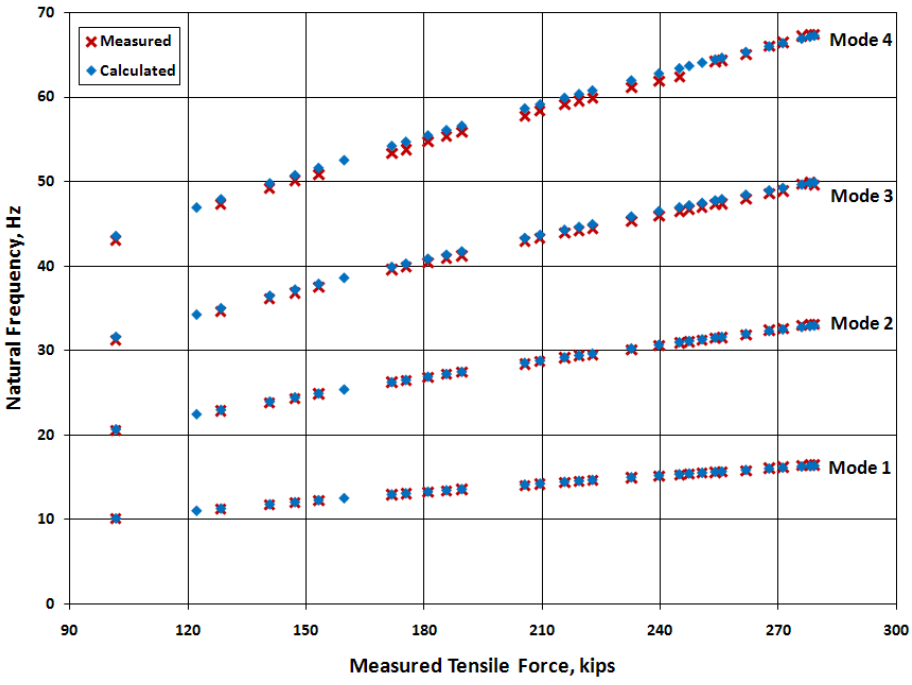

(b) All Modes

Figure 5.15: Variation Frequency in with Measured Tensile Force – Specimen 4

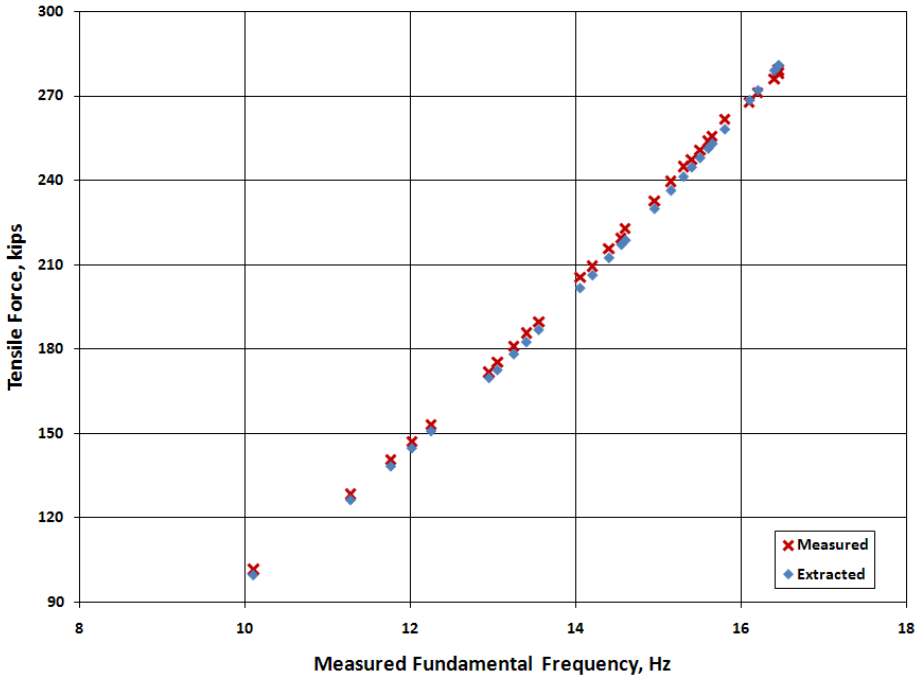

(a) Mode 1

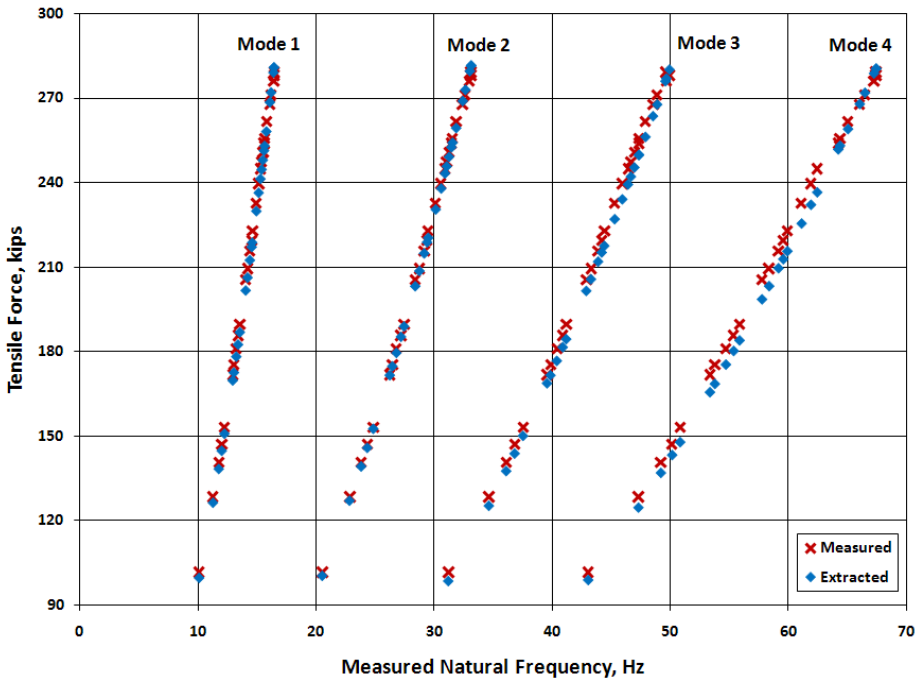

(b) All Modes

Figure 5.16: Variation in Tensile Force with Measured Frequency – Specimen 4

5.3.4 Specimen 5

The normalized frequency ratio is plotted versus the normalized tension ratio for Specimen 5 in the four plots in Figure 5.17.

The measured response of Specimen 5 is very similar to the response of Specimen 3. In the first two modes, the measured normalized frequency ratios tended to be slightly greater than the calculated normalized frequency ratios for a given level of damage. In the third and fourth mode, the measured and calculated normalized frequency ratios were essentially the same.

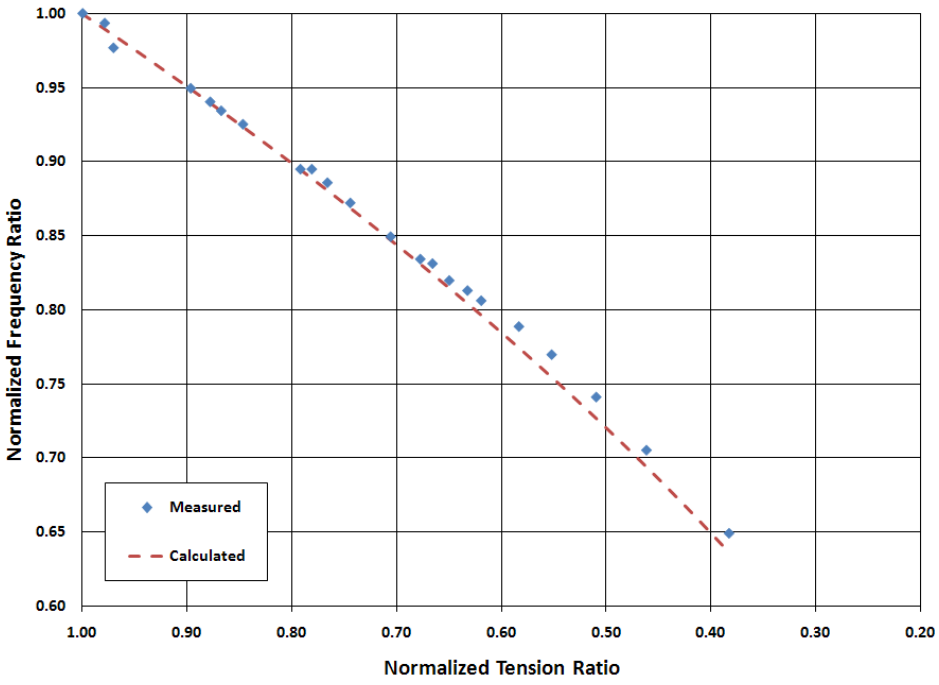

(a) Mode 1

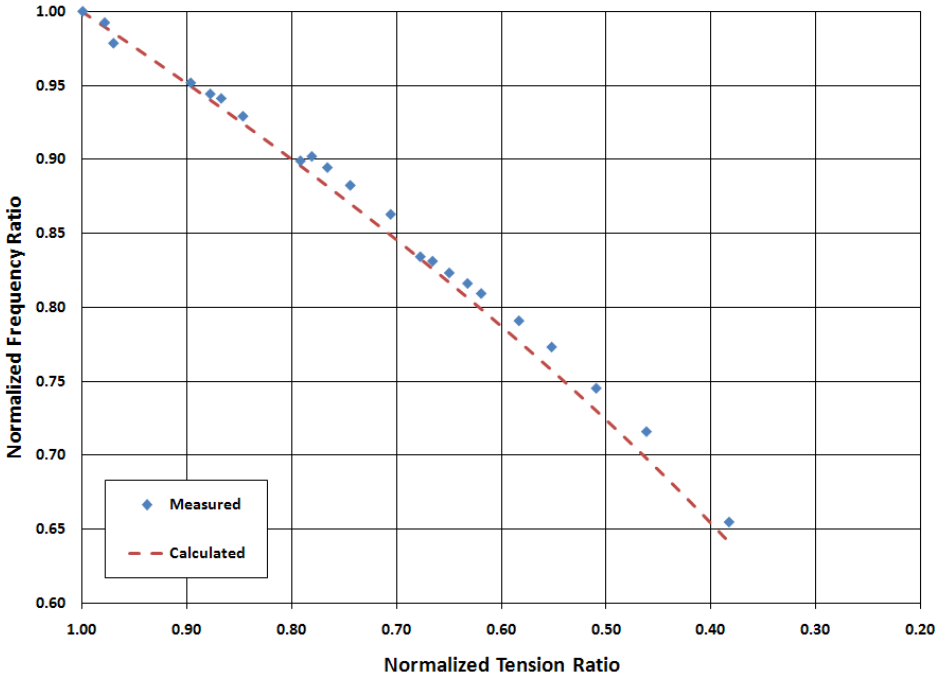

(b) Mode 2

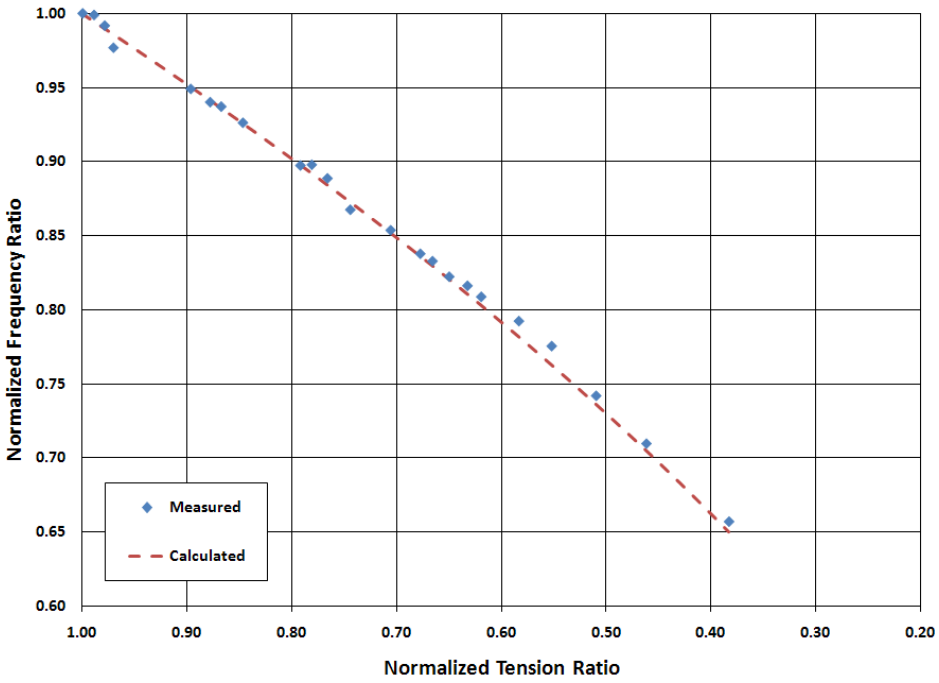

(c) Mode 3

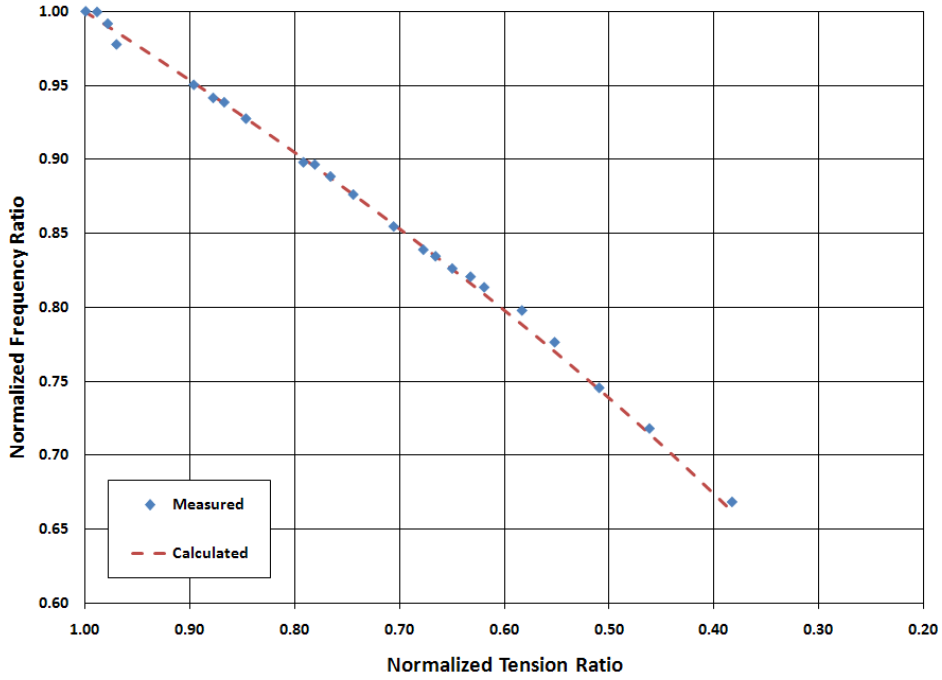

(d) Mode 4

Figure 5.17: Sensitivity of Natural Frequencies to Variation of Tensile Force – Specimen 5

The measured trends for all four modes are plotted in Figure 5.18. The final tension was 38.3% of the initial tension force. The measured frequencies at the conclusion of the test ranged from 64.9% of the initial for mode 1 to 66.9% of the initial for mode 4.

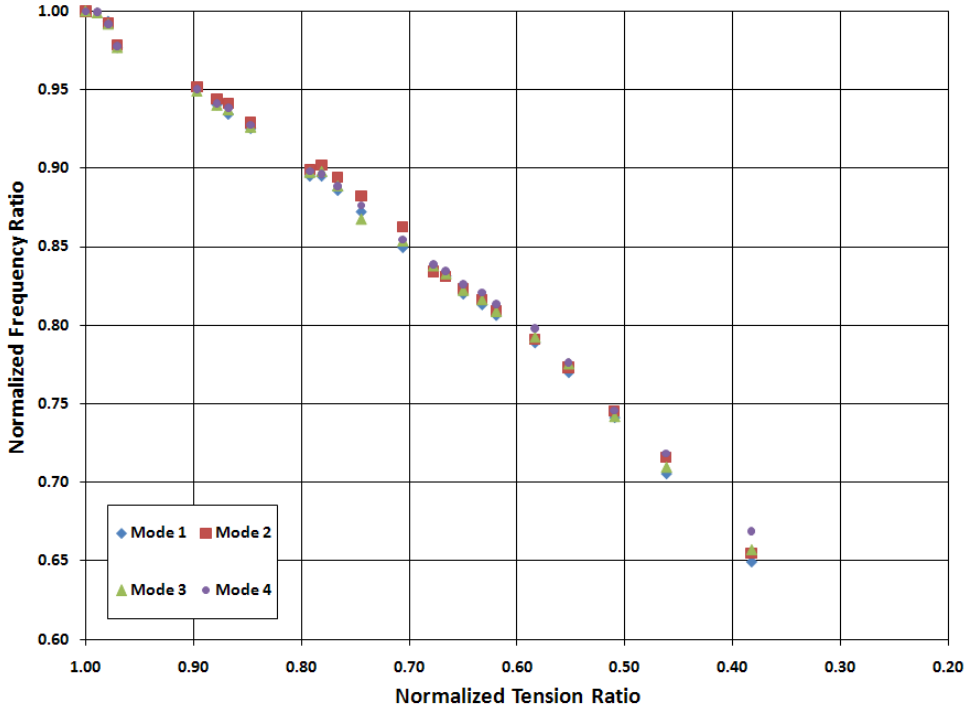

Figure 5.18: Sensitivity of Measured Natural Frequencies to Variation of Tensile Force – Specimen 5

Measured and calculated values of the fundamental natural frequency are plotted as a function of the measured tensile force in Figure 5.19. The calculated frequencies overestimated the measured natural frequencies by 0 to 3% for each mode.

Measured and extracted values of the tensile force are plotted as a function of the measured fundamental natural frequency in Figure 5.20. The extracted tensile forces underestimated the measured tensile forces by 0 to 6% for each mode.

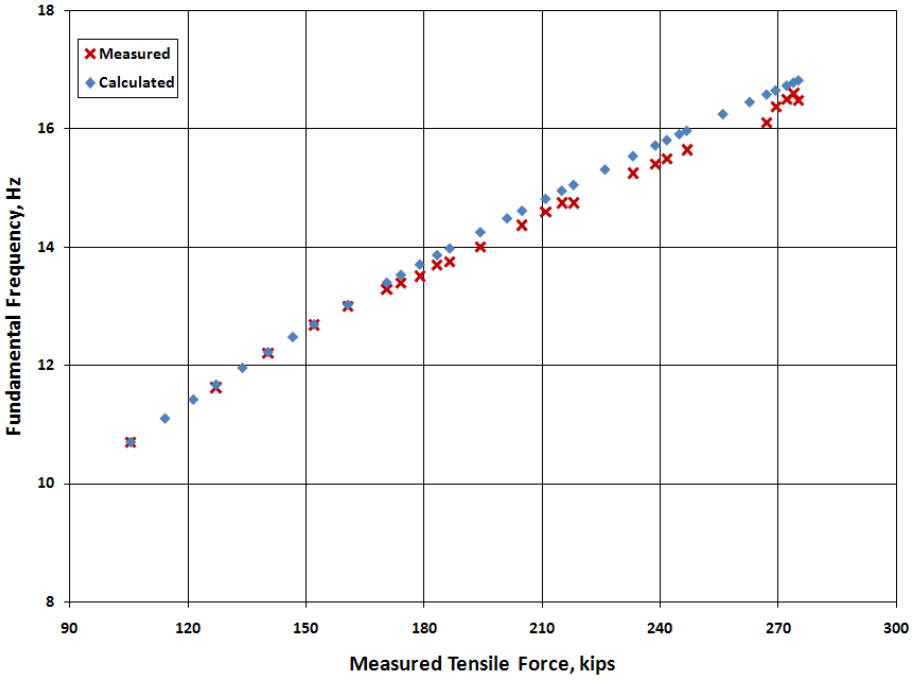

(a) Mode 1

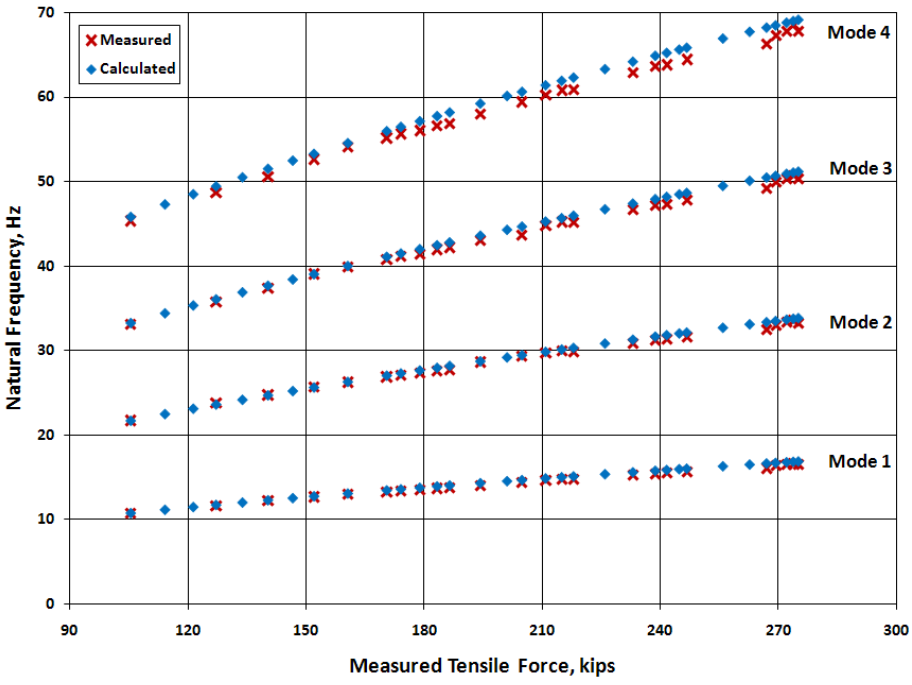

(b) All Modes

Figure 5.19: Variation in Frequency with Measured Tensile Force – Specimen 5

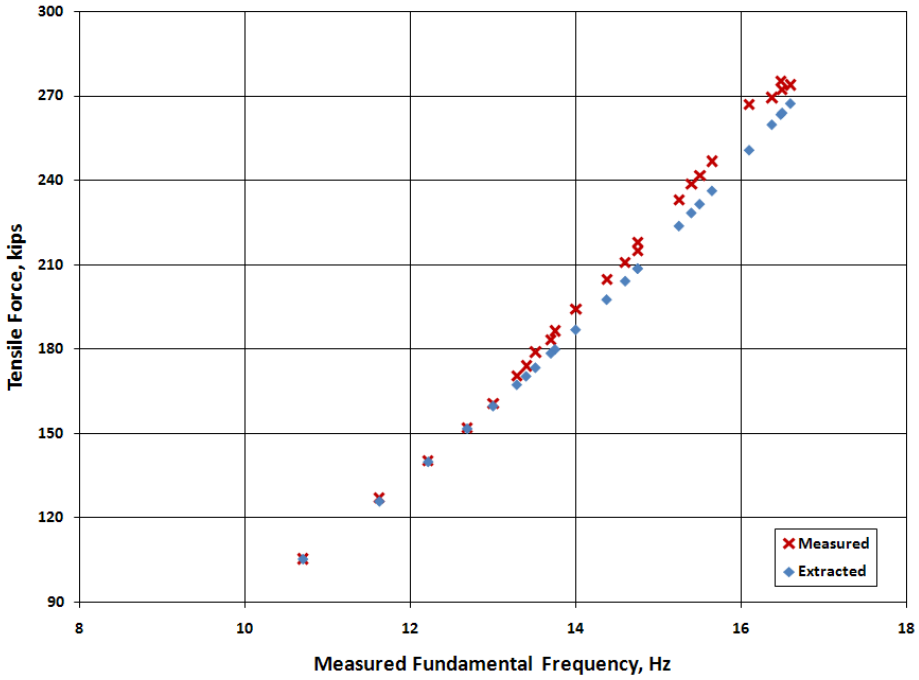

(a) Mode 1

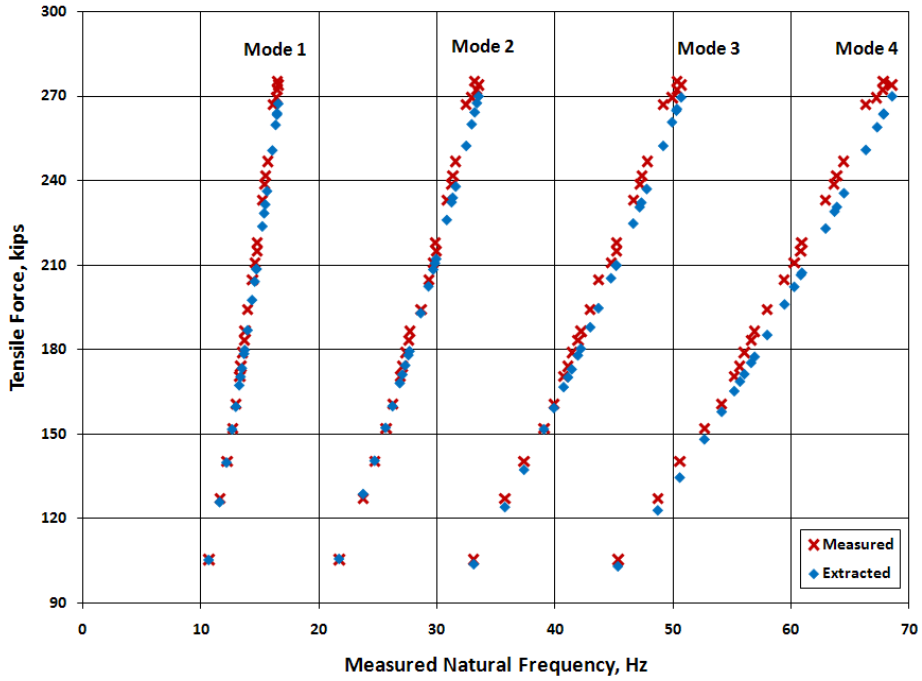

(b) All Modes

Figure 5.20: Variation in Tensile Force with Measured Frequency – Specimen 5

5.4 SUMMARY

A comparison between the measured specimen response and the Morse approximation of the stiff string model was presented in this chapter. With direct knowledge of the tensile force, mass, and length of the specimen, and a simple idealization of the flexural stiffness, the stiff string model provides a strikingly accurate representation of the natural frequencies for the external tendon specimens as they were subjected to increasing levels of local damage.

While a comparison of the measured and calculated frequencies with a known tensile force validates the model, its application is not appropriate for practical applications. Instead, a comparison between the measured and extracted tensile forces corresponding to a measured natural frequency is more pertinent. In most cases, the measured tensile forces exceeded the tensile forces extracted from the stiff string approximation. The error between the tensile force extracted from the measured frequencies and the measured tensile force for the specimens with steel anchor blocks was slightly less than the error for specimens with concrete anchor blocks.

Figure 5.21 summarizes the frequency distribution of the differences between the measured and extracted tensile forces using Equation 5.1, with the nominal structural parameters for each specimen and the measured natural frequencies for the first mode. Positive values in Figure 5.21 correspond to cases where the measured tensile force exceeded the extracted tensile force. The total variation for the four specimens ranged from -2.5 to 6.5%, with approximately 70% of the values in the range of 0 to 4.5%.

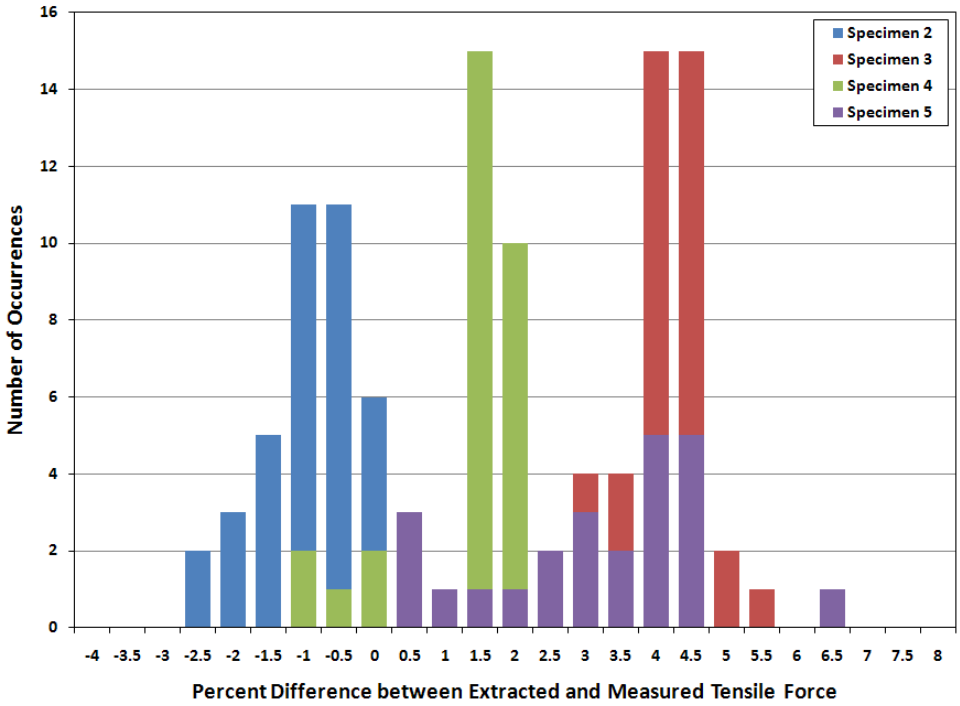

Figure 5.21: Frequency Distribution – Percent Difference in Extracted and Measured Tensile Force (combined plot)

As shown in Figure 5.22, the variation between measured and extracted tensile forces was within a 3% band for Specimens 2, 3, and 4, while Specimen 5 exhibited a 7% band of variation. More than 95% of the extracted tensile forces were within ±2% of the measured tensile forces for the specimens with steel anchor blocks. In contrast, only 12% of the extracted tensile forces were within ±2% of the measured tensile forces for the specimens with concrete anchor blocks. This observation indicates that the effective length of these specimens may exceed the clear distance between the concrete anchor blocks. However, additional experimental tests are required to determine the appropriate effective length for use in the Morse approximation.

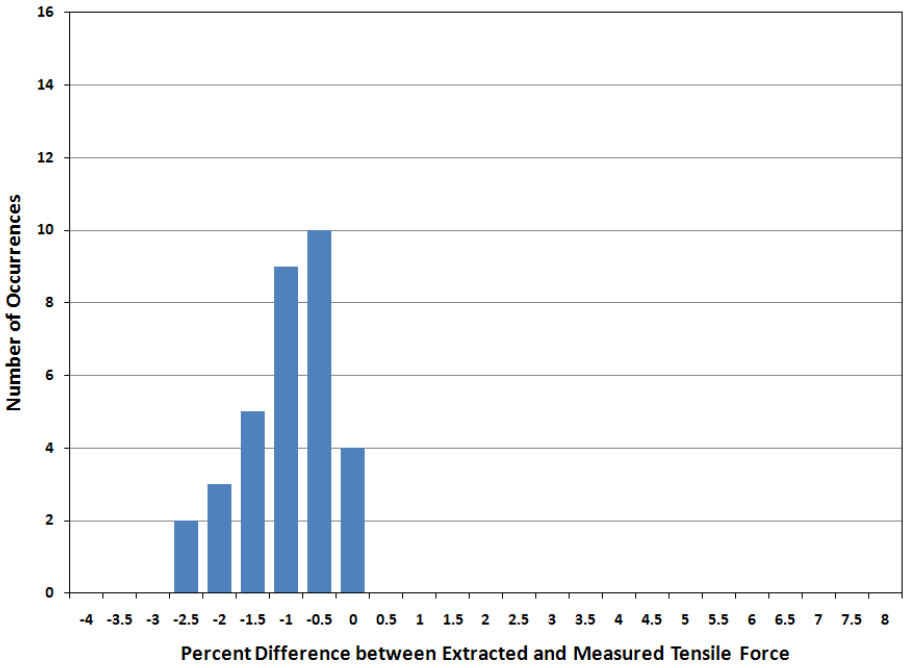

(a) Specimen 2

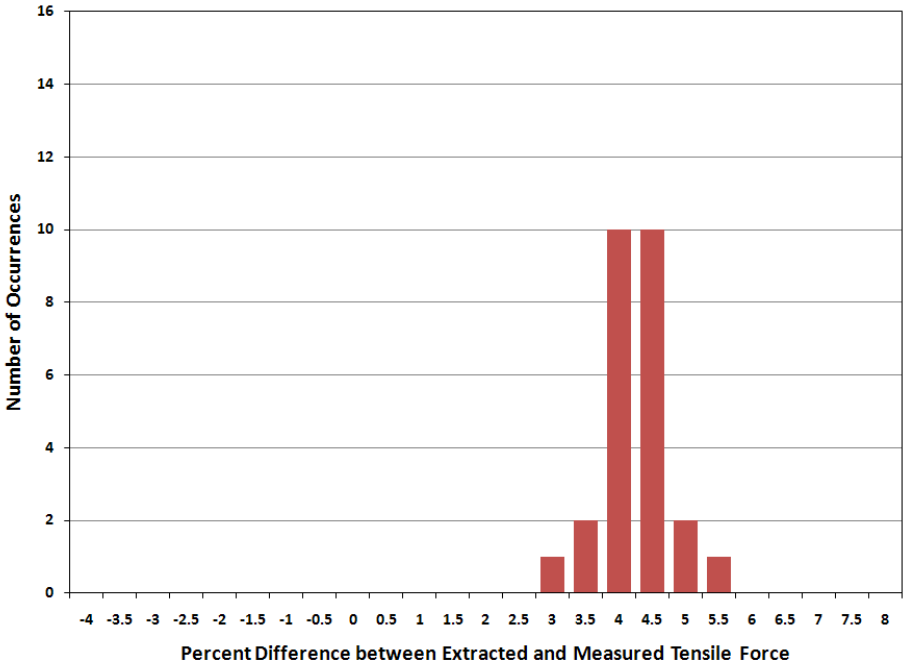

(b) Specimen 3

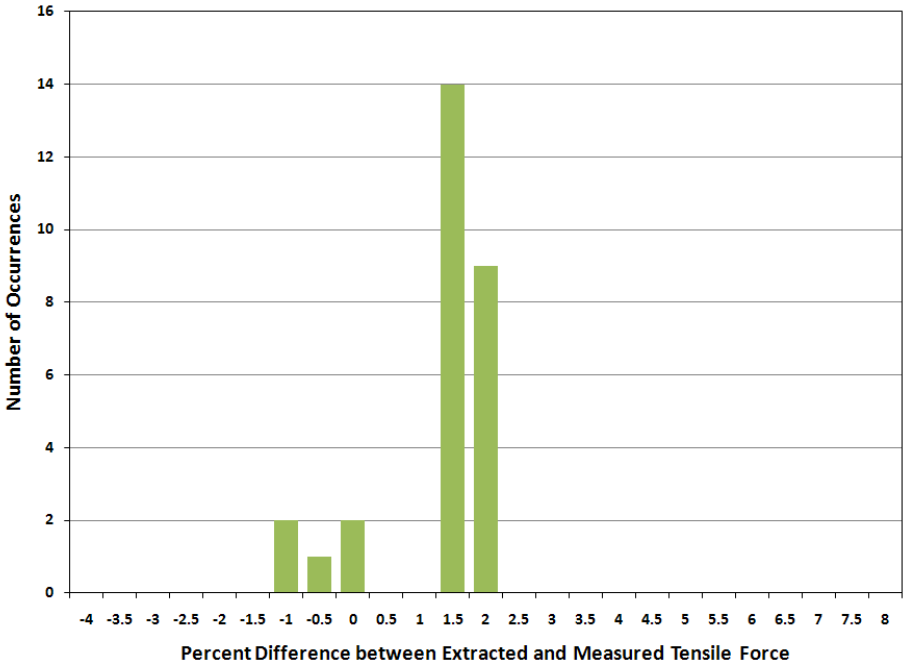

(c) Specimen 4

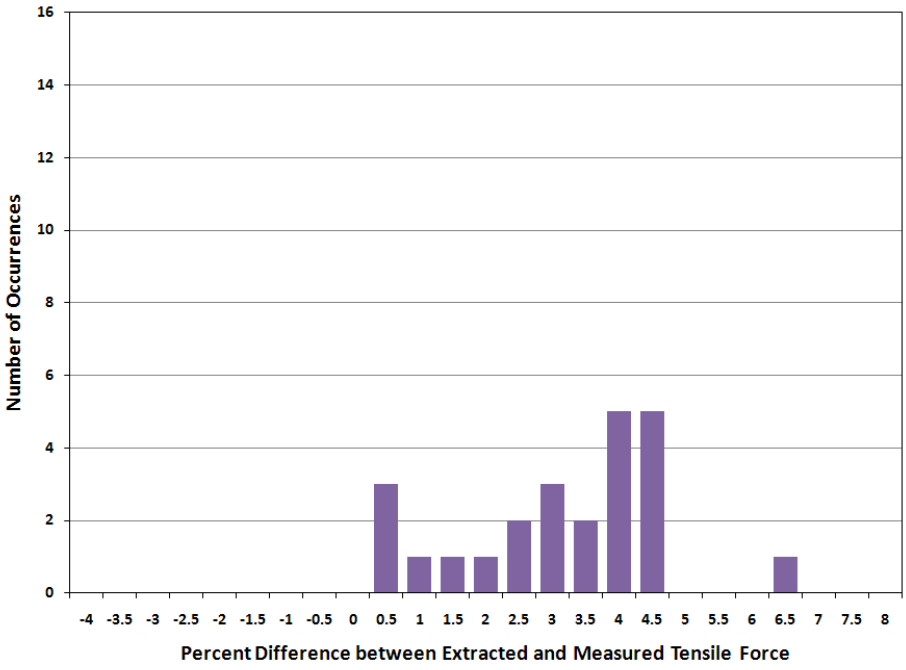

(d) Specimen 5

Figure 5.22: Frequency Distribution – Percent Difference in Extracted and Measured Tensile Force (individual plots)

CHAPTER 6

Field Measurements

6.1 OVERVIEW OF TESTING

U.S. Route 183 is a highway running across the United States from Texas to South Dakota. A portion of the highway in Austin, Texas is supported on a segmental bridge with external post-tensioned tendons (Figure 6.1). The bridge, constructed in 1997, consists of 218 spans ranging in length from 90 ft to 115 ft. The bridge was designed in accordance with the AASHTO Standard and Interim Specifications for Highway Bridges and the AASHTO Guide Specifications for Design and Construction of Segmental Concrete Bridges.

Figure 6.1: US 183 Bridge, Austin, Texas

Vibration tests were performed on the four tendons in one span in the bridge, located directly east of Interstate 35. The span was constructed with four external tendons, deviated into three sections, as shown in Figure 6.2. Each tendon was grouted and contained nineteen, 0.6-in. diameter, seven-wire strands stressed to 70% GUTS (guaranteed ultimate tensile strength).

The response of the span was measured during ninety-six free-vibration tests. A three-dimensional accelerometer, placed L/6 from each end of each segment, was used to measure the response of each tendon. For each deviated section of each tendon, eight free-vibration tests were conducted with four free-vibration tests performed at each end of the tendon segment. An impact hammer was used to induce either horizontal or vertical accelerations in the tendon (Figure 6.3). Each free-vibration test was repeated two times.

(a) Cross Section at Deviator (not to scale)

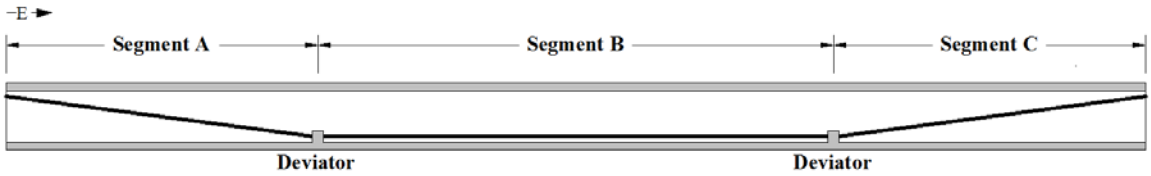

(b) Typical Span Profile (not to scale)

Figure 6.2: US 183 Bridge Cross Section and Profile

Figure 6.3: Vertical Vibration Test, US 183 Bridge

6.2 MEASURED FREQUENCY RESPONSE

The measured natural frequencies (Table 6.1) exhibited very little variation between tendons in the same segment. Regardless of whether a vibration test was performed at the west or east end of a particular tendon segment, the measured natural frequencies were identical. Slight differences were observed in the natural frequencies for vibrations in the vertical and horizontal directions.

In general, the measured frequencies in segments A and C were within ± 3% (Figure 6.4). The lower natural frequencies for segment B, compared with segments A and C, are due to its longer length (Figure 6.5). Also, the fifth mode for segment B was clearly present in the frequency spectrum. The absence of the fifth mode for segments A and C was due to the rate at which the acceleration data were acquired.

Table 6.1: Summary of Vibration Tests on US 183 Bridge

Segment	Direction	Mode	Natural Frequency (Hz)			
			Tendon 1	Tendon 2	Tendon 3	Tendon 4
A	Vertical	1	20.05	19.85	19.8	19.95
		2	41	40.4	40.4 / 41.05*	40.65
		3	63.65	62.35	62.2 / 63.6*	62.85
		4	88.5	86.2	85.75 / 88.45*	87.15
	Horizontal	1	19.95	20.1	20.1	20.1
		2	40.7	41.1	41.05	41
		3	62.9	63.9	63.6 / 62.2*	63.7
		4	87.1	89.1	88.45 / 85.75*	88.7
B	Vertical	1	11.75	11.75	11.8	11.65
		2	23.7 / 23.95*	23.7	23.7	23.45
		3	35.9 / 36.35*	35.85	35.85	35.6
		4	48.55 / 49.2*	48.45	48.4	48.1
		5	61.75 / 62.6*	61.55	61.5	61.2
	Horizontal	1	11.9	11.95	11.95	11.85
		2	23.95 / 23.7*	24.05	24.05	23.95
		3	36.35 / 35.9*	36.55	63.6	36.4
		4	49.2 / 48.55*	49.65	88.45	49.5
		5	62.6 / 61.75*	63.45	63.4	63.35
C	Vertical	1	20.2	20.1	20.15	19.95
		2	41	40.9	40.4	40.55
		3	63.05 / 64.25*	62.85	62.2	62.5
		4	86.95 / 89*	86.75	88.45	86.25
	Horizontal	1	20.5	20.35	20.35	20.3
		2	41.7 / 41*	41.6	41.55	41.5
		3	64.25 / 63.05*	64.3	63.6	64.45
		4	89	89.6	88.45	89.7

*Denotes the presence of dual peaks. The larger amplitude is displayed first.

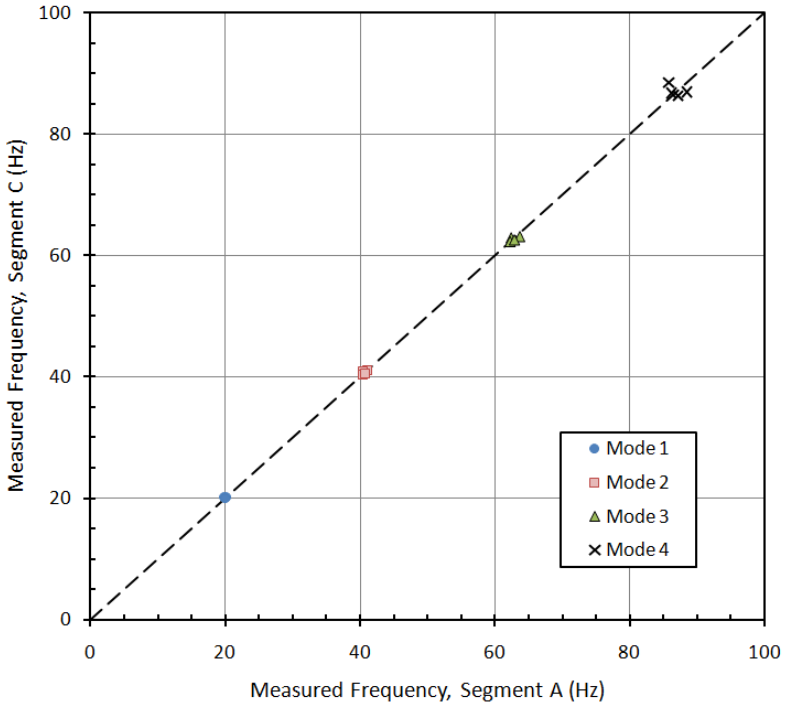

Figure 6.4: Comparison of Measured Frequency Response in Segments A and C

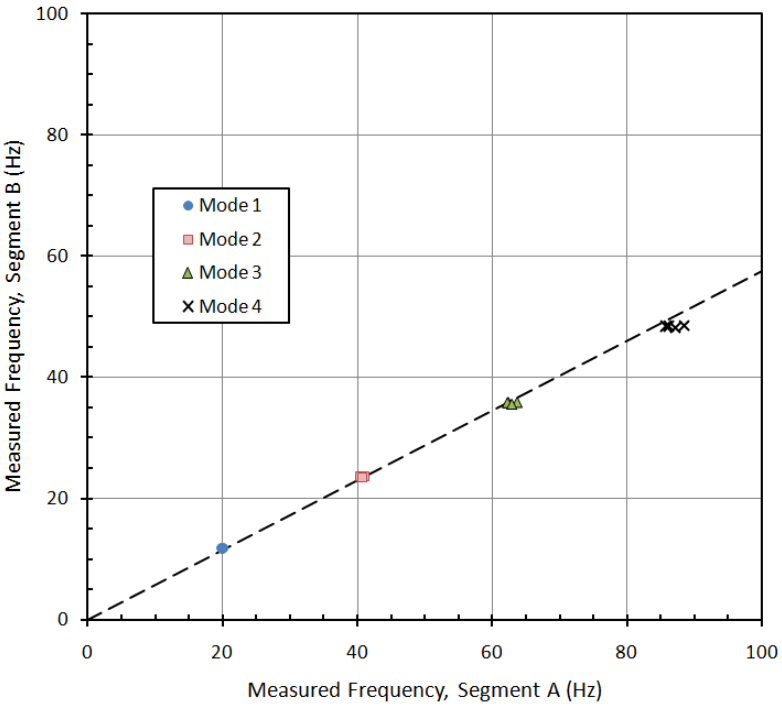

Figure 6.5: Comparison of Measured Frequency Response in Segments A and B

6.3 DUAL PEAKS

As experienced with the laboratory specimens, dual peaks were observed in the frequency spectrum for the US 183 vibration tests. In most cases, if a dual peak existed, it was present in both the vertical and horizontal directions of vibration. In segment A, dual peaks were observed in tendon 3 only. For segments B and C, dual peaks were observed in tendon 1. The frequency spectra corresponding to the horizontal and vertical directions of vibration for segment B of tendon 1 are shown in Figure 6.6.

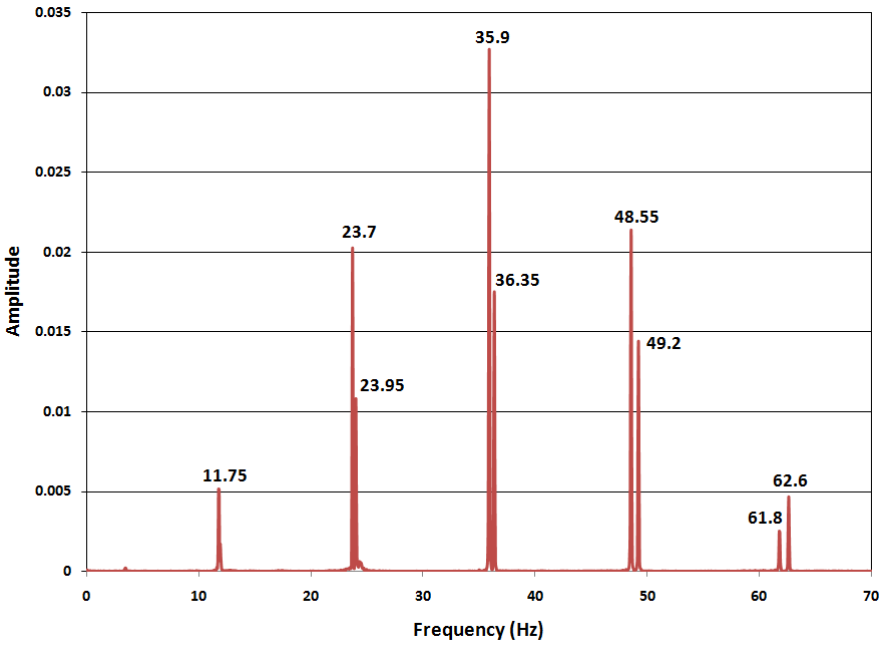

(a) US 183 – Segment B, Tendon 1 - Vertical Excitation

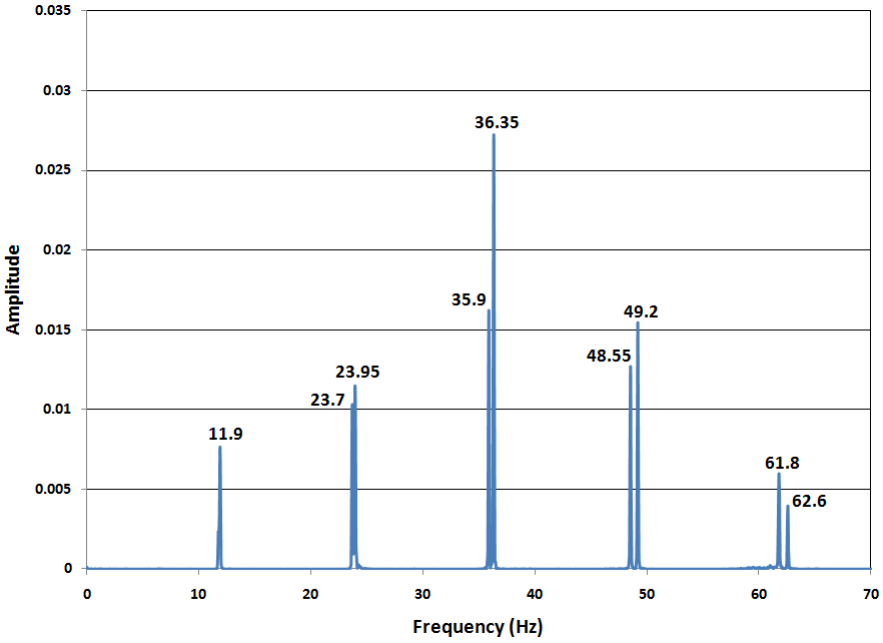

(b) US 183 – Segment B, Tendon 1 – Horizontal Excitation

Figure 6.6: US 183 Vibration Test – Double Peaks in the Frequency Spectrum

The dual peaks are attributed to variations in the strand arrangement along the length of the tendon. The idealized strand arrangement is shown in Figure 6.7(a). At deviator locations, the strands are expected to be concentrated at the top of the duct (Figure 6.7b).

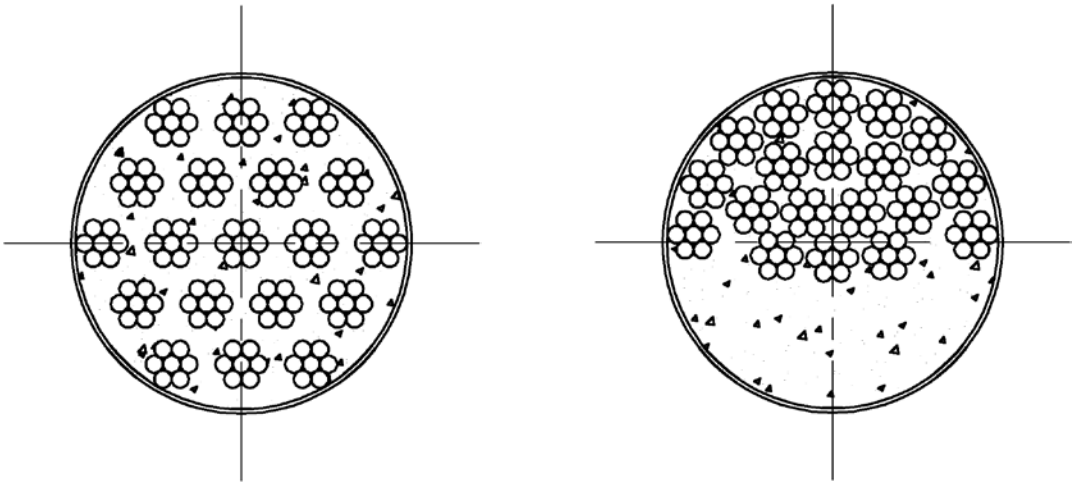

(a) Idealized Section (b) Assumed Deviator Section

Figure 6.7: US 183 Bridge - Tendon Cross Section

The calculated flexural stiffness's for the idealized section and assumed deviator section for bending about both the vertical and horizontal axis are reported in Table 6.2 and detailed in Appendix A. The values of flexural stiffness are essentially the same for vertical and horizontal bending for the idealized cross section. However, using the idealized deviator cross section, the horizontal flexural stiffness is 10% larger than the vertical flexural stiffness. These results are consistent with the higher measured frequencies for free vibration in the horizontal direction.

Table 6.2: US 183 Bridge - Calculated Flexural Stiffness

Section	Flexural Stiffness (kip-in^2)		Vertical / Horizontal Stiffness
	Vertical Bending	Horizontal Bending	
Idealized	132600	132600	1.000
Deviator	122200	135100	0.905

6.4 CALCULATED RESPONSE

An attempt was made to compare the measured frequencies of the tendons with those calculated using the stiff string model. Assumed values of the structural parameters used in the calculations are summarized in Table 6.3.

Table 6.3: Assumed Structural Parameters for US 183 Bridge

Parameter	Value
Flexural Stiffness	132,600 kip-in^2
Unit Mass	0.65 lb-sec^2/ft^2
Tension Force (70% GUTS)	780 kips
Length (Segments A & C)	27 ft. - 5 in.
Length (Segment B)	45 ft. - 3 in.
λ^2 (Segments A & C)	0.00010
λ^2 (Segment B)	0.00028
γ (Segments A & C)	25.2
γ (Segment B)	41.6

The flexural stiffness was calculated assuming an idealized cross-section (Figure 6.7a) and typical modulus of elasticity values for prestressing strand and grout. The unit mass was calculated by ignoring the mass of the duct and using the average density of the grout from the laboratory specimens. The tensile force was assumed to be equal to the design level of initial prestress - 70% GUTS. The clear length of each segment was measured directly at the mid-depth of the cross section. The parameters λ^2 and γ were calculated using the equations in Section 5.1.5. The unit mass, flexural stiffness and tensile force were assumed to be constant along the entire length of the tendon.

The idealized variation between the tensile force and frequency is plotted in Figure 6.8. All calculations are based on the approximate solution for the stiff string model developed by Morse (Section 5.1).

Clear differences may be observed between the calculated response of the shorter segments (A and C) compared with the longer segment (B). The frequencies corresponding to the higher modes in the shorter segments are more sensitive to changes in the tensile force.

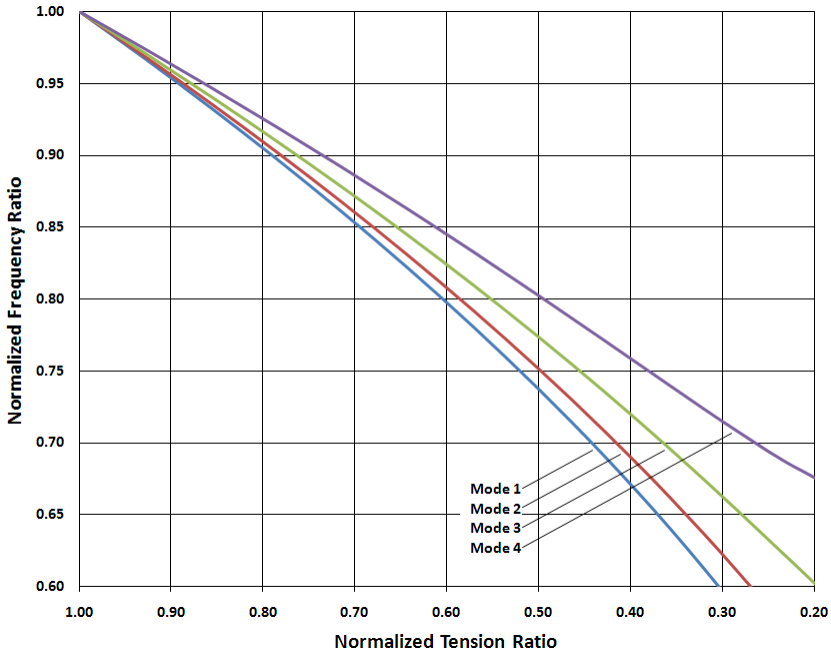

(a) Segments A and C

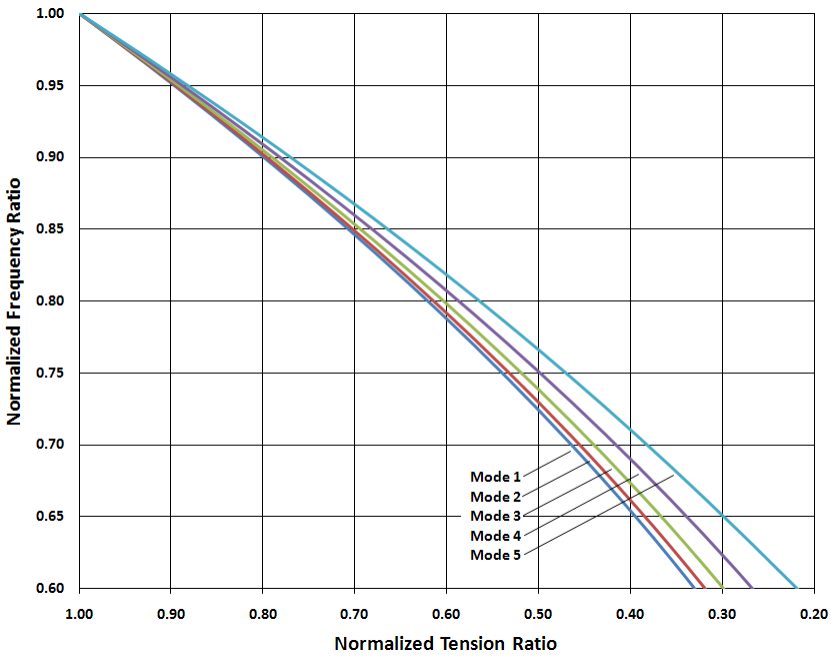

(b) Segment B

Figure 6.8: US 183 Bridge – Calculated Relationship between the Tensile Force and Natural Frequency using Morse Approximation

The non-dimensional parameters λ^2 and γ give a good indication of system behavior. As mentioned in Section 5.1.5, sag can be ignored as λ^2 approaches zero and gamma of approximately 50 was determined to be the cutoff value between beam and cable action. For all segments, the value of λ^2 was comparable to the higher stressed laboratory specimens (Table 5.2). The value of gamma for Segment B ($\gamma = 41.6$) was also comparable to the lab specimens ($\gamma > 40$). Conversely, the value of gamma for Segments A and C ($\gamma = 25.2$) was much lower than the lab specimens.

The following two sections use the measured data in two separate ways to observe the behavior of the bridge tendons. In Section 6.4.1, the measured natural frequencies were inputted into the Morse approximation and a tensile force was computed for each mode separately. This value was compared with the theoretical design tensile force of the tendons. In Section 6.4.2, the design tensile force was inputted into the Morse approximation and a theoretical natural frequency was computed for each mode. The measured natural frequencies were then compared with the calculated frequencies.

6.4.1 Tensile Force Extracted from the Measured Natural Frequencies

The tensile forces extracted from the measured frequencies using the stiff string model are compared with the design tensile force in Table 6.4. For segments A and C (Figure 6.9 and Figure 6.10), the extracted tensile forces were 15 - 20% less than the design levels for the first mode. As the mode number increased, the differences between the extracted tensile forces and the design tensile force became larger. The differences ranged from 25 – 30% for mode 4.

Table 6.4: Comparison of Tensile Force Extracted from Measured Frequencies in Vertical Direction and Design Tensile Force for US 183 Bridge

Segment	Tendon	Design Tensile Force (kips)	Extracted Tensile Force (kips)					Extracted / Design Tensile Force				
			Mode 1	Mode 2	Mode 3	Mode 4	Mode 5	Mode 1	Mode 2	Mode 3	Mode 4	Mode 5
A	1	780	643	638	628	603	-	0.83	0.82	0.81	0.77	-
	2		629	616	594	556	-	0.81	0.79	0.76	0.71	-
	3		625	616	591	547	-	0.80	0.79	0.76	0.70	-
	4		636	625	607	575	-	0.82	0.80	0.78	0.74	-
Segment	Tendon	Design Tensile Force (kips)	Extracted Tensile Force (kips)					Extracted / Design Tensile Force				
			Mode 1	Mode 2	Mode 3	Mode 4	Mode 5	Mode 1	Mode 2	Mode 3	Mode 4	Mode 5
B	1	780	654	653	644	633	638	0.84	0.84	0.83	0.81	0.82
	2		654	653	642	630	611	0.84	0.84	0.82	0.81	0.78
	3		660	653	642	628	610	0.85	0.84	0.82	0.81	0.78
	4		643	638	632	619	602	0.82	0.82	0.81	0.79	0.77
Segment	Tendon	Design Tensile Force (kips)	Extracted Tensile Force (kips)					Extracted / Design Tensile Force				
			Mode 1	Mode 2	Mode 3	Mode 4	Mode 5	Mode 1	Mode 2	Mode 3	Mode 4	Mode 5
C	1	780	654	638	612	571	-	0.84	0.82	0.79	0.73	-
	2		646	635	607	567	-	0.83	0.81	0.78	0.73	-
	3		650	616	591	602	-	0.83	0.79	0.76	0.77	-
	4		636	622	598	557	-	0.82	0.80	0.77	0.71	-

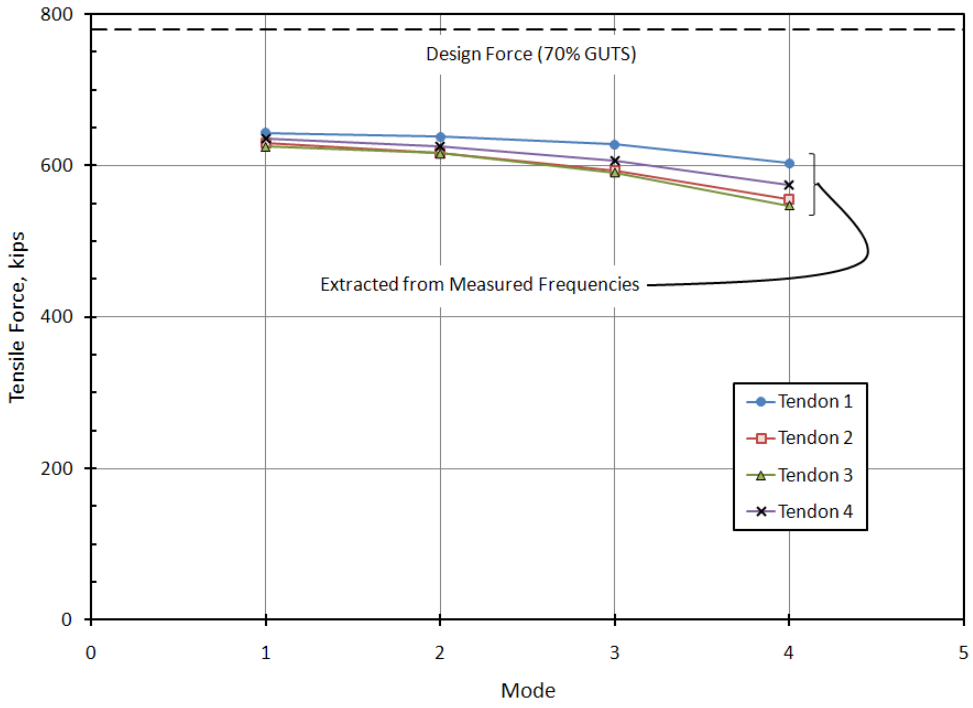

Figure 6.9: Variation of Tensile Forces Extracted from Measured Frequencies for Segment A

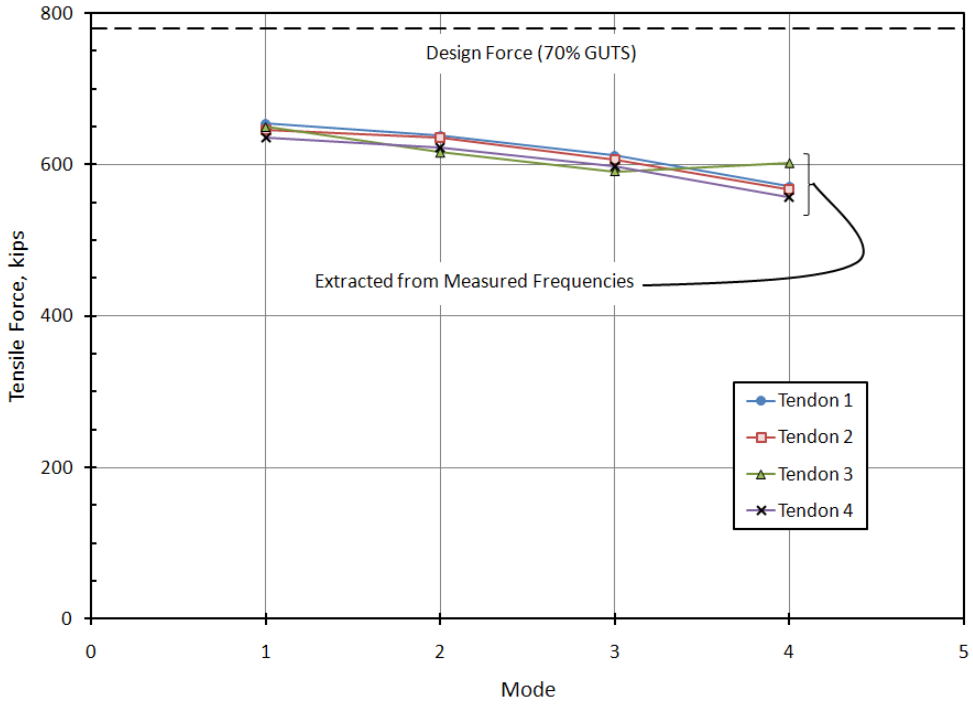

Figure 6.10: Variation of Tensile Forces Extracted from Measured Frequencies for Segment C

The trends were similar for segment B (Figure 6.11), but the magnitudes of the differences were smaller. The extracted tensile forces for segment B were 15 to 18% less than the design force for the first mode and 18 to 23% less than the design force for the fifth mode. These results indicate that the Morse approximation becomes less reliable for values of γ less than 40.

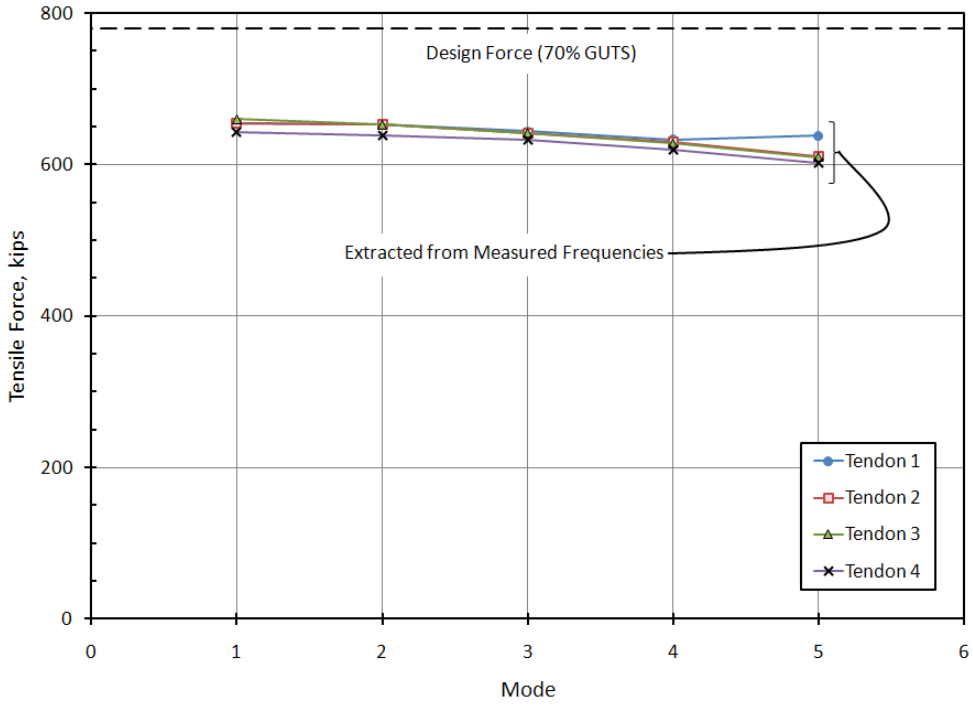

Figure 6.11: Variation of Tensile Forces Extracted from Measured Frequencies for Segment B

6.4.2 Calculation of Natural Frequencies from Design Tensile Force

The measured frequencies are compared with those calculated using the Morse approximation of the stiff string model in Table 6.5. For the comparisons, the measured frequencies in the vertical directions are used. If dual peaks were observed in the measured response, the dominant peak was used in the comparison. Similar to the laboratory tests, the calculated frequencies were greater than the measured frequencies in each case. Differences between the measured and calculated frequencies were generally between 9 to 12%, compared with -1 to 4% for the laboratory specimens. As the mode number increases, the error between the calculated and measured natural frequency increased.

Table 6.5: Comparison of Measured Frequencies in Vertical Direction and Calculated Frequencies Using Stiff String Model for US 183 Bridge

Segment	Tendon	Calculated Natural Frequency (Hz)					Calculated / Measured Frequency				
		Mode 1	Mode 2	Mode 3	Mode 4	Mode 5	Mode 1	Mode 2	Mode 3	Mode 4	Mode 5
A	1	21.86	44.64	69.28	96.71	-	1.09	1.09	1.09	1.09	-
	2						1.10	1.10	1.11	1.12	-
	3						1.10	1.10	1.11	1.13	-
	4						1.10	1.10	1.10	1.11	-
Segment	**Tendon**	**Calculated Natural Frequency (Hz)**					**Calculated / Measured Frequency**				
		Mode 1	**Mode 2**	**Mode 3**	**Mode 4**	**Mode 5**	**Mode 1**	**Mode 2**	**Mode 3**	**Mode 4**	**Mode 5**
B	1	12.76	25.72	39.10	53.09	67.91	1.09	1.09	1.09	1.09	1.08
	2						1.09	1.09	1.09	1.10	1.10
	3						1.08	1.09	1.09	1.10	1.10
	4						1.09	1.10	1.10	1.10	1.11
Segment	**Tendon**	**Calculated Natural Frequency (Hz)**					**Calculated / Measured Frequency**				
		Mode 1	**Mode 2**	**Mode 3**	**Mode 4**	**Mode 5**	**Mode 1**	**Mode 2**	**Mode 3**	**Mode 4**	**Mode 5**
C	1	21.86	44.64	69.28	96.71	-	1.08	1.09	1.10	1.11	-
	2						1.09	1.09	1.10	1.11	-
	3						1.08	1.10	1.11	1.09	-
	4						1.10	1.10	1.11	1.12	-

6.5 SUMMARY

Vibration tests were performed on one span of the US 183 bridge in Austin, Texas. It would have been interesting to test the tendons in multiple spans to determine if the observed trends were consistent, but several constraints severely limited the amount of field testing conducted in this investigation. Nevertheless, valuable information on the accuracy of the Morse approximation of the stiff string model was obtained.

Because less information was known about the structural parameters used to model the response of the tendons, the errors associated with the Morse approximation increased. In addition, in extracting the tensile force from the measured natural frequencies, errors increased as the mode number increased. This trend was especially apparent in segments A and C, which had a gamma much less than segment B and the laboratory specimens. This observation implies that the accuracy of the Morse approximation decreases as the tendon response approaches that of an axially-loaded beam.

CHAPTER 7

Summary

The primary objective of this investigation was to determine how the tensile force and natural frequencies changed as local damage accumulated in external post-tensioned tendons in the laboratory. A secondary objective was to determine if the Morse approximation of the stiff string model was sufficient to reproduce the measured experimental trends.

A technique was developed to corrode single wires in succession in the laboratory specimens. Therefore, the local damage accumulated in a quantifiable fashion. Variations in the natural frequencies and tensile force were monitored as local damage increased and the sensitivity of the measured frequency response to variations in the tensile force was evaluated. The Morse approximation was used to extract tensile forces from the measured frequencies to determine the variability inherent in the non-destructive approach.

7.1 SUMMARY OF LABORATORY TESTS

Four external tendons were tested in the laboratory during this project. Each specimen was grouted and contained seven, 0.6-in. diameter, seven-wire strands. The configuration of the anchor blocks and the level of initial stressing were the two primary experimental parameters. Two specimens were stressed to 40% GUTS (guaranteed ultimate tensile strength), while the other two were stressed to 70% GUTS. For each level of initial prestress, one tendon had concrete anchor blocks, while the other had steel anchor blocks. The different end conditions were selected to determine the effective length of the tendons.

During each test, the tensile force in the specimen was monitored using a load cell and strain gages attached to the strands. The strain gages also monitored the redistribution

in stress in the tendon. The natural frequencies were determined from the measured acceleration response as the specimen was subjected to a series of free-vibration tests.

7.1.1 Sensitivity of Tensile Force to Damage Accumulation

The tensile force in the tendons tested in the laboratory was monitored as damage accumulated. For specimens 2 and 3, the strains in individual strands were also monitored. As the level of damage increased in a tendon, the reduction in tensile force was fairly consistent among the four specimens. A 60% reduction in the cross-sectional area of the strands resulted in a 40 to 50% reduction in the tensile force. The specimens with higher levels of initial prestress experienced a larger reduction than the specimens with lower levels of initial prestress.

The loss in tensile force was not linear with the loss of cross-sectional area of the strand. Two mechanisms contributed to stress redistribution. Friction between wires permitted redistribution of stress among wires within a given prestressing strand and the grout was capable of transmitting tensile stresses among strands. The level of stress redistribution was greater for the specimens with the lower level of initial prestress.

7.1.2 Sensitivity of Natural Frequencies to Damage Accumulation

The natural frequencies were not as sensitive to the level of induced damage as the tensile force. A 60% reduction in the cross-sectional area of the strands corresponded to a 20 to 30% reduction in the fundamental frequency. The specimens with higher levels of initial prestress were more sensitive to the damage than the specimens with lower levels of initial prestress.

Dual peaks were observed in a relatively small number of the frequency measurements. The peaks are believed to be caused by differences in the moment of inertia of the tendon in the horizontal and vertical directions. There did not appear to be any correlation between the presence/absence of dual peaks and the type of anchor block used at the end of the test specimens.

7.2 SUMMARY OF FIELD MEASUREMENTS

In applying the Morse approximation to the US 183 bridge, a greater number of structural parameters had to be assumed. Consequently, the errors associated with the approximation increased. In addition, in extracting the tensile force from the natural frequencies, errors increased as the mode number increased. This was especially apparent in the shorter length segments, which had a gamma much less than the longer length segment and the laboratory specimens. This observation implies that the accuracy of the Morse approximation decreases as the tendon response approaches that of an axially-loaded beam.

7.3 INHERENT VARIABILITY USING THE VIBRATION METHOD TO EVALUATE EXTERNAL TENDONS

Sagues (2006) and Lee (2007) used the stiff string idealization and the approximate solution proposed by Morse (1948) to represent the dynamic response of external tendons. Four parameters, related to the geometry and material properties of the tendon are used in this idealization: unit mass, length, tensile force, and flexural stiffness. All four parameters are assumed to remain constant along the length of the tendon.

For the laboratory specimens tested in this investigation, the tensile force was measured throughout the experiments. The unit mass was taken as the average of two measurements and the length was taken as the clear distance between the inner faces of the anchor blocks. Simple approximations were made to estimate the moduli of elasticity for the grout and prestressing strand and the moment of inertia was calculated based on an idealized cross section. The tensile forces extracted from the measured fundamental frequencies were within -2.5 to 6.5% of the measured tensile forces. The trends were similar for all four test specimens and were not sensitive to the level of initial prestress or the level of induced damage, but did appear to depend on the type of anchor block. While these differences are not significant, the results demonstrate that even under ideal circumstances, the tensile forces extracted from Morse's approximation will typically

underestimate the actual tensile forces in grouted tendons. Approximately 70% of the extracted tensile forces were between 0 to 4.5% of the measured tensile forces.

When evaluating the measured response of the tendons of the US 183 bridge, the differences between the extracted tensile forces and the design tensile force were considerably larger than the differences between the extracted and measured tensile forces for the laboratory specimens. This comparison is not completely valid, because the actual tensile force in the tendons may not be equal to the design tension force. It is possible that the actual tensile force in each tendon was less than the design tensile force due to the accumulation of losses during the thirteen years that the bridge has been subjected to service loads. However, other explanations for the differences are also possible:

a. Less information was known about the geometric and structural properties of the bridge tendons than the laboratory specimens. The unit mass of the bridge tendons could not be measured and the relative positions of the individual strands in each tendon duct were expected to vary along the length due to the presence of the deviators. Therefore, larger errors in the idealized structural parameters used in the Morse approximation are expected for the bridge tendons, which would lead to larger differences between the extracted and actual tensile forces.
b. The Morse approximation appears to have more inherent error for the shorter tendon segments ($\gamma = 25.2$) compared to the longer tendon segments ($\gamma = 41.6$) and the laboratory specimens ($\gamma > 40$).

Due to the consistency of the measured data from similar tendons and the lack of visual indications of damage, differences between the laboratory specimens and the bridge tendons are believed to be caused by larger levels of inherent error in the Morse approximation, rather than a 15 to 20% reduction in the tendon tensile force. The data in this investigation support the conclusions reached in the Mid-Bay Bridge study (Corven, 2001) that vibration testing is most appropriately used in comparing relative differences between equally stressed segments of a particular tendon. Differences on the order of

20% between tensile forces extracted from the measured frequencies and the design tensile forces are considered to be within the inherent variability of vibration testing.

APPENDIX A

Flexural Stiffness Calculations

A.1 LABORATORY SPECIMENS

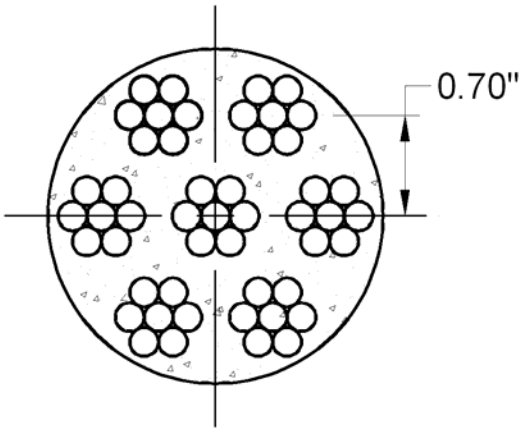

Nominal Dimensions

Strand diameter = 0.6 in

Strand area = 0.217 in^2

Effective strand diameter = 0.53 in

Duct ID = 2.28 in

E_s = 29500 ksi

f'_g = 4000 psi

E_g = 3605 ksi

Moment of Inertia

$I_{o,strand} = \pi * d^2 / 64 = 0.0037\ in^4$

$I_{duct} = \pi * d^2 / 64 = 1.33\ in^4$

layer	# strands	d (in)	A_s (in^2)	$A_s d^2$ (in^4)
1	2	0.70	0.43	0.21
2	3	0	0.65	0.00
3	2	-0.70	0.43	0.21

$I_{strands} = 7 * I_{o,strand} + \Sigma A d^2 = 0.452\ in^4$

$I_{grout} = I_{duct} - I_{strands} = 0.875\ in^4$

$I = I_s + (E_g/E_s) * I_{grout} = 0.558$ in^4

$E_s * I =$ **EI = 16475 k-in^2**

A.2 US 183 BRIDGE TENDONS – IDEALIZED VERTICAL FLEXURAL STIFFNESS

Nominal Dimensions

Strand diameter = 0.6 in

Strand area = 0.217 in^2

Effective strand diameter = 0.53 in

Duct ID = 3.94 in

E_s = 29500 ksi

f'_g = 4000 psi

E_g = 3605 ksi

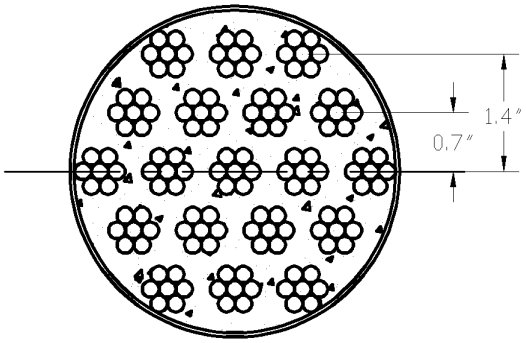

Moment of Inertia

$I_{o,strand} = \pi * d^2 / 64 = 0.0037\ in^4$

$I_{duct} = \pi * d^2 / 64 = 11.83\ in^4$

layer	# strands	d (in)	A_s (in^2)	$A_s d^2$ (in^4)
1	3	1.4	0.65	1.28
2	4	0.7	0.87	0.43
3	5	0	1.09	0.00
4	4	-0.7	0.87	0.43
5	3	-1.4	0.65	1.28

$I_{strands} = 19 * I_{o,strand} + \Sigma Ad^2 = 3.474\ in^4$

$I_{grout} = I_{duct} - I_{strands} = 8.355\ in^4$

$I = I_s + (E_g/E_s) * I_{grout} = 4.495\ in^4$

$E_s * I =$ **$EI = 132597\ k\text{-}in^2$**

A.3 US 183 BRIDGE TENDONS – IDEALIZED HORIZONTAL FLEXURAL STIFFNESS

Nominal Dimensions

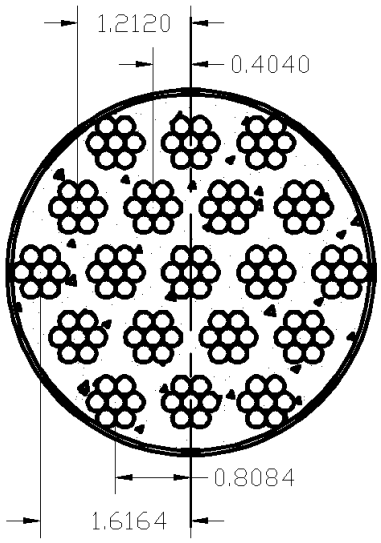

Strand diameter = 0.6 in

Strand area = 0.217 in^2

Effective strand diameter = 0.53 in

Duct ID = 3.94 in

E_s = 29500 ksi

f'_g = 4000 psi

E_g = 3605 ksi

Moment of Inertia

$I_{o,strand} = \pi * d^2 / 64 = 0.0037\ in^4$

$I_{duct} = \pi * d^2 / 64 = 11.83\ in^4$

layer	# strands	d (in)	A_s (in^2)	$A_s d^2$ (in^4)
1	1	1.6164	0.22	0.57
2	2	1.212	0.43	0.64
3	3	0.8084	0.65	0.43
4	2	0.404	0.43	0.07
5	3	0	0.65	0.00
6	2	-0.404	0.43	0.07
7	3	-0.8084	0.65	0.43
8	2	-1.212	0.43	0.64
9	1	-1.6164	0.22	0.57

$I_{strands} = 19 * I_{o,strand} + \Sigma Ad^2 = 3.473\ in^4$

$I_{grout} = I_{duct} - I_{strands} = 8.356\ in^4$

$I = I_s + (E_g/E_s) * I_{grout} = 4.494$ in^4

$E_s * I =$ **$EI = 132570\ k\text{-}in^2$**

A.4 US 183 Bridge Tendons – Assumed Deviator Section - Vertical Flexural Stiffness

Nominal Dimensions

Strand diameter = 0.6 in

Strand area = 0.217 in^2

Effective strand diameter = 0.53 in

Duct ID = 3.94 in

E_s = 29500 ksi

f'_g = 4000 psi

E_g = 3605 ksi

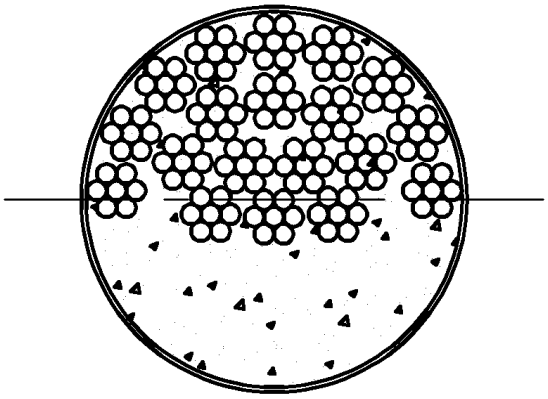

Moment of Inertia

$I_{o,strand} = \pi * d^2 / 64 = 0.0037\ in^4$

$I_{duct} = \pi * d^2 / 64 = 11.83\ in^4$

layer	# strands	d (in)	A_s (in^2)	$A_s d^2$ (in^4)
1	1	0.1797	0.22	0.01
2	2	0.1516	0.43	0.01
3	2	0.0893	0.43	0.00
4	2	0.3422	0.43	0.05
5	2	0.3787	0.43	0.06
6	2	0.6748	0.43	0.20
7	2	0.8736	0.43	0.33
8	1	1.0036	0.22	0.22
9	2	1.171	0.43	0.60
10	2	1.4921	0.43	0.97
11	1	1.6063	0.22	0.56

$I_{strands} = 19 * I_{o,strand} + \Sigma Ad^2 = 3.073\ in^4$

$I_{grout} = I_{duct} - I_{strands} = 8.756\ in^4$

$I = I_s + (E_g/E_s) * I_{grout} = 4.143$ in^4

$E_s * I =$ **$EI = 122229\ k\text{-}in^2$**

A.5 US 183 BRIDGE TENDONS – ASSUMED DEVIATOR SECTION - HORIZONTAL FLEXURAL STIFFNESS

Nominal Dimensions

Strand diameter = 0.6 in

Strand area = 0.217 in^2

Effective strand diameter = 0.53 in

Duct ID = 3.94 in

E_s = 29500 ksi

f'_g = 4000 psi

E_g = 3605 ksi

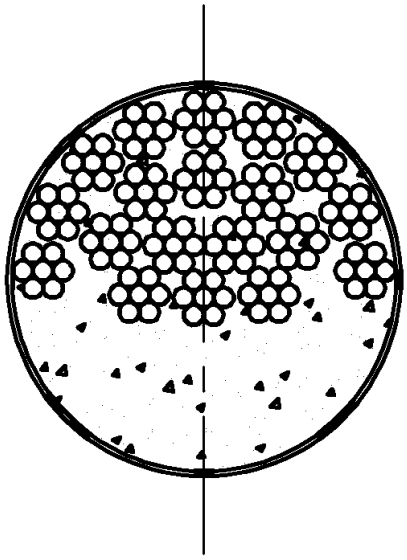

Moment of Inertia

$I_{o,strand} = \pi * d^2 / 64 = 0.0037\ in^4$

$I_{duct} = \pi * d^2 / 64 = 11.83\ in^4$

layer	# strands	d (in)	A_s (in^2)	$A_s d^2$ (in^4)
1	2	1.6125	0.43	1.13
2	2	1.4609	0.43	0.93
3	2	1.1117	0.43	0.54
4	2	0.9351	0.43	0.38
5	2	0.649	0.43	0.18
6	2	0.6	0.43	0.16
7	2	0.5879	0.43	0.15
8	2	0.3027	0.43	0.04
9	1	0	0.22	0.00
10	1	0	0.22	0.00
11	1	0	0.22	0.00

$I_{strands} = 19 * I_{o,strand} + \Sigma Ad^2 = 3.571\ in^4$

$I_{grout} = I_{duct} - I_{strands} = 8.259\ in^4$

$I = I_s + (E_g/E_s) * I_{grout} = 4.580\ in^4$

$E_s * I =$ **$EI = 135105\ k\text{-}in^2$**

REFERENCES

Bean, M. J., 2006, Bending Fatigue Performance of Small-Scale Stay Cables, Master's thesis, the University of Texas at Austin.

Corven Engineering, 2001, Mid-Bay Bridge Post-Tensioning Evaluation, Final Report, to Florida Department of Transportation District 3, Tallahassee, Florida.

Corven Engineering, 2002, New Directions for Florida Post-Tensioning Bridges, Florida Department of Transportation, Tallahassee, Florida, 2002.

Evans J.J., Ridge IML, Chaplin CR, 2001, Wire Failure in Ropes and Their Influence on Local Wire Strain Behavior in Tension-Tension Fatigue, Journal of Strain Analysis, 36:2:231-244.

Irvine, H.M., 1981, Cable Structures. 1st ed. New York: Dover Publications.

Kim B.H., Park T., 2007, Estimation of Cable Tension Force Using the Frequency-Based System Identification Method, Journal of Sound and Vibration, Elsevier 304:660-676.

Lee J.K., 2007, Evaluation of External Post-Tensioned Tendons Using Vibration Signatures, University of Texas, Austin, TX: PhD dissertation.

MacDougall C., Bartlett F.M., 2005, Mechanical Model for Unbonded Seven-Wire Tendon with Symmetric Wire Breaks, Journal of Engineering Mechanics, ASCE 131:12:1239-1247.

MacDougall C., Bartlett F.M., 2006 Mechanical Model for Unbonded Seven-Wire Tendon with Single Broken Wire, Journal of Engineering Mechanics, ASCE 132:12:1345-1353.

Morse P.M., 1948 Vibration and sound, 2nd edition, New York, NY: McGraw-Hill.

Pebley, A., 2005, Bending Stresses in Stay-Cables during Large-Amplitude Vibrations – Alfred Hartmann Bridge Case Study, Master's thesis, University of Texas at Austin.

Poser, M., 2001, Full-Scale Bending Fatigue Tests on Stay Cables, Master's thesis, University of Texas at Austin.

Russell J.C., Lardner T.J., 1998, Experimental Determination of Frequencies and Tension for Elastic Cables, Journal of Engineering Mechanics, ASCE 124:10:1067-1072.

Sagüés A.A., Kranc S.C., Eason T.G., 2006, Vibrational Tension Measurement of External Tendons in Segmental Post-Tensioned Bridges, Journal of Bridge Engineering, ASCE 11:5:582-589.

Tilly, G., 2002, Performance and Management of Post-Tensioned Structures, Structures and Buildings, Volume 152, Issue 1.

Weiher, H., Zilch, K., 2006, Condition of Post-Tensioned Concrete Bridges – Assessment of the German Stock by a Spot Survey of Damages, First International Conference on Advances in Bridge Engineering, June 26-28.

Wood S.L., Poser M., Frank K.H., Bean M.J., Dowd J.A., Eggers J.C., et al., 2008, Bending Fatigue Response of Grouted Stay Cables, Austin, TX: Center for Transportation Research, Report 0-1401-1.

Zui H., Shinke T., Namita Y., 1996, Practical Formulas for Estimation of Cable Tension by Vibration Method, Journal of Structural Engineering, ASCE 122:6:651-656.